MODELING and SIMULATION of BLOOD PRESSURE in RATS

by

SUSANNE HENTSCHEL

THESIS

for the degree of

MASTER OF SCIENCE

(Master i Anvendt matematikk og mekanikk)

Faculty of Mathematics and Natural Sciences
University of Oslo

November 2008

Det matematisk- naturvitenskapelige fakultet
Universitetet i Oslo

Modeling and Simulation of Blood Pressure in Rats

Susanne Hentschel

November 17, 2008

Preface

The idea of this thesis came up when *Hans Petter Langtangen* (*Simula Research Laboratory*) heard a presentation given by *Torill Berg* (*University of Oslo; Medical Department*). It was his idea to use Berg's measurements for simulation studies. Before I started working on this thesis, I had already worked for Simula for some months. During this time, I was introduced to many interesting topics and research in general. All that I have learned from the people at the *Simula Research Laboratory* had a great influence on this thesis.

The main work of the thesis started in January 2008 and was finished in November 2008. The result contains a fusion of the different fields that were part of my studies and I therefore consider my thesis worthy to complete my Master's degree in *Computational Science*, at the *Department of Mathematics*, *University of Oslo*.

I would like to thank *Kent-Andre Mardal* from the *Simula Research Laboratory* for taking over as my main supervisor. He introduced me to the field of inverse modeling that turned out to be a very powerful tool for the posed problem. He helped me a great deal to maneuver through this matter, where there is little useful literature to find.

Another thanks goes to *Torill Berg* who provided me with data and covered the medical side of the project. I appreciated her interest in my field, that was totally new to her, and the patience with which she helped me to understand the physiological principles.

Thanks to *Hans Petter Langtangen* and *Joakim Sundnes* for contributing with ideas and help, as well as to *Harish Narayanan* who volunteered in reading and correcting toward the end of my thesis.

Susanne Hentschel,
November 2008

Contents

List of Figures

List of Tables

List of Abbrevations

C	compliance
C_{lv}	left ventricular compliance
C_{rv}	right ventricular compliance
C_{sa}	systemic arterial compliance
C_{sv}	systemic veinous compliance
C_{pa}	pulmonary arterial compliance
C_{pv}	pulmonary veinous compliance
CVS	cardiovascular system
CO	cardiac ouput
HR	heart rate
MAP	mean arterial pressure
MP	mean pressure
P	pressure
P_{lv}	left ventricular pressure
P_{rv}	right ventricular pressure
P_{sa}	systemic arterial pressure
P_{sv}	systemic veinous pressure
P_{pa}	pulmonary arterial pressure
P_{pv}	pulmonary veinous pressure
Q	blood flow
Q_{ao}	flow through the aortic valve
Q_{dia}	flow during diastole
Q_{mi}	flow through the mitral valve
Q_{sys}	flow during systole
R	resistance
R_{ao}	resistance of the aortic valve
R_{mi}	resistance of the mitral valve
R_{pul}	pulmonary resistance
R_{pv}	resistance of the pulmonary valve
R_{sys}	systemic resistance
R_{tr}	state (closed/open) of the transcuspid valve
S_{ao}	state (closed/open) of the aortic valve
S_{mi}	state (closed/open) of the mitral valve
S_{pv}	state (closed/open) of the pulmonary valve
S_{tr}	state (closed/open) of the transcuspid valve
SV	stroke volume
t	time
$T = \frac{1}{HR}$	duration of heart beat
t_s	time where systole occurs
T_s	time from t_d to t_s
t_d	time where diastole occurs
T_d	time from t_s to t_d
$TPVR$	total peripher vascular resistance
V	volume

V_{lv}	left ventricular volume
V_{rv}	right ventricular volume
V_{sa}	systemic arterial volume

Part I.

Introduction

0.1. Motivation and Background

It was in the late 18^{th} century that scientists were able to measure blood pressure for the first time. Soon correlations between extraordinary blood pressure measurements and malfunctioning of the cardiovascular system could be revealed [34]. Today, cardiovascular disease is the most frequent cause of death. In the recent decades a lot of effort has been put into understanding the complex mechanisms that control the dynamics of blood pressure [34].

This thesis is connected to on-going research by the use of a data base, provided by Prof. Torill Berg. Berg has studied the regulation of blood pressure in rats, and during the years collected numerous measurements.

0.2. Aim and Structure

The aim of this thesis was to develop a model that reproduces the experimental data. To be able to model the cardiovascular system, its structure and dynamics have to be clear. Decomposing the system into subparts simplifies the understanding of its components. Hence the cardiovascular system is first studied as a basic passive system in static conditions. When the submodel is understood, it is extended to a dynamic model. The mentioned points are organized in the following way:

PART I As background for the mathematical and computational modeling, the physiological basics of the cardiovascular system are introduced (Chapter 1). This section on the cardiovascular system also includes definitions of the most important parameters used in medical research on this field. The introduction also presents the data measured by Prof. Berg and literature about modeling the cardiovascular system.

PART II After introducing some common mathematical blood pressure models in Chapter 4, Chapter 5 focuses on the analysis of the mathematical models including common properties, stability and equilibria. Up to this point, the thesis does not differ from what can be found in literature, since many studies use similar approaches. However, the data basis provided by Berg contains measurements that differ from the data used in other simulation studies. Parameter estimation (Chapter 6) is therefore a key chapter. It contains an *a priori* approach based on conditions derived from physical characteristics of the cardiovascular system. In addition to this 'direct' estimation of parameters, Section 6.2 also provides an inverse parameter estimation. Finally, the simulations, results and errors in the different models conclude part II. At this point the basis for the dynamic part is built.

PART III The goal of Chapter 8 is to present possible solutions for adding dynamic response to the previously described static model. Unlike the rest of

the thesis, the ideas presented in part III are only preliminary. More future work is required to successfully model the dynamic response.

PART IV The thesis will be concluded by a discussion on the applicability and future prospects of different models.

Appendix The appendix includes additional plots from the simulations and a brief description of the code for the different simulations. The code itself is available on the internet [12].

0.3. Abbreviations

A list with all abbreviations used in this document can be found in the beginning of the document. The parameters are often given a subscript, referring to the part of the Cardiovascular System that is described.

1. Physiology of the CVS

1.1. The Cardiovascular System

All factors that have an impact on blood pressure are part of the Cardiovascular System (CVS) or at least coupled to it. The CVS includes both the complex network of blood vessels, where blood is transported between different organs and the heart that pumps the blood (Figure 1.1, [14]).

On its way from the heart to the body, blood passes through vessels with distensible walls, called compliance vessels. Their main characteristic is that blood is transported with a minimum of energy loss by keeping the mean pressure close to constant [15]. During systole (when the heart ejects blood) compliance vessels expand and store parts of the entering blood. The stored blood is released during diastole (when the heart refills). As a consequence, the oscillating flow that is produced by the heart, becomes almost stationary when it arrives in the organ vessels (capillaries). Figure 1.2 shows how pressure changes from the heart to the capillaries.

When blood approaches the organs, the network of blood vessels densifies gradually. The diameters for single vessels decrease, but the over-all cross section of parallel vessels becomes vast (Figure 1.2, [30]). Due to their small diameters, these vessels have increased resistance and reduced flexibility and are therefore called resistance vessels. The resistance causes a pressure fall. The resulting low velocity in the distal capillaries enables exchange of products with the surrounding tissues.

The vessel system leading back to the heart (venal system) is symmetric with the arterial system. In the organs, the venal system is a vast network with vessels of small diameter. Closer to the heart, there are less veins with larger diameter. A main difference to the arterial system is that veins are more flexible to allow blood transport in spite of the low pressure.

Furthermore, the CVS consists of two parallel systems, i. e., the systemic and pulmonary circulations. The first supplies the body with nutrients and oxygen, whereas the pulmonary system transports blood between heart and lungs and allows gas exchange in the lungs. The systemic circulation includes vessels from the left ventricle to all other organs and back to the right ventricle. The circulation from the right ventricle to the lungs and back to the left ventricle is part of the pulmonary circulation. The ventricles and the vessel network are separated by valves preventing retrograde flow.

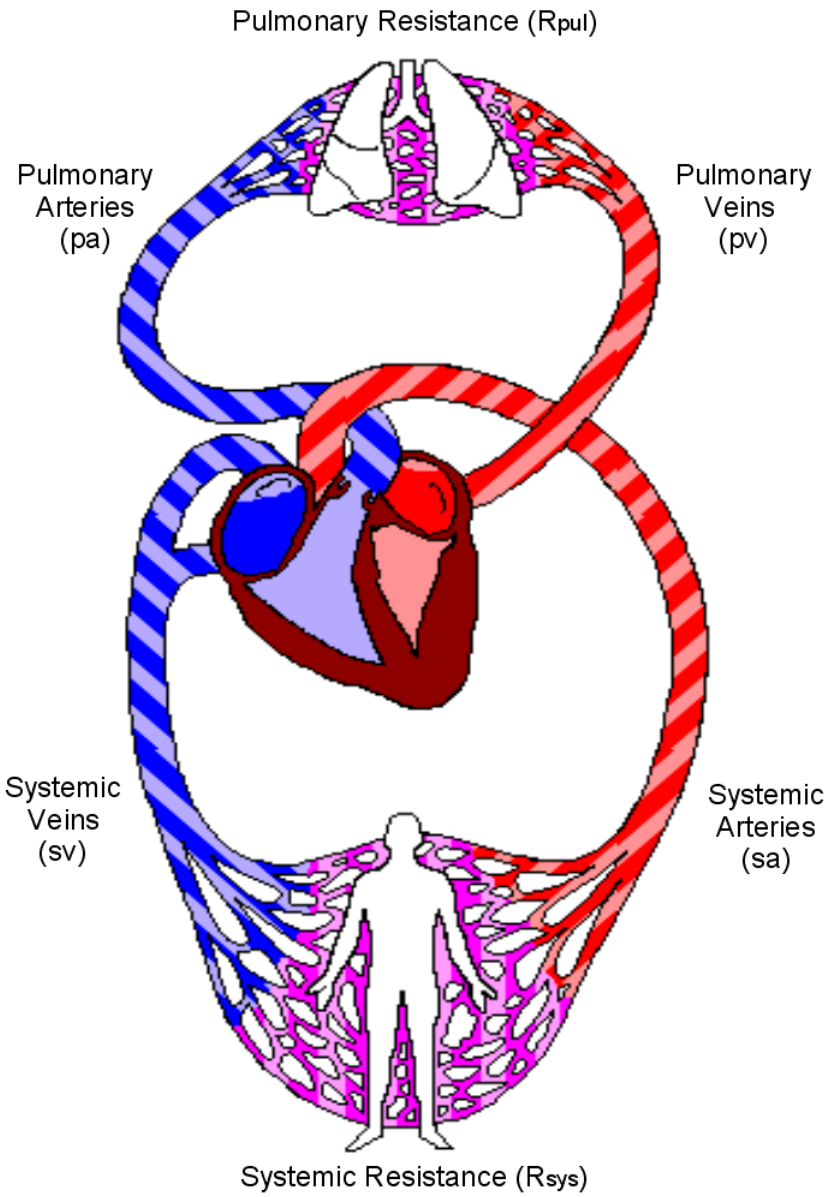

Figure 1.1.: The cardiovascular system of the human body.

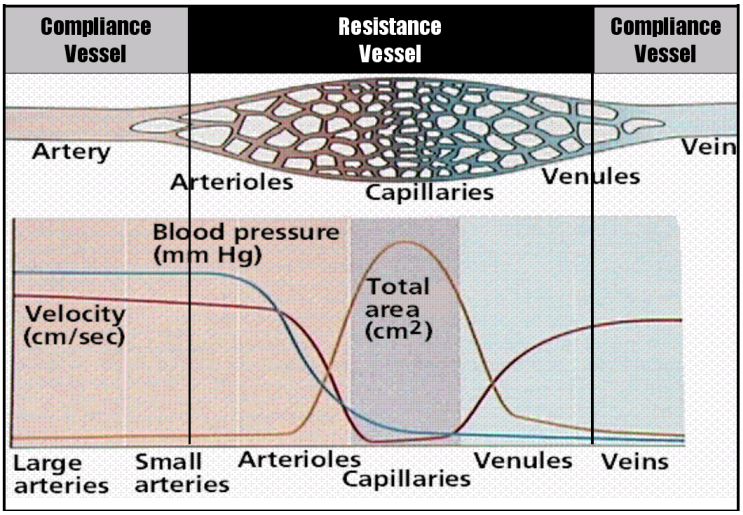

Figure 1.2.: Illustration of the mean pressure distribution, blood velocity and cross section area along the vessel system.

Systemic arterial pressure is described by its minimum and maximum values, i. e. diastolic and systolic pressure, respectively. It is important to note that the systole starts where the arterial pressure has its minimum, but the systole does not end with maximum arterial pressure. Hence, there is a difference in the terms diastolic/systolic and diastole/systole. Figure 1.3 shows the relation between the main pressure and flow curves [20].

The blood volume ejected by the heart during each contraction is called the stroke volume. Cardiac output is determined by the stroke volume multiplied by the number of heart beats per minute (heart rate). Stroke volume and cardiac output refer to output from the left ventricle unless otherwise indicated.

$$CO = SV \cdot HR = SV/T \tag{1.1}$$

with

CO ... cardiac output

SV ... stroke volume

HR ... heart rate

T ... duration of heart beat

By dividing mean arterial pressure by cardiac output we get the total peripheral vascular resistance ($TPVR$).

$$TPVR = MAP/CO = (MAP \cdot T)/SV \tag{1.2}$$

with

MAP ... mean arterial pressure

T ... duration of heart beat

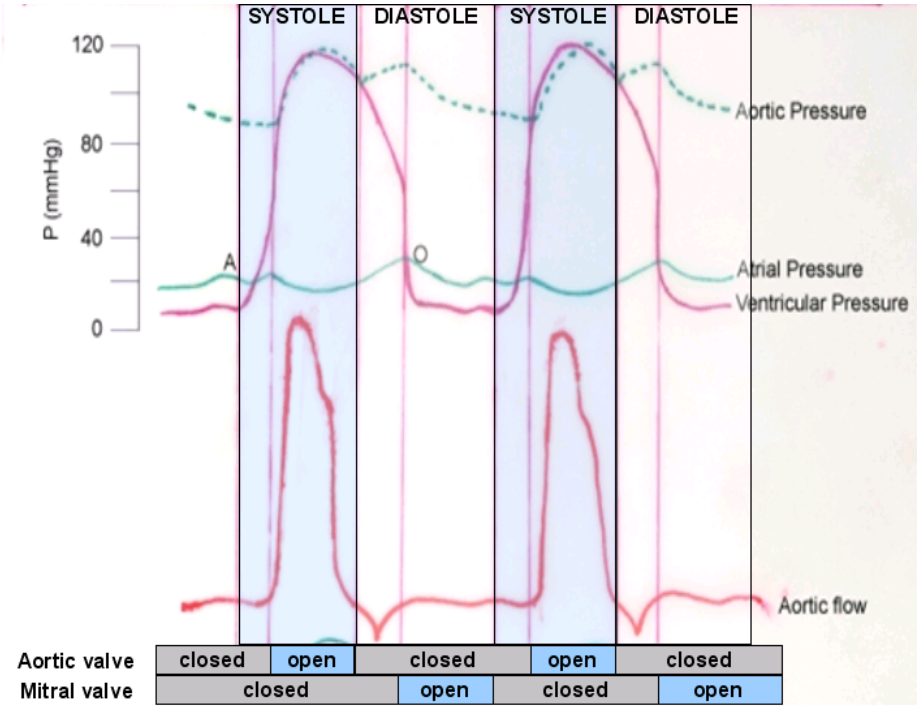

Figure 1.3.: Aortic, ventricular and atrial pressure and aortic flow in the heart cycle.

Another important factor is the heart's performance, which is influenced by contractility, preload and afterload. Contractility is the heart's ability to pump. It is influenced by the pressure that stretches the ventricle (the preload) and the pressure the heart is pumping against (the afterload).

1.2. Dynamics of the CVS

1.2.1. The Baroreceptor Loop

Dynamic behaviour of the CVS is controlled by the baroreceptor loop. The latter is a global feedback mechanism attempting to keep the mean arterial pressure constant. When the mean pressure changes, the baroreceptors function to adapt heart rate, cardiac contractility and $TPVR$ so that the pressure can return to the desired value.

When baroreceptors, the receptors in the aorta, detect a fall in pressure, they send a signal to the central nervous system. To react on the incoming signal, the center of blood pressure control in the brain stem keeps track of two main characteristics; the mean arterial pressure and its rate of change. The baroreceptors are sensitive to deviations of the actual and the nominal values, however the sensitivity depends on the rate of change. If the observed changes occur rapidly, the CVS is adapted more radically.

1.3. Hypertension

When the pressure remains altered for a long period of time, the nominal value is adapted to this new condition. The result is hypertension, where the abnormal elevated pressure is seen as normal and therefore stays constantly high [8]. Hypertension is the most common disease in the CVS. The mechanisms responsible for the development of hypertension are not fully understood. Many factors may play a role, such as Sodium intake, renal function, sympathic nervous system, humoral factors, local autoregulation and elasticity of the vessel walls, wall shear and blood viscosity [34].

2. Experiments and Extracted Data

2.1. Experiments and Measurements

Preparation of animals. 12–14 weeks old male spontaneous hypertensive rats (SHR, Okamoto, SHR/NHsd strain) and their normotensive controls (WKY, Wistar Kyoto) on conventional rat chow diet (0.7 % NaCl) were allowed food and water ad lib until the time of the experiment. The rats were anesthetized with pentobarbital sodium (65–75 mg/kg, intraperitoneally). Systolic blood pressure and diastolic blood pressure were monitored through a catheter in the femoral artery, and left vetriclar pressure by a catheter in the left ventricle, inserted via the right carotid artery. The catheters were filled with heparinized (100 I.U./ml) buffered saline (PBS: 0.01M Na-phosphate, pH 7.4, 0.14M NaCl), and connected to SensoNor 840 transducers (SensoNor a/s, Horten, Norway). The rats were then connected to a respirator and were ventilated with air throughout the experiment. Thoracotomy was performed through the right, forth inter-costal space, and a perivascular flow probe (2SB) was placed around the ascending aorta. The probe was coupled to a T206 Ultrasonic Transit-Time Flowmeter (Transonic Systems, Ithaca, N.Y., USA) and recorded flow in the ascending aorta, also used to describe cardiac output (i. e., minus cardiac flow). The thorax was subsequently closed. The flowprobe and transducers were coupled to an amplifier and computer for storage and computation of data. Body temperature was maintained by external heating, guided by a thermo sensor inserted inguinally into the abdominal cavity.

Experimental design. Data were first collected during a control period of 10 min. Then, data were collected during a period adrenergic activation of the CVS, achieved by stimulation of endogenous noradrenalin release from sympathetic nerve endings using tyramine. Tyramine hydrochloride was infused through a catheter in the femoral vein (1.26 μ mol/min/kg in PBS (0.01 mol/L Na-phosphate, pH 7.4, 0.14 mol/L NaCl), 217 μ l/min/kg for 15 min).

2.2. Acquisition and Analysis of Data

The electronic signals (2500 signals/sec) from the probe and the transducers were transferred to a computer with a Dash 16 ADC card (Metrabyte Corp., Computer Boards Inc., Tauton, MA). The program for calibration, data acquisition, plotting and evaluation was written in ASYST v.4.0 software (Macmillan Software Co., New York, NY). The data were collected in a background circular buffer that returns 50 points of data on each of 4 channels at 20 msec intervals, giving a resolution of several hundred points per heart beat. The systolic and

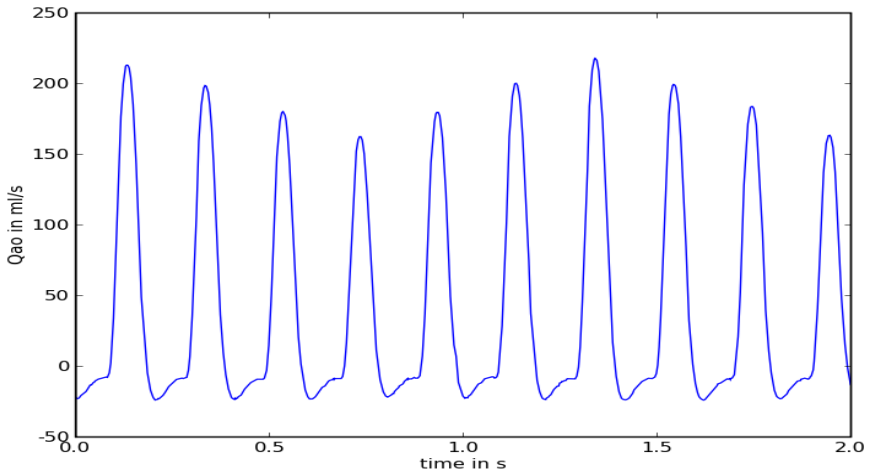

Figure 2.1.: Example of raw data of high resolution measurements of flow over 2 seconds.

diastolic blood pressure were identified by the voltage crossing a slowly drifting midline.

Mean Arterial Blood Pressure was calculated:

$$MAP = 2/3P_{dia} + 1/3P_{sys}, \tag{2.1}$$

with

P_{sys} ... systolic arterial blood pressure

P_{dia} ... diastolic arterial blood pressure.

Recent research has shown that this approximation is not accurate for every heart rate. Mean arterial pressure can be better approximated by a heart rate dependent formula as given in [33]. In this work however, we have decided to follow Berg and use Equation 2.1 for all heart rates.

TPVR was calculated as in 1.2, with mean arterial pressure from 2.1.

Heart Rate was determined from the periodicity of the oscillations in the cardiac output curve.

Pressure and Aortic Flow. The normal protocol was to store the pressure and aortic flow values at each systole and diastole only, and the intermediate signals were discarded to make the amount of data manageable. However, when greater fidelity was required, pressing an assigned key on the computer keyboard instructed the program to store all signals collected during the last two seconds (5000 signals from the left ventricular pressure transducer and 5000 signals from the flow probe) into a separate file.

Averaging High Resolution Measurements. High resolution measurements contained several pulses with a varying number from rat to rat. Due to the invasive experiments, the rats' pulses were not always regular (see Figure 2.1). Highly unregular pulses had to be sorted out. For comparing single pulses, they had to be extracted from the signal. The simplest characteristic in every pulse is that its slope changes sign only once if we define the starting point to also be at a point of changing slope sign. To sort out period after period, three points needed to be found: the first point where the slope is positive (Point I), the first point (Point II) where the slope is negative after Point I, and the first point (Point III) with positive slope after Point II. To decrease the chance that the interval from Point I to Point III is a complete period, every period was required to contain at least 100 points. Before averaging the single pulses to one curve, pulses with markedly different duration or maximum, were removed. The duration of each pulse was compared to the mean of the others and was only accepted if it differed less than $\pm$ 10 dt. The maximum of each pulse was compared to the overall mean maximum, where a deviation of $\pm$ 20 mmHg was allowed. Then, the pulses were averaged in a way that all the maxima occur on the same index. An example of separated flow curves and their average can be found in Figure 2.2.

Occurrence of Systolic and Diastolic Arterial Pressure. Since it is not known when the measurements of systolic and diastolic arterial pressure were taken, the time of occurrence had to be estimated. Figure 1.3 shows that diastolic pressure coincides with an enormous slope change in the aortic flow curve. The latter could be defined by the maximum of the third derivative of aortic flow. However, the time of the systolic pressure is not as easy to find. As an approximation, the maximum of aortic flow was used, even though it occurs slightly before the pressure peak [24]. Defining systolic arterial blood pressure at the flow peak would be correct for for rigid vessel walls. The delay, that we do not take into account, occurs due to the flexibility of the vessel walls.

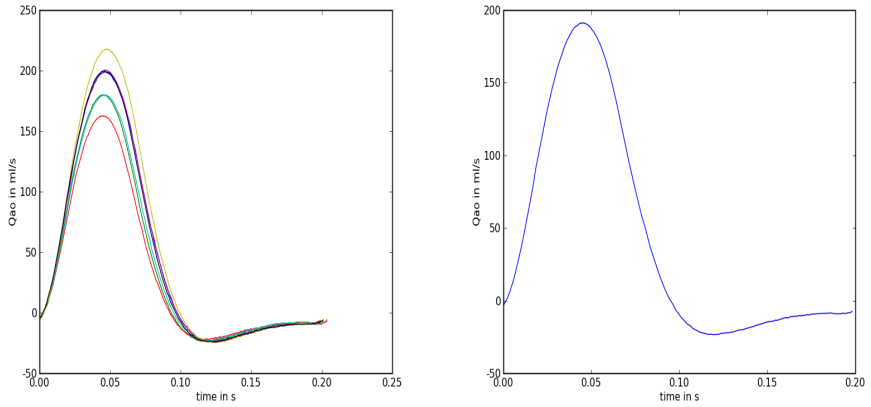

Figure 2.2.: High resolution flow data from Figure 2.1 clipped into single periods and averaged in a single curve.

3. Literature Review

3.1. Basic Models for the CVS

In Chapter 1, we have seen that the CVS is composed of three main parts: the heart, resistance and compliance vessels. These three components form the basis of models found in literature. Both the implementation of the single components and the degree of complexity vary in the different approaches.

3.1.1. Complexity and Analysis of the Models

The most common basic model includes the whole CVS packed together in six compartments. Its popularity results from being the simplest model that contains all the main parts of the CVS. A detailed description and analysis of the six compartment model is presented in [4]. The latter discusses also the dynamics, equilibria and stability of the six compartment model. Parameter identification is accomplished both *a priori* (combining literature and own measurements) and *a posteriori* (based on dynamic measurements).

It is also possible to model the CVS in simpler ways. The simplest way is to remove five compartments from the complete model and set conditions for the incoming and outgoing signals. Another way is to lump several compartments to one. In this way, the complexity is reduced at the expense of the physical meaning of some the lumped parameters. Such models can were found in [15] and [17]. Both provide physiological background and develop the models by gradually extending a One-Compartment Model. Following this path of going from basic to more complex models is a good approach for applications with many unknown parameters. [15] covers also the implementation of models in Matlab, but numerical analysis is not included.

A majority of models are based on a linear relation between resistance and flow even though it is known that non-linear relations (such the form as given in [36]) are more physiologically appropriate [1]. Figure 3.1 from [28] shows how the simulated arterial pressure from a linear model compares to measured data. The pressure maximum occurs too late and is clearly lower than the measured systolic pressure. The gradients for both rising and falling pressure are not steep enough around the systolic pressure. The pressure oscillations around the closing of the aortic valve can not be reproduced by the linear model. The diastolic part of the curve is simulated quite exact. With the available arterial pressure measurements, the deviation between simulated and real pressure can not be seen so clearly. However, it is important to notice, that the location systolic pressure are not correct. Even though we can manage to increase the modeled systolic pressure by changing the compliance, the model produces a shape that differs from reality.

3.1.2. The Pumping Activity of the Heart

As the heart is the pump of the system, it defines the wave form of the signal that is sent through the body. It is therefore very important to model the heart correctly. A typical approach to define the pumping activity of the heart, is by a time-varying compliance or volume function. In both cases, there are models that use mathematical functions with fitted parameters ([2], [35]) and functions derived from physical quantities. The latter are often more complex but they allow interpretations of the physical meaning of changing certain parameters.

The most important physical models are presented below. [15] uses Sagawa's approach (Equation 3.1) of modeling the heart with time-varying compliance. This approach was first introduced in 1978 [16] and is now widely in use.

$$C_{lv}(t) = \begin{cases} C_{LVD}\left(\frac{C_{LVS}}{C_{LVD}}\right)^{\frac{1-\exp(-t/\tau_s)}{1-\exp(-T_s/\tau_s)}} & 0 \leq t \leq T_s \\ C_{LVS}\left(\frac{C_{LVD}}{C_{LVS}}\right)^{\frac{1-\exp(-(t-T_s)/\tau_d)}{1-\exp(-(T-T_s)/\tau_d)}} & T_S \leq t \leq T \end{cases} \tag{3.1}$$

with

C_{LVD} ... maximum value of C_{lv}
C_{LVS} ... minimum value of C_{lv}
τ_s ... time constant for decreasing C_{lv}
τ_d ... time constant for increasing C_{lv}
T ... duration of one heart beat
Ts ... duration of one systole

In contrast to Sagawa's formula for compliance, one may focus on volume changes in the heart without extracting compliance and pressure, as can be seen in [4]. However, Berg's measurements allow us to include left ventricular pressure explicitly while the volume is unknown.

A discussion and comparison of different models of the heart is given in [27] and [9]. Both present similar definitions of compliance which are independent of load. The more compact definition was found in [27], with a single function valid over the whole period:

$$E_{lv} = 1/C_{lv} = 2a(V_{lv} - b) + c\frac{(1 - \exp\left(-(\frac{t}{\tau_c})\right)^{\alpha})\exp\left(-(\frac{t-t_d}{\tau_r}\right))^{\alpha}}{(1 - \exp\left(-(\frac{t_p}{\tau_c})\right)^{\alpha})\exp(-(\frac{t_p-t_d}{\tau_r}))^{\alpha}} \tag{3.2}$$

with

E_{lv} ... left ventricular elastance

V_{lv} ... left ventricular volume

t_d ... starting point of relaxation process

t_p ... time of peak generated pressure

a, b, c ... parameters, defined by curve fitting

τ_c, τ_r ... time constants

Being highly dependent on contractility, [27] appraises this definition to be a reliable indicator for the heart performance. Nevertheless, the formula requires the left ventricular volume which is an unknown, time-dependent function. Thus Sagawa's approach has to be chosen, despite of the limitations.

3.2. Models of CVS Control Mechanisms

Most groups working with the CVS also study its dynamics. Typically, they focus on short term regulation, in particular the mechanisms of the baroreceptor loop. Their approaches may be divided into two groups: Models that reproduce and fit measured data ([23], [11], [2], [35]) and models that reveal physiological details in the baroreceptor control mechanism ([11], [19]). A good example of the first model type is that [23] fits the heart rate so that the modeled pressure is close to the measured pressure. From a physiological point of view, this models lacks the influence of the blood pressure derivative (Section 1.2.1) and the modeled heart rate is not compared to measurements. A collection of control mechanisms appealing to the second group are explained in [9]. Among those are models for central nervous system, control of the ventricles, control of the vasculature. Another example for modeling the central nervous system's effect on blood pressure control is given in [19].

Some groups tried to gain more insight in the dynamics of the CVS by applying system identification techniques as described in [3], [22] and [21]. The applied mathematical tools in the latter ones were not studied or consulted. However, they might be useful for later work.

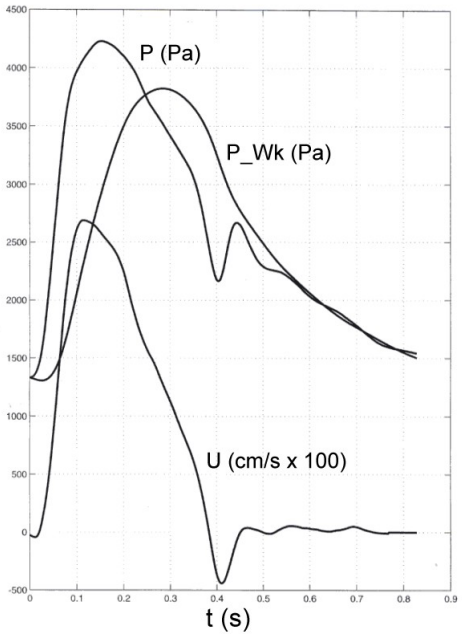

Figure 3.1.: Measured pulmonary arterial pressure and velocity compared with modeled pulmonary arterial pressure in a dog.

Part II.

Finding Basic Models for Static Conditions

4. Models of the Cardiovascular System

As presented in Chapter 1, the CVS is composed of different vessel types. We have seen that these vessel types can be classified as compliance and resistance vessels. In this chapter, we introduce the physical laws of these two vessel types and describe how they can be connected to different models. A detailed description of the models and their equations is given in [15] and [17].

A linear relation of the changing volume $V(t)$ in a compliance vessel is given by the equation

$$V(t) = V_d + C\,P(t). \tag{4.1}$$

V_d denotes the volume that the vessel would have when dead. Depending on the actual pressure $P(t)$, the vessel walls expand or relax. The extent of the expansion of the vessel walls depends on the vessel's compliance C, that describes the vessel's flexibility. In most models, arteries with a large diameter are considered to be compliance vessels. Parallel compliance vessels can be lumped into one compliance vessel, also called compliance compartment.

In contrast to flow through compliance vessels, flow through a resistor causes a considerable pressure drop given by the relation

$$Q(t) = \frac{\Delta P(t)}{R} = \frac{P_{in}(t) - P_{out}(t)}{R}, \tag{4.2}$$

with

$Q(t)$ ... flow through the resistor
$P_{in}(t)$ ... inflow pressure
$P_{out}(t)$ ... outflow pressure
R ... resistance of the resistor.

The resistor may replace a single vessel or a network of many bifurcating and converging vessels. It models the overall pressure drop in a given region.

A more complex formulation of the pressure drop over a resistor is given in [36] and can replace Equation 4.2:

$$\frac{dQ(t)}{dt} = \frac{P_{in}(t) - P_{out}(t) - QR}{L}, \tag{4.3}$$

with the additional parameter

L ... length of the resistor.

By applying the law of conservation of volume, the two vessel types can be connected:

$$\frac{dV}{dt} = \frac{d(C\,P)}{dt} = Q_{in}(t) - Q_{out}(t) \tag{4.4}$$

with

$Q_{in}(t)$ ... inflow
$Q_{out}(t)$ ... outflow.

The rate of volume change in the compliance vessels must equal the difference between inflow and outflow. By using resistance and compliance vessels as basic tools, one can set up a variety of different models. Some examples are introduced in the next sections.

4.1. One-Compartment Model

The simplest approach is shown in Figure 4.1, which models arterial pressure by applying Equation 4.4. The inflow into the systemic arteries is defined by a given time dependent function. The outflow equals the flow through the systemic resistance:

$$Q_{out} = \frac{P_{sa} - P_{sv}}{R_{sys}} \tag{4.5}$$

with

P_{sa} ... systemic arterial pressure
P_{sv} ... systemic veinous pressure
R_{sys} ... systemic resistance

Equation 4.4 can then be formulated as

$$C_{sa}\frac{d(P)}{dt} = Q_{in}(t) - \frac{P_{sa}(t) - P_{sv}(t)}{R_{sys}} \tag{4.6}$$

with

C_{sa} ... systemic arterial compliance

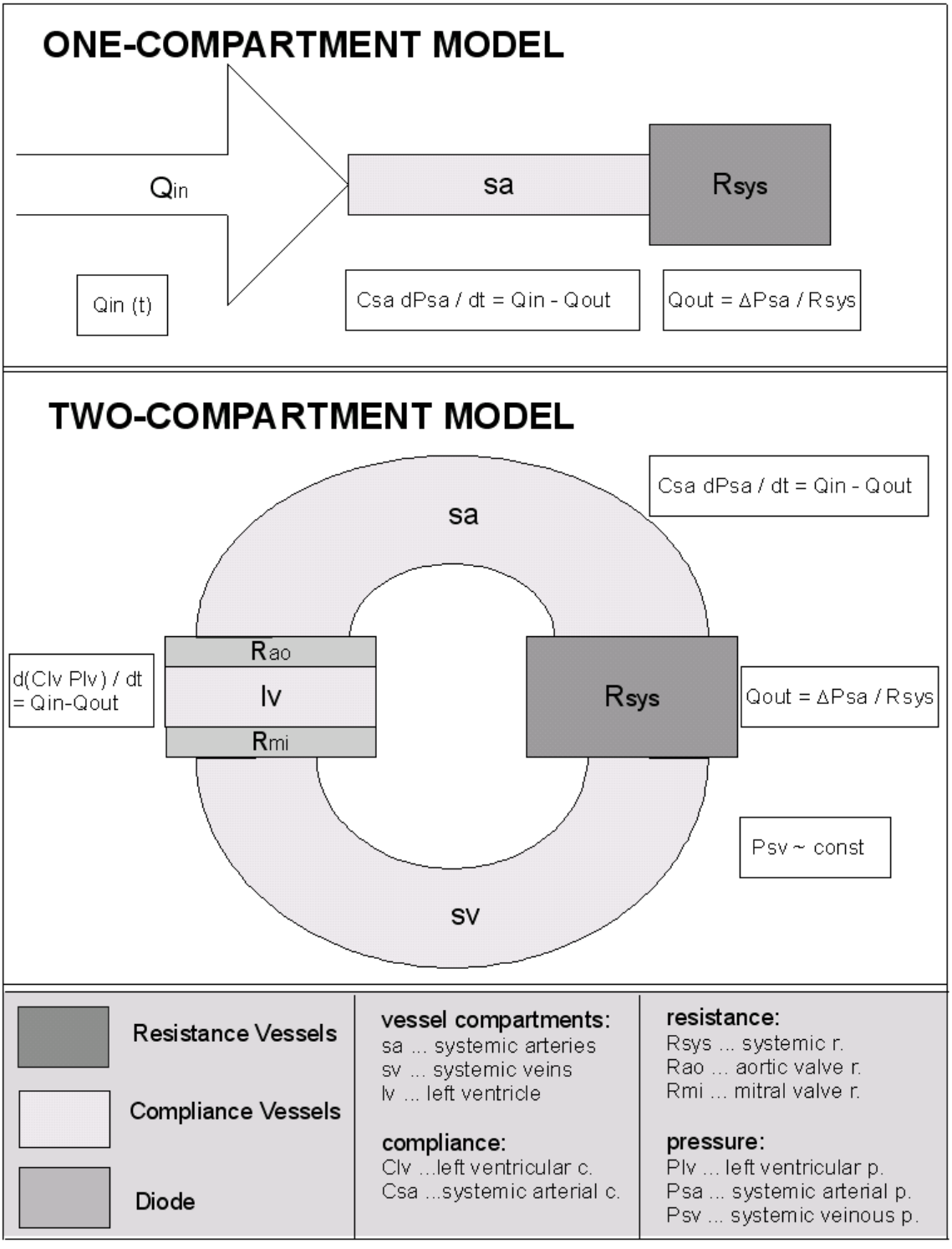

Figure 4.1.: One-Compartment and Two-Compartment Model of the cardiovascular system.

Assuming that arterial pressure is much greater than venous pressure ($P_{sa} >> P_{sv}$), arterial pressure is defined by:

$$\dot{P_{sa}} = \frac{Q_{in} - P_{sa}/R_{sys}}{C_{sa}}. \tag{4.7}$$

Discretizing this equation by using the forward Euler method provides an explicit scheme for the One-Compartment Model:

$$P_{sa}(t_{i+1}) = P_{sa}(t_i)\Delta t \frac{Q_{in}(t_i) - \frac{P_{sa}(t_i)}{R_{sys}}}{C_{sa}}. \tag{4.8}$$

4.2. Two-Compartment Model

The previous section showed a simple way of modeling blood pressure in the arteries, but the input and the output are not connected. We will now develop a Two-Compartment Model 4.1 that represents the CVS as a circular system. Before we can model the CVS as a circular system, we need to model the heart that generates the inflow into the systemic arteries. For simplicity, the heart is only represented by the left ventricle.
By defining the heart as a compliance vessel with time-dependent compliance,

$$\frac{dV_{lv}}{dt} = \frac{d}{dt} C_{lv}(t) P_{lv}(t), \tag{4.9}$$

with

V_{lv} ... volume of the left ventricle
C_{lv} ... left ventricular compliance
P_{lv} ... left ventricular pressure,

the law of conversation of volume can be applied:

$$\frac{d(C_{lv}P_{lv})}{dt} = Q_{in} - Q_{out}. \tag{4.10}$$

The inflow and the outflow of the heart are defined by the flow through the heart's valves. To maintain the flow direction, the valves are modeled as diode-like resistors, with low resistance in the desired flow direction and high resistance in the opposite direction. By including an additional state variable S, the definition of flow through a resistor can be extended to flow through a diode. The variable S indicates if the valve is open ($S = 1$) or closed ($S = 0$).

Finally we connect the systemic resistor and the mitral valve diode with a compliance vessel. This vessel represents systemic veins that transport the

blood back to the heart. Since venous pressure is very small compared to the arterial pressure, it is assumed constant. As a consequence, the volume in the venous compliance compartment is not changing.

Then inflow and outflow of the heart can then be formulated by:

$$\begin{aligned} Q_{in} &= Q_{mi} = S_{mi}\frac{P_{sv} - P_{lv}}{R_{mi}} \\ Q_{out} &= Q_{ao} = S_{ao}\frac{P_{lv} - P_{sa}}{R_{ao}} \end{aligned} \tag{4.11}$$

with

Q_{mi} ... flow through the mitral valve
Q_{ao} ... flow through the aortic valve
R_{mi} ... resistance of the mitral valve
S_{mi} ... state of the mitral valve
S_{ao} ... state of the aortic valve
R_{ao} ... resistance of the aotric valve.

Merging Equation 4.11 and Equation 4.10 gives

$$\frac{d(C_{lv}P_{lv})}{dt} = S_{mi}\frac{P_{sv} - P_{lv}}{R_{mi}} - S_{ao}\frac{P_{lv} - P_{sa}}{R_{ao}}. \tag{4.12}$$

Similarily we insert Equation 4.11 into Equation **??**:

$$C_{sa}\dot{P_{sa}} = S_{ao}\frac{P_{lv} - P_{sa}}{R - ao} - \frac{P_{sa}}{R_{sys}}. \tag{4.13}$$

The equations are coupled (both depend on systemic and left ventricular pressure) and nonlinear, since the valves' state depend on the current pressure. [15] suggested to discretize the equations with backward Euler. On each time step, the calculated pressure and the valves' states have to be stable. First, the valves are set and the pressure is calculated. If the calculated pressure demands another state of one or both valves, the valves are reset and the pressure is re-calculated. This process is repeated until the result is stable. More information on convergence of this method can be found in [15].

The complete scheme is given by

$$\begin{aligned} & C_{sa}\frac{P_{sa}(t_i) - P_{sa}(t_{i-1})}{\Delta t} = \\ =& S_{ao}(t_i)\frac{P_{lv}(t_i) - P_{sa}(t_i)}{R_{ao}} - \frac{P_{sa}(t_i)}{R_{sys}} \\ & \frac{C_{lv}(t_i)P_{lv}(t_i) - C_{lv}(t_{i-1})P_{lv}(t_{i-1})}{\Delta t} = \\ =& S_{mi}(t_i)\frac{P_{sv}(t_i) - P_{lv}(t_i)}{R_{mi}} - S_{ao}(t_i)\frac{P_{lv}(t_i) - P_{sa}(t_i)}{R_{ao}} \end{aligned} \tag{4.14}$$

4.3. Six-Compartment Model

The previous sections gave examples of models that are basically built up by connecting resistors with compliance vessels. However, introducing a Six-Compartment Model allows one to build a system containing both pulmonary and systemic circulation.

A model which has been widely used is one which includes both the systemic and pulmonary circulation (see Figure 4.3) with left and the right ventricle. The systemic circulation is almost identical to that in the last example. However, in this model, the systemic veins empty into the right ventricle instead. From there, the pulmonary arteries lead into the pulmonary resistor, representing the lungs. The model is completed by the pulmonary veins, which transport blood from the lungs back into the left ventricle. All compartments in this model are analogous to the ones used in the previous models.

Thus, the circulatory system is modeled as a closed circuit including six resistors connected by six compliance vessels. This leads to a system of almost linear equations where the valve states depend on the unknown pressure values. In contrast to the other models, the Six-Compartment Model is the only model which contains all important parts of the cardiovascular system.

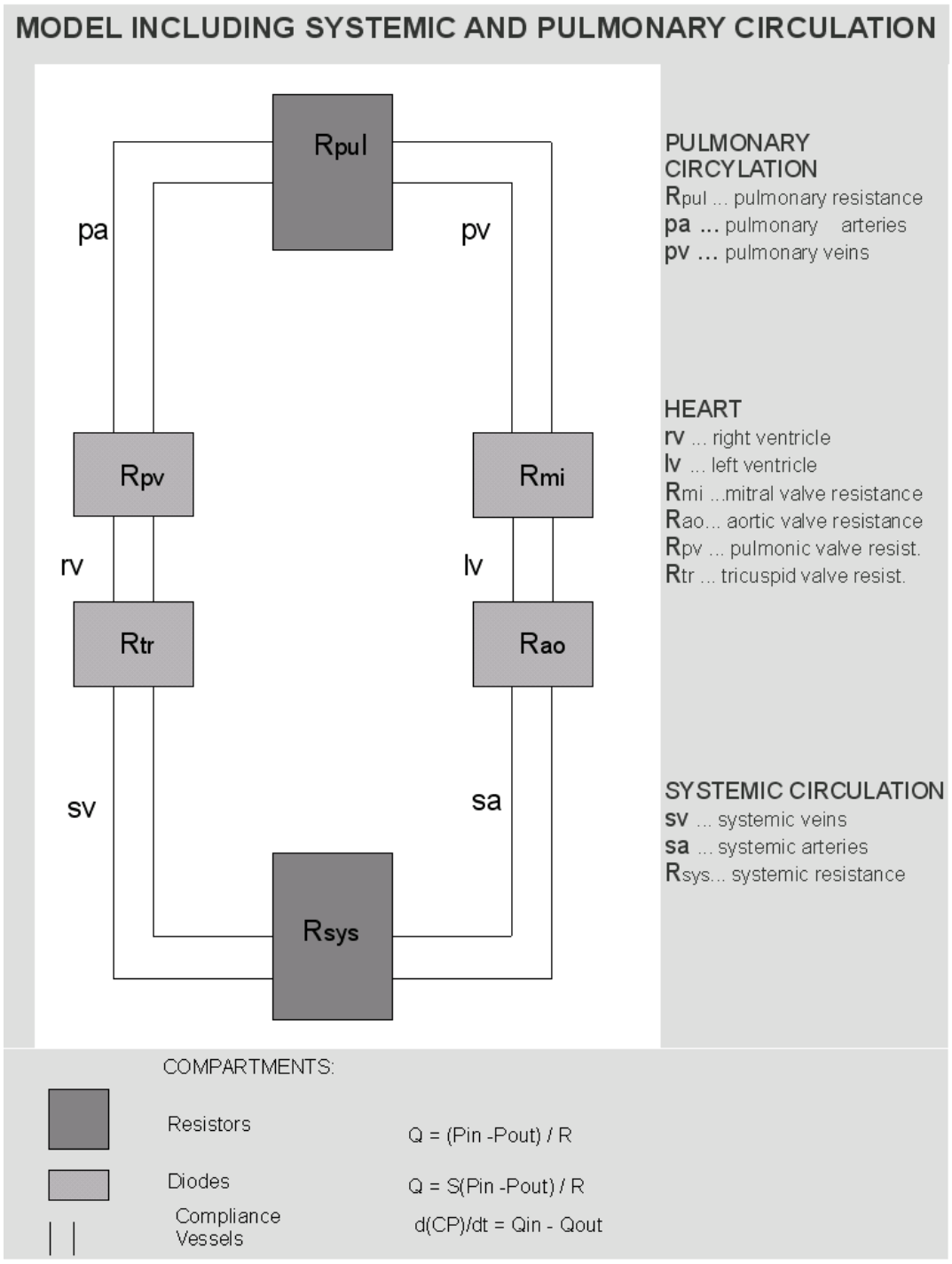

Figure 4.2.: The CVS with systemic and pulmonary circulation.

5. Analysis

After having introduced models of the CVS, this chapter provides some analysis of the One-Compartment model. The purpose is to show the parameter's influence on the solution.

5.1. Analytical Analysis for the One-Compartment Model

The One-Compartment Model is a first order ODE with constant coefficients and an initial condition:

$$\begin{aligned} &\dot{P(t)} - AQ(t) + BP(t) = 0 \\ &P(0) = P_0 \\ &A = \frac{1}{C} \\ &B = \frac{1}{RC} = \frac{A}{R} \end{aligned} \tag{5.1}$$

Solving the equation in general gives

$$P(t) = \frac{A \int_0^t Q(t) e^{Bt} dt + C}{e^{Bt}} \tag{5.2}$$

Approaching this general solution through several steps gives an idea of how the different variables and constants influence each other.

Setting $B = 0$ (meaning that resistance is infinite) and $Q = const$ leads to a the linear solution

$$P(t) = AQt + P_0. \tag{5.3}$$

This solution is meaningful in a physical sense: finite resistance and constant flow lead to pressure increasing linearly with time.

Changing B to a nonzero constant gives:

$$P(t) = \frac{AQ}{B} + \left(P_0 - \frac{AQ}{B}\right) \exp(-Bt) \tag{5.4}$$

I. e. finite resistance and constant flow let the pressure approach a constant value. The closer the initial value P_0 is chosen to the final constant, the faster the equilibrium state is reached. This equation is a good description of the

mean pressure behaviour and how the initial condition influences the solution.

To introduce a more realistic but simple function with a fluctuation flow pattern, a simple sine function was chosen.

$$Q(t) = a \sin\left(\frac{2\pi}{T}t\right) + b, \text{ with amplitude } a > 0 \tag{5.5}$$

This function provides three characteristics that can also be found in the real flow function: amplitude (a), mean value (b) and duration of one period (T).

This leads to the solution

$$\begin{aligned} P(t) &= \frac{A\int_0^t (a\sin\left(\frac{2\pi}{T}t\right) + b)e^{Bt}dt + C}{e^{Bt}} \\ &= \frac{Aa}{B^2 + (T/2\pi)^2}\left[B\sin\left(\frac{2\pi}{T}t\right) - \frac{T}{2\pi}\cos\left(\frac{2\pi}{T}t\right)\right] + \frac{Ab}{B} + Ce^{-Bt}, \end{aligned} \tag{5.6}$$

with

$$C = P_0 + \frac{Aa}{B^2 + (T/2\pi)^2}\frac{T}{2\pi} - \frac{Ab}{B}$$

$$\begin{aligned} P(t) =& \frac{Ab}{B} + \frac{Aa}{B^2 + (T/2\pi)^2}\left[B\sin\left(\frac{2\pi}{T}t\right) - \frac{T}{2\pi}\cos\left(\frac{2\pi}{T}t\right)\right] \\ &+ \left(P_0 + \frac{Aa}{B^2 + (T/2\pi)^2}\frac{T}{2\pi} - \frac{Ab}{B}\right)e^{-Bt}. \end{aligned} \tag{5.7}$$

Inserting $B = A/R$, $B = 1/C$, $B \gg T/2\pi$ and letting $t \to \infty$,

$$P(t) \approx bR + \frac{a}{1/CR^2}\left[\frac{1}{CR}\sin\left(\frac{2\pi}{T}t\right) - \frac{T}{2\pi}\cos\left(\frac{2\pi}{T}t\right)\right] \tag{5.8}$$

We see that the mean level of the flow function and the resistance influence the mean level of the pressure while the amplitude of the pressure oscillations are influence by the flow's amplitude, the resistance and the compliance.

5.2. Equilibrium State

The principle of the CVS is to maintain blood supply to all parts of the body according to changing needs. Whenever the needs are constant, the system will approach an equilibrium. Assuming that the body's needs can be met by the pumping capacity of the heart, the equilibrium will be reached when the needs stay constant sufficiently long. In part I, the goal was to develop a model for constant conditions, thus, equilibria are a very good indicator for checking the validity of the model.

For the basic model to mimic physiology correctly, it must approach the correct equilibrium under static conditions. Static conditions require constant

resistance in all resistance vessels and constant compliance in all compliance vessels, except for the heart.

Equilibrium is reached when the last and the first point in every period have the same value, and the mean blood pressure remains constant. Integrating the equation from the One-Compartment Model (Equation 4.7) over one period gives:

$$C \underbrace{(P(0) - P(T))}_{=0} = SV - \frac{1}{R} \int_0^T P dt. \tag{5.9}$$

Equilibrium resistance is though given by

$$R = \frac{1}{SV} \int_0^T P dt = \frac{MAP * T}{SV} \tag{5.10}$$

with

MAP ... mean arterial pressure

SV ... stroke volume,

where

$$MAP = \frac{1}{T} \int_0^T P dt \tag{5.11}$$

The given resistance is identical with the definition of TPVR (Equation 1.2). Also, the compliance does not have any impact on the equilibrium, neither is it coupled to the mean pressure.

Applying the same idea to the model of N compliance and N resistance compartments, gives:

$$\frac{\int_0^T P_{i-1} dt - \int_0^T P_i dt}{R_{i-1}} - \frac{\int_0^T P_i dt - \int_0^T P_{i+1} dt}{R_i} = 0 \tag{5.12}$$

for i = 1, ... , N, except for the heart compartments, which cannot be described with constant compliance and resistance.
Writing Equation 5.12 with

$$MP_i = \frac{1}{T} \int_0^T P_i dt \tag{5.13}$$

gives

$$\frac{MP_{i-1} - MP_i}{R_{i-1}} - \frac{MP_i - MP_{i+1}}{R_i} = 0. \tag{5.14}$$

In equilibrium, all blood that the heart pumps into the system, passes through all compartments — meaning that the integral of the flow through each compartment over one period must equal the stroke volume:

$$\int_0^T Q_i = SV \text{ for i = 1,..., N} \tag{5.15}$$

6. Adapting Models to Measured Data

6.1. A Priori Parameter Estimation

6.1.1. The One-Compartment Model

Before simulating the One-Compartment Model, the outflow from the heart, systemic resistance, systemic compliance, and an initial condition had to be estimated. For the outflow from the heart, the high resolution cardiac output measurements were applied. Further, systemic resistance was set to $TPVR$ (calculated by Equation 1.2), where mean arterial pressure was approximated by Equation 2.1.

Since systemic compliance was unknown, it had to be estimated by applying Equation 4.7. With two available pressure measurements per period, we could approximate the time derivative of pressure as slope between the two points. Of the two possible slopes, the one from systolic to diastolic pressure resulted in smaller simulation errors and was therefore chosen for the later experiments. The remaining parameters in Equation 4.7 had to match the approximation of the pressure derivative, i. e. flow was set to the mean flow that occurs from diastolic to systolic pressure, while pressure was approximated by the total mean pressure.

$$\frac{C_{sa}\left(P_{sa}(t_d) - P_{sa}(t_s)\right)}{t_d - t_s} = Q_{mean\_t_s - t_d} - \frac{MAP}{R_{sys}} \tag{6.1}$$

with

t_s ... time of systolic arterial pressure

t_d ... time of diastolic arterial pressure,

where the mean flow from systolic to diastolic pressure is given by:

$$Q_{mean\_t_s - t_d} = \frac{1}{t_d - t_s} \int_{t_s}^{t_d} Q dt. \tag{6.2}$$

The compliance is then given by:

$$C_{sa} = (t_d - t_s) \left(Q_{mean\_t_s - t_d} - \frac{MAP}{R_{sys}} \right) / \left(P_{sa}(t_d) - P_{sa}(t_s) \right). \tag{6.3}$$

Reformulating Equation 6.3 with 1.2 gives:

$$C_{sa} = (t_d - t_s)(Q_{mean\_t_s - t_d} - CO) / \left(P_{sa}(t_d) - P_{sa}(t_s) \right). \tag{6.4}$$

According to [32], the compliance that is described by simulation models (apparent compliance) is not the correct description of true compliance. [32]

suggest to multiply apparent compliance by a factor of at least 1.5, to approximate true compliance. The factor will be accounted for in the simulations. Since the input flow curve starts at the beginning of systole, the initial condition was set to diastolic pressure.

6.1.2. Two-Comparment Model

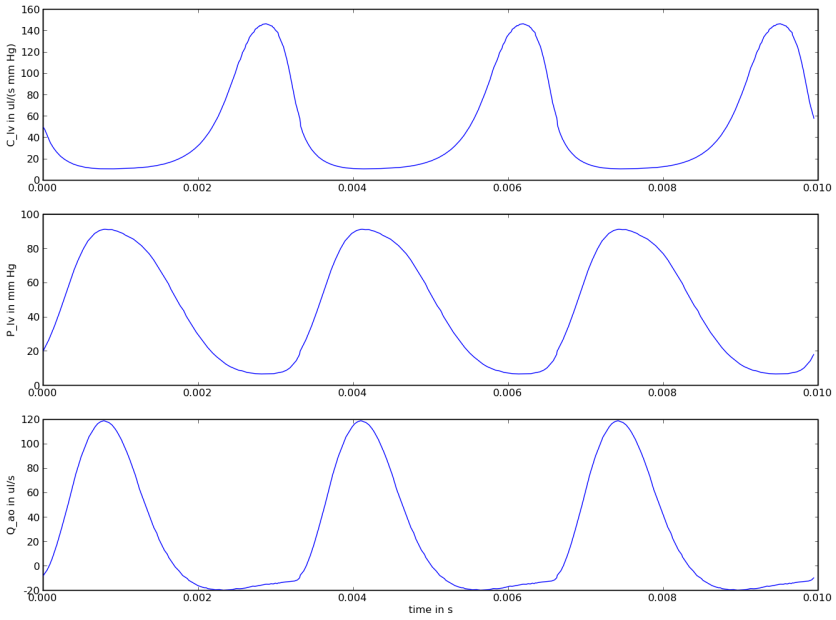

Figure 6.1.: Three periods of left ventricular compliance derived from left ventricular pressure and flow through the mitral valve.

Extending the One-Compartment Model to a loop demanded a good representation of the pumping activity of the heart. Due to the high resolution measurements from the left ventricle and from the cardiac output, the ventricle's compliance could be approximated quite exactly by using Equation 4.14.

$$\frac{C_{lv}(t_i)P_{lv}(t_i) - C_{lv}(t_{i-1})P_{lv}(t_{i-1})}{\Delta t} = Q_{mi}(t_i) - Q_{ao}(t_i) \tag{6.5}$$

With an open mitral valve, the flow through it is given by:

$$Q_{mi}(t_i) = (P_{sv} - P_{lv}(t_i))/R_{ao}. \tag{6.6}$$

To include the valves' functions, negative flow through both of the valves was set to zero

$$Q_{mi} = Q_{mi} * Q_{mi} > 0, \qquad Q_{ao} = Q_{ao} * Q_{ao} > 0. \tag{6.7}$$

Left ventricular compliance was found by solving Equation 6.5 for $C_{lv}(t_i)$. Depending on the initial condition, the calculated curve of left ventricular compliance changed from period to period. To find the solution that is (almost) in immediate equilibrium, different initial conditions were tried out. The values used for approximating left ventricular compliance were taken from the last of 15 calculated periods (Figure 6.1). For being able to adjust left ventricular compliance to dynamic changes, the discrete values were used to define the parameters in Sagawas's function (Equation 3.1, see Section 7.2).

By reusing the estimations for systemic resistance and compliance from the the One-Compartment Model, the only unknowns were the resistance of aortic and mitral valve and the systemic venous pressure. According to [15], the unknown venous pressure may be assumed small compared to arterial pressure. However, like the valve resistances, systemic venous pressure influences the volume that is transported through the subsequent vessel compartment. When trying to simulate the equilibrium state, the volume that passes through each compartment per heart beat should equal the stroke volume. Hence, the mentioned parameters have to be adapted to maintain the transported volume. Additionally, the pressure drop from ventricular to arterial pressure during systole depends on the resistance of the aortic valve (Equation 4.2). By integrating Equation 4.2, the conditions of transported volume per heart beat and pressure drop over the aortic valve could be combined.

$$\begin{aligned} SV &= \frac{1}{R_{ao}} \int_{t_{vo}}^{t_{vc}} (P_{lv} - P_{sa})\, dt \\ &\approx \frac{1}{R_{ao}} \int_{t_{vo}}^{t_{vc}} P_{lv} dt - MAP * (t_{vc} - t_{vo}) \end{aligned} \tag{6.8}$$

with

t_{vo} time where aortic valve opens
t_{vc} time where aortic valve closes

Mean arterial pressure during systole was set to the total mean pressure. Besides of this simplification, the exactness of the equation depends on how accurately the closing and opening of the aortic valve can be detected from the given data.

An easier approach for estimating the resistance of the aortic valve is to apply Equation 4.2 at the time step of systolic pressure.

$$Q_{ao}(ts) = \frac{1}{R_{ao}} \left(P_{lv}(ts) - P_{sa_{sys}} \right) \tag{6.9}$$

On the one hand, the latter case does not necessarily fulfill the flow condition, but on the other, it is based on exactly measured values and simplifies calculation of the aortic resistance compared to Equation 6.8.

The resistance of the mitral valve may be defined analogue to Equation 6.8.

$$SV = \frac{1}{R_{mi}} \int_{t_{vo}}^{t_{vc}} (P_{sv} - P_{lv})\, dt = \frac{1}{R_{mi}} \left(P_{sv} * (t_{vc} - t_{vo}) - \int_{t_{vo}}^{t_{vc}} P_{lv} dt \right) \quad (6.10)$$

with

t_{vo} ... time where mitral valve opens

t_{vc} ... time where mitral valve closes

Since the flow through the mitral valve was not measured, the formula could not be simplified as in the case of the aortic valve.

The pressure drop over the systemic resistance results in the condition

$$SV = \frac{T}{R_{sys}} (MAP - P_{sv})\,. \quad (6.11)$$

For $P_{sv} = 0$, this equation is equal to the definition of $TPVR$. Hence, with a nonzero venous pressure $TPVR$ as systemic resistance, the condition of maintained flow can not be fulfilled. Redefining systemic resistance by Equation 6.11 is a way of dealing with this dilemma. In that case, another condition is required. It may seem reasonable to assume that the resistance in the two valves is equal, so that venous pressure is found from Equation 6.10 and the valves' resistances from Equation 6.8 or 6.9.

Finally, the an initial condition for ventricular and arterial pressure was set to diastolic pressure.

6.1.3. Six-Compartment Model

For the Six-Compartment Model, the parameters of the systemic system could be reused from the Two-Comparment Model. However, the parameters from the pulmonary system and the right ventricle are much harder to find. The only known condition for these compartments is, that the flux per heart beat must equal the stroke volume when the system is in equilibrium. Some research papers (like [7], [37]) on rats state that pulmonary resistance corresponds to about 10% of systemic resistance. The same relation is assumed for mean pressure in pulmonary and systemic arteries. A part from these rough guesses, we do not have any more information about the pulmonary system.

6.2. Inverse Problem with Method of Lagrangian Multipliers

6.2.1. Formulation with Linear Flow-Resistance Relation

In Chapter 3, we presented a selection of modeling ideas for the CVS. The mentioned references include different methods for defining unknown parameters in dynamic systems. However, these techniques were considered little flexible. Since we wanted to develop a solver that can easily be applied to different model equations, we needed a flexible tool. Hence, we have chosen the method of Lagrangian Multipliers with variational formulation. The goal of this method is to minimize an error norm (of some modeled and known values), while the model equation is fulfilled. The method allows unknown model parameters that are fitted to approximate the solution to some desired values. The method is therefore called inverse method. Since the model equation does not match the error norm equally well in every point, the equations for every point are weighted with so-called Lagrange Multipliers.

The variational formulation was chosen due to available symbolic finite elements software [26] that enabled to produce a very flexible parameter identification solver. The formulations below are inspired from [4] and [23].

We want to minimize the function f

$$f(P) = 1/2 \int_0^T (DP - d)^2 \cdot dt, \tag{6.12}$$

while the ODE

$$\begin{aligned} C\dot{P} &= Q - P/R \\ P(0) &= P_0 \end{aligned} \tag{6.13}$$

is fulfilled. Here, $D(t)$ is a function weighting the time-steps in P for comparison with the associated measurements given by the function $d(t)$.

The variational formulation of the ODE as a function g with $A = 1/C$ and $B = 1/R$ is given by

$$g(P, A, B) = \int_0^T \left(\dot{P} - AQ + ABP\right) \Phi_i \cdot dt = 0, \ \forall i \in 1, 2, \cdots, n, \tag{6.14}$$

where Φ_i is a test function for the i-th time interval.

The inverse problem can then be formulated as

$$\begin{aligned} \nabla f &= \lambda^T \nabla g \\ g &= 0, \\ P(0) &= P_0, \end{aligned} \tag{6.15}$$

where the Lagrange Multipliers are collected in the vector λ.

The system can be reduced to one PDE

$$\nabla L\left(P, A, B, \lambda\right) = 0, \tag{6.16}$$

by defining L as

$$L(P, A, B, \lambda) = f - \lambda^T g, \tag{6.17}$$

and ∇ as

$$\nabla = \begin{bmatrix} \partial/\partial p_i \\ \partial L/\partial A \\ \partial/\partial B \\ \partial/\partial \lambda_i \end{bmatrix} \tag{6.18}$$

Since the problem is non-linear it has to be solved iteratively. Here we choose the Newton Raphson method:

$$x^i = (P^i, A, B, \lambda^i) \tag{6.19}$$

$$\mathcal{J}_L(x^i) \cdot (x^i - x^{i-1}) = \nabla L(x^{i-1}). \tag{6.20}$$

P,Q and λ are defined as follows:

$$\begin{aligned} P &= \sum_{i=1}^{n} p_i \Phi_i(t) \\ Q &= \sum_{i=1}^{n} q_i \Phi_i(t) \\ \lambda &= [\lambda_1, ..., \lambda_n]^T. \end{aligned} \tag{6.21}$$

To simplify the formulation we define a new variational parameter W

$$W = \sum_i \lambda_i \Phi_i, \tag{6.22}$$

as the sum over the products of Lagrange Multipliers and test function in the associated time interval.
The gradient of L includes the following components

$$\frac{\partial L}{\partial p_i} = \int_0^T (\bar{D}P - \bar{d})\bar{D}\Phi_i \cdot dt - \int_0^T (\dot{\Phi}_i + AB\Phi_i)W \cdot dt \tag{6.23}$$

$$\frac{\partial L}{\partial A} = W \int_0^T Q \cdot dt - BW \int_0^T P \cdot dt \tag{6.24}$$

$$\frac{\partial L}{\partial B} = -AW \int_0^T P \cdot dt \tag{6.25}$$

$$\frac{\partial L}{\partial \lambda_i} = -\int_0^T (\dot{P} - AQ + ABP)\Phi_i \cdot dt \tag{6.26}$$

with

$$\begin{aligned} \bar{d}[i] &= d(t_i) \\ \bar{D}[i,j] &= D(t_j) \end{aligned} \tag{6.27}$$

giving:

$$\begin{aligned} \nabla L &= \begin{bmatrix} \partial L/\partial p_i \\ \partial L/\partial A \\ \partial L/\partial B \\ \partial L/\partial \lambda_i \end{bmatrix} \\ &= \begin{bmatrix} (\bar{D}\mathbf{Mp} - \bar{d})^T \bar{D} - (\mathbf{K} + B\mathbf{M})\lambda \\ \left((\mathbf{Mq})^T - B(\mathbf{Mp})^T\right)\lambda \\ -A(\mathbf{Mp})^T\lambda \\ -(\mathbf{K} + B\mathbf{M})\mathbf{p} + A\mathbf{Mq}. \end{bmatrix} \end{aligned} \tag{6.28}$$

The Jacobian of the gradient of L is given by

$$\begin{aligned} \mathcal{J}_L &= \left[\nabla\frac{\partial L}{\partial p_i}, \nabla\frac{\partial L}{\partial A}, \nabla\frac{\partial L}{\partial B}, \nabla\frac{\partial L}{\partial \lambda_i}\right] \\ &= \begin{bmatrix} (\bar{D}\mathbf{M})^T\bar{D} & 0 & -\mathbf{M}\lambda & -(\mathbf{K} + AB\mathbf{M}) \\ 0 & 0 & 0 & (\mathbf{M}(\mathbf{q} - B\mathbf{p}))^T \\ -\mathbf{M}\lambda & 0 & 0 & -A\mathbf{Mp} \\ -(\mathbf{K} + AB\mathbf{M}) & \mathbf{M}(\mathbf{q} - B\mathbf{p}) & -A\mathbf{Mp} & 0, \end{bmatrix} \end{aligned} \tag{6.29}$$

with

$$\mathbf{M}_{ij} = \int_0^T \Phi_i \Phi_j dt \tag{6.30}$$

$$\mathbf{K}_{ij} = \int_0^T \dot{\Phi}_i \Phi_j dt \tag{6.31}$$

depending on the chosen element types. The initital condition has to be set manually to the equation.

6.2.2. Uniqueness of Solution

To ensure that the solution for this saddle point problem is unique, boundedness, coercivity and the inf-sup-condition have to be fulfilled. Since analysing a nonlinear problem analytically is difficult, problem was linearized by assuming that the factor $A \cdot B$ is known. In the following we have $AB := B$. The resulting problem found below is formulated similar to [5].

Find $(u, W) \in X \times L_2$ with

$$\begin{aligned} &a(u,v) + b(v,W) = f(v) - a(u_0, v) \quad \forall\ v \in X \\ &b(u,m) = 0 \quad \forall\ m \in L_2, \end{aligned} \tag{6.32}$$

where

$u = [P, A]$ with $u \in X = H^1 \times R$

$v \in H^1$

$m \in L_2$

$$a_1(P, v) = \int_0^T D^T P v \cdot dt$$

$$a_2(A, v) = 0$$

$$b(u, z) = \int_0^T \left(\dot{P} - AQ + BP\right) m \cdot dt.$$

For Q and B we know that:

$0 < B < C$,

$|Q(t)| \leq C < \infty \; \forall \; t \; \in R$.

Further, the constant C is used to replace constant values in the equations.

Boundedness

$$\begin{aligned} a(u, v) &= \int_0^T D^2 P v \cdot dt \\ &\leq \int_0^T D^2 \cdot dt ||P||_{L_2} ||v||_{L_2} \\ &\leq \int_0^T D^2 \cdot dt ||P||_{H^1} ||v||_{L_2} \\ &\leq \int_0^T D^2 \cdot dt \left(||P||_{H^1}^2\right)^{1/2} ||v||_{L_2} \\ &\leq \int_0^T D^2 \cdot dt \left(||P||_{H^1}^2 + ||A||\right)^{1/2} ||v||_{L_2} \\ &\leq \beta_1 ||u||_X ||v||_{L_2} \end{aligned} \tag{6.33}$$

$\int_0^T D^2 \cdot dt \leq \beta_1$ holds since D is only nonzero in few points.

$$\begin{aligned} b(u, m) &= \int_0^T \left(\dot{P} - AQ + BP\right) m \cdot dt \\ &\text{with} \int_0^T AQ \cdot dt > 0 \\ &\leq \left[\int_0^T \dot{P} \cdot dt + \int_0^T BP\right] \cdot dt ||m||_{L_2} \end{aligned} \tag{6.34}$$

with Poincare

$$\begin{aligned} &\leq \left[\int_0^T \dot{P} \cdot dt + \int_0^T CB\dot{P}\right] \cdot dt ||m||_{L_2} \\ &\leq \beta_1 ||\dot{P}||_{L_2} ||m||_{L_2} \\ &\leq \beta_1 ||u||_X ||m||_{L_2} \end{aligned}$$

Coercivity

$$a(u,u) \geq \alpha ||u||^2 = \alpha \left(||P||^2_{H^1} + |A|^2 \right) \tag{6.35}$$

This inequality was assumed to be fulfilled, however it remains to prove that the inequality holds. We know that a physically reasonable solution for P is an oscillating function with an upper and a lower bound. Since the pumping activity of the heart has limits, the lenght of the periods can not become arbitrarily small. Further, the sign of the time derivative P_t changes once within every period. Hence, $||P||^2_{H^1}$ can assumed to be bounded.

Inf-Sup Condition

$$\sup_{P \in H^1, A \in R} \frac{b(u,m)}{\left(||P||_{H^1} + A^2 \right)^{1/2}} \geq \beta ||m|| \quad \forall m \in L_2 \tag{6.36}$$

If the inequality holds for a particular $A \in R$ and a particular $P \in H^1$, it must also hold for the supremum of the two quantities. With $A = \bar{A}$ and P so that $g(\bar{P}, \bar{A}) = m$, the equation simplifies to

$$\frac{(m,m)}{\left(||P||_{H^1} + A^2 \right)^{1/2}} \geq \beta ||m|| \quad \forall m \in L_2. \tag{6.37}$$

It remains to be shown that

$$\left(||\bar{P}||^2_{H^1} + A^2 \right)^{1/2} \leq \beta ||m||_{L_2}. \tag{6.38}$$

However, similarily to coercivity, we assume that $||P||_{H^1}$ is bounded. We have not been able to prove that $||P||_{H^1}$ is bounded but the numerical simulations indicate that this is the case.

6.2.3. Implementation Issues

Preconditioner

Inverse problems can lead to ill-conditioned matrices [38]. By applying an appropriate preconditioner, the condition number can be improved. The applied preconditioner gave good results for a certain range of step lenghts. However, more investigation is necessary to furhter improve the numerical results. The eigenvalue analysis was performed on the linearized variant of the Lagrange formulation (see Analysis above). As can be seen in Table 6.1, in most cases, the condition number of the preconditioned system is clearly smaller than in the unconditioned system. Further, we see, that for deacreasing step length, the condition number of the preconditioned system close to constant, while the condition number of the the unconditioned increases. Figure 6.2 shows how sorted absoluted values of the eigenvalues for preconditioned and unconditioned system behave. For the unconditioned system, the values are spread while the preconditioned values are constant – with a few exceptions.

Furthermore, notice that the components in the preconditioners are standard elliptic preconditioners that can be constructed with e. g. multigrid methods. Hence, applying e. g. Minimal Residual method to this preconditioned system will give an order optimal algorithm.

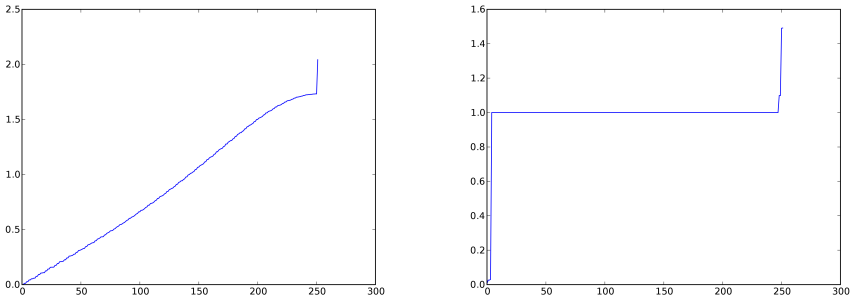

Figure 6.2.: Absolute values of the eigenvalues of the unconditioned and the preconditioned inverse system.

Table 6.1.: Condition numbers for unconditioned and preconditioned Systems with Different Step Length

Δt	unconditioned	conditioned
$32T/\text{len}(Q_{ao})$	$1.2 \cdot 10^3$	$2.7 \cdot 10^3$
$16T/\text{len}(Q_{ao})$	$1.5 \cdot 10^3$	$3.5 \cdot 10^2$
$8T/\text{len}(Q_{ao})$	$2.6 \cdot 10^3$	$2.9 \cdot 10^2$
$4T/\text{len}(Q_{ao})$	$5.0 \cdot 10^3$	$3.1 \cdot 10^2$
$2T/\text{len}(Q_{ao})$	$9.9 \cdot 10^3$	$3.2 \cdot 10^2$
$T/\text{len}(Q_{ao})$	$9.9 \cdot 10^3$	not converged

Implementation Structure

Even though the analysis was only accomplished for the linearized variant, we managed to successfully implement the original equation. So far, only compliance and systemic arterial pressure were set as unknowns, while systemic resistance was approximated by $TPVR$. The system of equations (6.20) was derived analytically by using the programming packages swiginac [31] and SyFi [26]. First all unknown parameters were expressed in their variational form (Equation 6.21 and 6.22), where the variational forms were based on symbols. After formulating the Lagrangian (Equation 6.17), the gradient and its Jacobian were calculated. Finally, the system of equations was solved with the package [13], where the symbols were substitued by their values for the current iteration step.

In contrast to the simulations for the analysis of the eigenvalues, the requirements and the initial condition were not set directly in the system of equations. For the requirements on pressure to equal systolic and diastolic pressure at certain points, the functions D_1 and d_1 were only set nonzero on these points. The

initial condition was added by the additional term

$$\mu \int_0^T (P(0) - P_0)^2 \cdot dt \tag{6.39}$$

with the additional Lagrange Multiplier μ. In this way, the conditions are not absolute and allowed the solution to differ from the desired values. Not knowing how well the model represents the rats' physiology, we did not want the conditions to affect the solution too much.

7. Simulation Results under Static Conditions

The preceding chapters provided all the necessary information to use mathematical models as simulation tool. We will now take a look at how well simulations can reproduce measurements. To make sure that the models develop the desired equilibrium state, the simulations were carried out for 30 heart beats. We defined the error at a certain time in the heart beat as the difference between the measured and the simulated pressure values. The errors of systolic and diastolic pressure were registered in the 30^{th} heart beat and are further denoted as systolic and diastolic error respectively. In the following, the errors and their connection to model parameters are analyzed. In the simulations, it is postulated for simplicity that the experimental data used in parameter estimation is recorded under equilibrium.

7.1. Simulation Results for the One-Compartment Model

7.1.1. One-Compartment Model with Pre-estimated Parameters

Relation of Diastolic and Systolic Errors. Figures 7.1.1, 7.1.1 and 7.1.1 are examples of simulations of different rats; the corresponding parameters can be found in Table 7.1. The first model is in equilibrium from the beginning while the other two need 7-15 beats to remain stable. The fact that models have a falling, rising or constant mean pressure before they reach the equilibrium indicates that the correctness of the applied model depends on the individual cases. There is no common factor for all the models that could improve the simulation results. Even the first model that is stable from the beginning has a large error in the systolic pressure. Comparing the all systolic and diastolic

Table 7.1.: Parameter examples for Different rats

Parameter	Rat#1	Rat#2	Rat#3
SV in μ l	124.33	76.0	48.53
$P_{sa}(t_{sys})$ in mmHg	95.23	93.55	68.58
$P_{sa}(t_{dia})$ in mmHg	68.58	64.14	55.59
R_{sys} in mmHg s/ml	2.4	2.8	2.8
C_{sa} in ml/mmHg	0.0059	0.0014	0.0036
$error(t_{sys})$ in mmHg	-8.8	0.3	-5.9
$error(t_{dia})$ in mmHg	0.0	-9.4	1.1

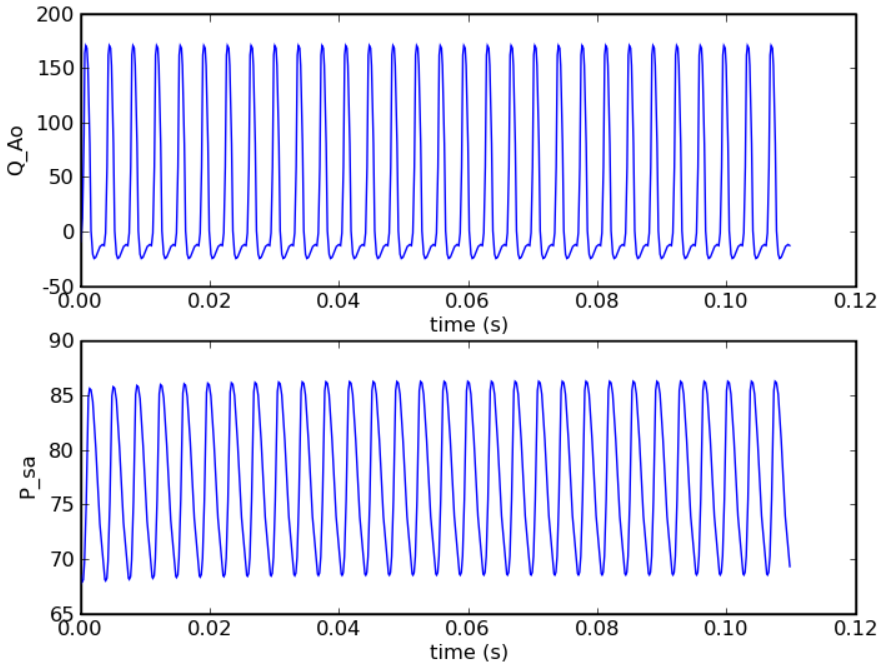

Figure 7.1.: One-Compartment Model: A simulation where the is in equilibrium state instantly ($Rat\#1$).

errors reveals two groups. In almost every case, only one of the errors (systolic and diastolic) is large while the other is close to zero (see Figure 7.4). The first group (Group I) is defined by well estimated systolic pressure and an underestimated diastolic pressure. Group II contains simulations, where the diastolic value is well approximated and the systolic value becomes too high. As can be seen from Figure 7.4, the latter case occurs more often.

In Section 3.1.1 we showed how the modeled pressure differs from the measured values in a dog. The pressure amplitude in the simulated curve was lower than in the measured curve. Group II corresponds to the case described in Figure 3.1, while Group I seems to be en translated variant of Group II. In the plots of errors versus other parameters, the dots seem to pile in two regions that are separated by a gap. These regions correspond to the two groups mentioned above. Since the number of plots is quite large the focus was set on the ones that show clear differences. The rest of the plots are attached in the appendix. All the correlated points in the plots are marked with a '+' for hypertensive and with a '×' for normotensive rats.

Duration of Systole. An interesting indicator for the error is the proportion of the interval from diastole to systole and the duration of the whole period (T_s/T), see Figure 7.5. First of all it is important to notice, that the values of the factor T_s/T can be grouped into points around 0.2 and around 0.75 even

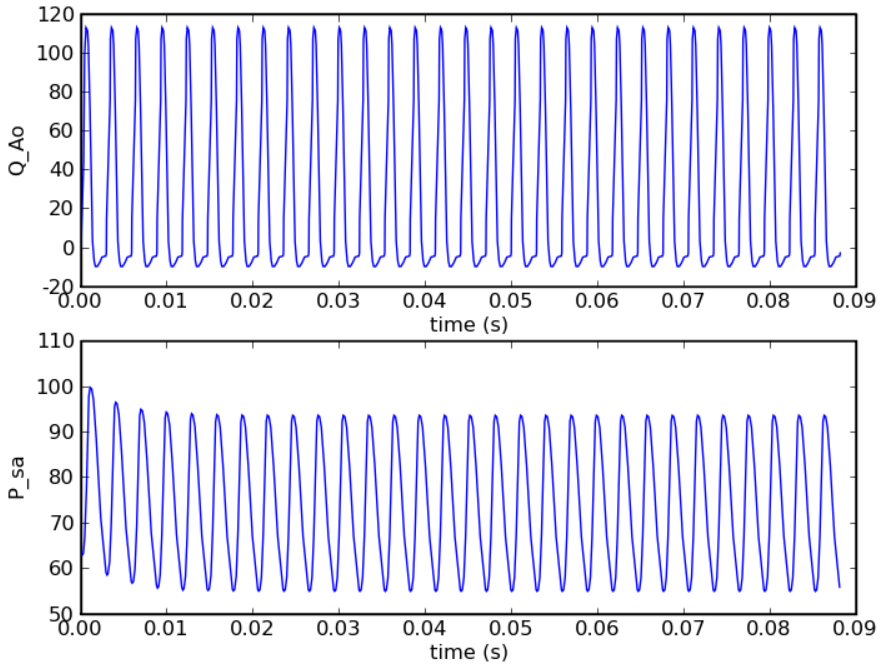

Figure 7.2.: One-Compartment Model: A simulation with falling mean pressure ($Rat\#2$).

though the duration of the period has a great variety for the different rats. Hence, the dependency of T_s/T of the heart rate as stated in [33] could not be observed in the given data.

The concentration of points around two factors corresponds to the groups mentioned earlier. For small factors, systolic errors were high (around -10 mmHg) while diastolic errors were close to zero (Group II). The opposite effect (Group I) was observed for high factors; the error of systolic pressure was close to zero while the diastolic error was high (around -10 mmHg). We see that the factor T_s/T is a strong indicator if the simulation reproduces either of the two pressure values quite accurately while the other has a remarkable deviation.

Compliance. The results show that low compliance leads to good simulations of systolic but bad for diastolic values. Higher compliance values resulted in small errors during diastole and large errors during systole. Despite of knowing that the applied model equation is not suitable for describing both systemic and diastolic pressure accurately, some of the error could be due to rough approximation of compliance. To improve the compliance values, it was checked how multiplying it with different factors would affect the results.

Figure 7.6 shows that the margin of errors gets smaller for higher factors. The mean diastolic error is smallest for the highest factor, but the systolic errors become too big (in their absolute value). Using Equation 1.6 (see Chapter

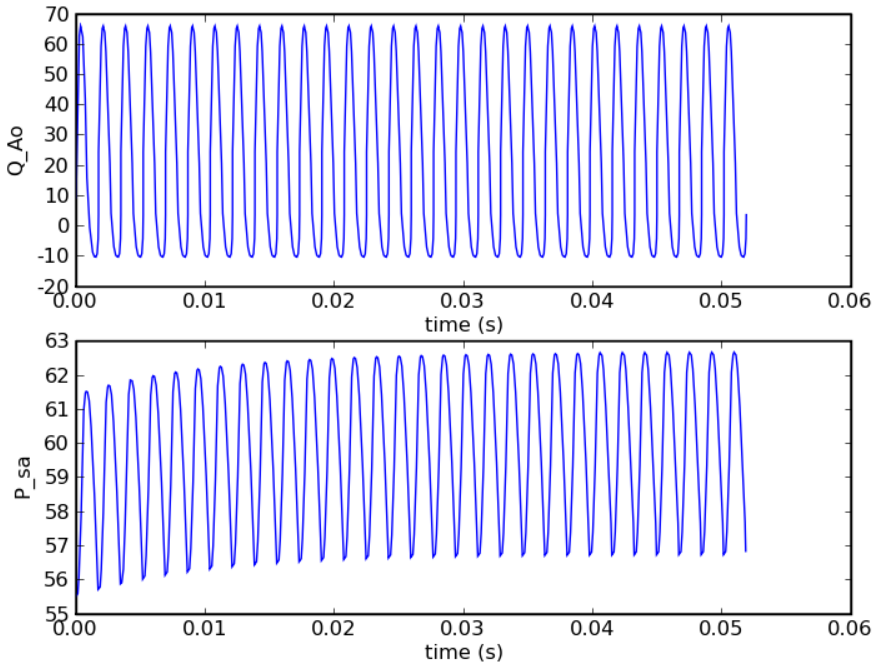

Figure 7.3.: One-Compartment Model: A simulation rising mean pressure ($Rat\#3$).

6) leads to good results for the major group of the experiments. The factor does not only help to verify the estimation of compliance but it also shows its influence on the systolic and diastolic pressure values. As expected, we can observe that higher compliance leads to lower pressure amplitudes. However, the correlation between changing compliance and the errors (and thus the pressure amplitudes) is not linear.

Resistance. Resistance was defined by $TPVR$ with the goal of establishing an equilibrium with the desired mean arterial pressure. Small and big errors were well distributed over high and low resistance and do not seem to influence the result.

By comparing the model parameters with resistance (see Appendix A), one can check how well the model assumptions are reproduced. It can be seen that arterial pressure rises for increasing resistances. For large stroke volume (77–140 μl) the resistance is very low and varies little. For low stroke volume ($\leq$ 58 μl) the resistance shows great variance. Over a certain resistance threshold, the heart has obviously great difficulties to pump the blood, so that the stroke volume does not exceed a certain value. This assumption can be amplified by considering how the amplitude of cardiac output correlates to resistance. We observed high amplitudes for the smallest resistance values and almost equal amplitudes for the rest of the resistance values. Additionally, heart rate and

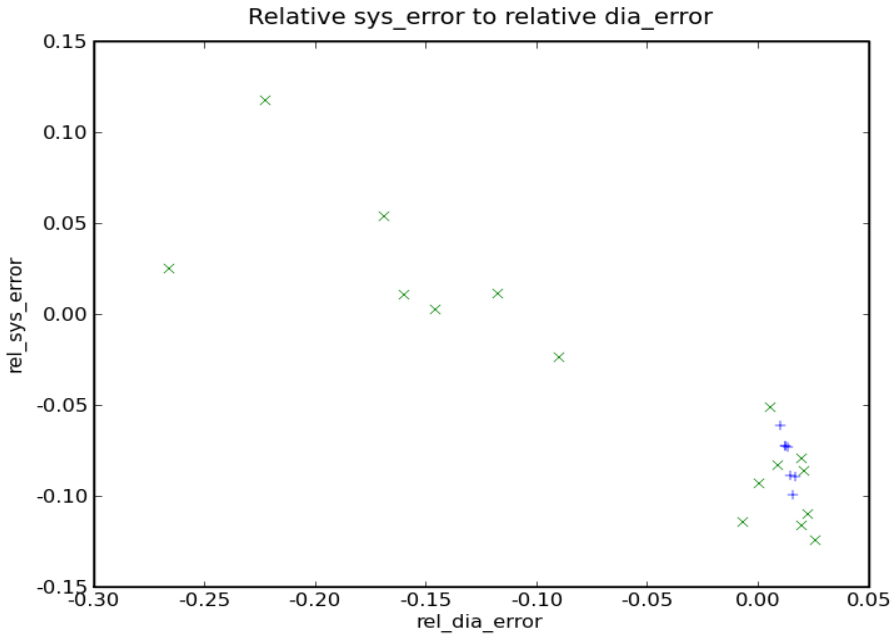

Figure 7.4.: Relation of relative errors in systemic and diastolic arterial pressure.

resistance are directly proportional. The last two findings might be connected by stating that lower (higher) resistance allows the heart to pump with lower (higher) frequency that leads to higher (lower) flow amplitudes. Knowing that the flow amplitude is mainly influenced by compliance, the correlation of compliance and resistance is not surprising.

Limitations. In all models, complex structures are collected in a few compartments. [10] points out that success of lumped elements depends on their application, but that the accuracy for average behaviour and the wave form is good in large vessels. The article also mentions that the linear approximations for compliance and resistance vessels is too simple for individuals with 'radically different physiology'. Finally [10] mentions the neglected inertial effect which occurs during blood acceleration that results in a different wave form. The lack of detail in Berg's measurements of the systemic arterial pressure, make it hard to evaluate the exactness of the model.

Conclusion. It seems that the One-Compartment Model is a good tool to give some additional information about the measured data. We have seen that comparing the simulation results for different parameters revealed two main groups. Marking hypertensive and normotensive cases with different colors in the plot showed that both types occur in both of the groups. For better insight, it is necessary to increase the number of simulated cases a lot in order to get to more concrete solutions.

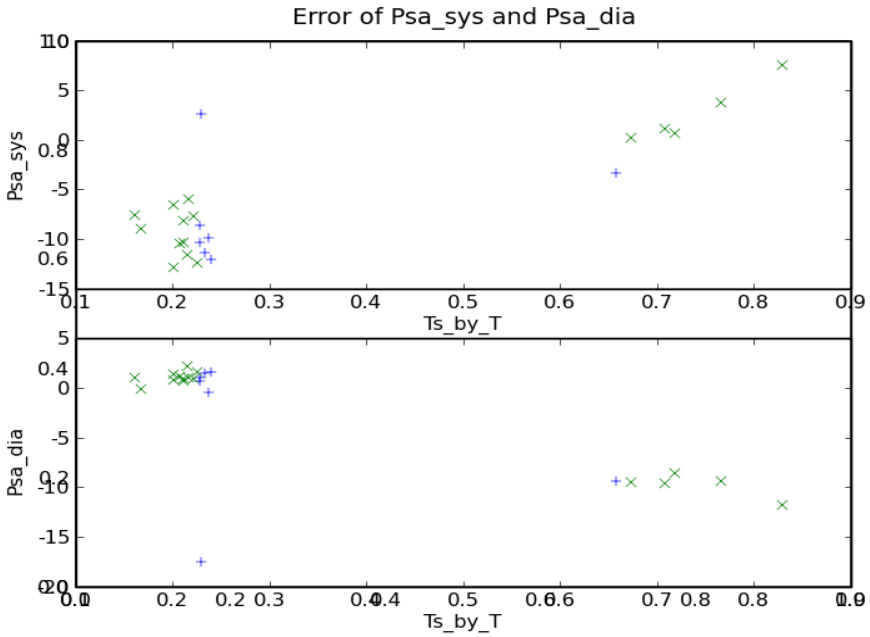

Figure 7.5.: How T_s/T influences the systemic and diastolic errors.

7.1.2. Inverse modeling of the One-Compartment Model

We have seen that forward modeling of the One-Compartment Model leads to non-neglectable errors. A possible reason was assumed to result from the rough estimation of systemic arterial compliance used in the forward model (see Chapter 6). In the following we will see if the result can be improved by applying the inverse algorithm to the same model. The figures for this section contain two subplots each. One subplot shows aortic flow, the other one includes calculated pressure and lines that mark the level of systolic and diastolic pressure.

Figure 7.7 reveals problems of the Inverse Modeling in this Simple Case: The pressure maximum occurred much later than the flow peak and during diastole, the pressure dropped too much. As a result of the late maximum, the amplitude of the pressure oscillation was much higher than expected.

For improving the result, the systolic pressure value was not demanded at the peak of the aortic flow, but where the pressure maximum naturally appears (as found from the first simulation). In Figure 7.8, we see that the pressure maximum now equals the measured systolic value and the end of the period is much closer to the diastolic value.

Due to its generality, the inverse solver could easily be adapted to replace the linear One-Compartment Model by a nonlinear Model. The latter was achieved by using the flow pressure relation given in equation 4.3. The time derivative of flow was calculated numerically from the given flow measurements and the length parameter L was set as unknown. The result can be seen in Figure 7.7.

Table 7.2.: Test Cases for Inverse Modeling

Parameter	Case#1	Case#2	Case#3
$max(P)$ in mmHg	112	85	85
$P_{sa}(T)$ in mmHg	37	51	55
C_{sa} in ml/mmHg	0.0010	0.0010	0.0106
$error(P_{max})$ in mmHg	27	0	0
$error(P_{sa}(T))$ in mmHg	-19	-4	-1
min(eigenvalue)	2.47e-03	9.99e-03	1.46e-06

Conclusion. We have seen that the starting diastolic value and the systolic value as pressure peak could be simulated well (Table 7.2). However, even though we tried to fit the last value to measured diastolic pressure, it lies below in all the models. Since the first and the last values are not equal, the model is not in equilibrium. For this reason, we decided to redo the inverse simulations over a time-interval of two periods. We used the same initial condition as for one period and trying to fit all the other systolic and diastolic points. The results for the linear cases are given in Figure 7.10. Again, we could achieve a better result by adapting the occurrence of the systole to the natural position of maximum pressure. For the non-linear model, the result was nonphysical.

Still, mean pressure is falling in time. As presented in Chapter 5, the level of mean pressure is defined by resistance. A possible reason could therefore be that the approximation of $TPVR$ was not be accurate enough. We tried to set resistance as unknown in the inverse model, but the resulting system of equations was singular. As mentioned above, the linear model underestimates systolic pressure. Since the inverse problem forms the model so that the measured systolic pressure is reached, the subsequent values lead to a wrong diastolic pressure in the end of the period.

7.1.3. Comparing the Linear Forward Model with different Compliance Values

By applying the different compliance values to the existing linear forward model, the results of the inverse and the forward model could be compared more easily. The results of the different forward models can be found in Table 7.3. Case#1 is based on the compliance value that pre-estimated by Equation 6.3. The compliance values for Case#2 and Case#3 were found by linear inverse modeling over one period, with the pressure maximum at the flow peak and at its natural occurrence respectively. The analogous cases over two periods are modeled in Case#4 and Case#5. We see that the sum of the errors is almost equal for every case except for Case#2. The difference of the result lies in the distribution of the total error over systolic and diastolic error. Comparing the forward models (see Appendix) reveals that the models that are in instant equilibrium develop simulate the diastolic pressure better than the systolic. The models that need some periods to reach the equilibrium have a falling mean pressure that results in underestimated diastolic pressure values, while the systolic pressure is

Table 7.3.: Errors for Forward Models with Different Compliance

Parameter	Case#1	Case#2	Case#3	Case#4	Case#5
C_{sa} in ml/mmHg	0.00118	0.00102	0.00216	0.00330	0.00223
$error(P_sa(t_d))$ in mmHg	0.32	16.17	-2.70	-8.38	-3.19
$error(P_{sa}(t_s))$ in mmHg	-9.41	-24.38	-7.13	-1.56	-6.65

estimated better.

7.2. Simulation and Results for the Two-Compartment Model

The conditions for simulations of static Two-Compartment Models were given in Section 6.1.2. For achieving a value as realistic as possible, the calculated discrete values for left ventricular pressure were used (Equation 6.5) to adjust the rest of the parameters. The plots of the results contain subplots of flow, pressure and compliance. The first subplot shows aortic flow (blue) and mitral flow (green), the second subplot shows the measured (red) and the simulated (green) left ventricular pressure curve, the simulated systemic arterial pressure (blue) and the measured systolic (red) and diastolic (light blue) arterial pressure. The calculated (green) left ventricular compliance and its representation used in the simulations (blue) are contained in the last subplot.

Trying to apply Equations 6.8 to 6.11 for estimating the unknown parameters did not succeed because the valves' states could not be defined correct enough. As a consequence, the parameters were set manually and iteratively to fit the conditions for a static system.

When setting the parameters so that the systolic arterial pressure is reproduced (Equation 6.9), the flow curve's maximum was overestimated by about 25%.

The differences between the measured flow curve and the simulated model might be due to the linear relation that was assumed between flow and resistance (Equation 4.2). We have seen earlier, that the nonlinear model in the One-Compartment Example gave markedly better results.

So far, we used a calculated function for left ventricular pressure that is not suitable for use in a dynamic model. The next step was therefore to replace it by Sagawa's compliance function. Almost all parameters were extracted from the known data or the calculated compliance function. We used least square fitting for finding τ_S and τ_D, however the solution was improved by manually finding values that improved the simulation results. With the result (see appendix A.6) being quite different from 7.11, it turned out that some adjustments for Sagawa's formula were necessary. Moving the maxima and minima helped to improve the approximation of the decreasing part of compliance (see A.7). However, we see that the transitions between systole and diastole of ventricular

Table 7.4.: Parameters and resulting Volume flow through Two-Compartment Model

Common Parameters		
Parameters	Values	
P_{sv} in mmHg	22.25	
R_{mi} in mmHg	0.16	
R_{ao} in ml/mmHg	0.016	
SV in ml	0.0855	
Different Results for the Models		
Parameter	calculated C_{lv}	approximated C_{lv}
$\int_0^T Q_{ao}$ in ml	0.0858	0.0889
$\int_0^T Q_{sys}$ in ml	0.0856	0.0889
$\int_0^T Q_{mi}$ in ml	0.0858	0.0767
error(P_{max}) in mmHg	0	1
error(P_{min}) in mmHg	8	6

pressure were not smooth. Further, the pressure maxima occurred too late and had a far too high value. As a consequence, the systemic arterial pressure did not reach the desired level. This fact could be changed by using an additional function for all values smaller than a certain threshold, i. e. values smaller than the threshold were replaced by the smooth function:

$$Clv(t) = min + Clvs\left[\exp\left\{(C_{lvs} - C_{lv\_old(t)})^{40}\right\}\right]^8,$$
$$\forall t : Clv\_old(t) < min$$

with

min ... the new desired minimum

C_{lvs} ... the minimum that would occur without this correction function

C_{lv_old} ... the Clv function before it is changed by this correction function. (7.1)

To ensure continuity in the new left ventricular compliance function the minimum for the rising part of the function had to be changed to

$$Clvs = min + Clvs. \tag{7.2}$$

The final result (Figure 7.12) is almost identical with Figure A.6. The used parameters and the average flow through the compartments in these two models can be found in Table 7.4.

As mentioned earlier, flow through the mitral valve depends on the venous pressure. The mitral valve is only open, when venous pressure is above left ventricular pressure. To ensure enough flow for the equilibrium situation, venous pressure had to be set to a very high value. As a consequence, the resistance

estimation given by Equation 6.11 would lead to far too low pressure values in the aorta. Instead of applying the latter, resistance was set to $TPVR$.

All the simulations for the Two-Compartment Model have been done with data from one rat. Trying to apply the final model to the data of other rats, turned out to be difficult. Besides that the unknown parameters would have to be redefined, the calculated compliance function of the left ventricle differed so much that a good adaptation would require manual adjustments for every rat.

7.3. Simulation of the Six-Compartment Model

All parameters of the pulmonary system and the right ventricle were basically unknown. Trying to manually adapt those parameters did not lead to a model that produced acceptable results. To succeed with a Six-Compartment Model requires measurements in more parts of the body.

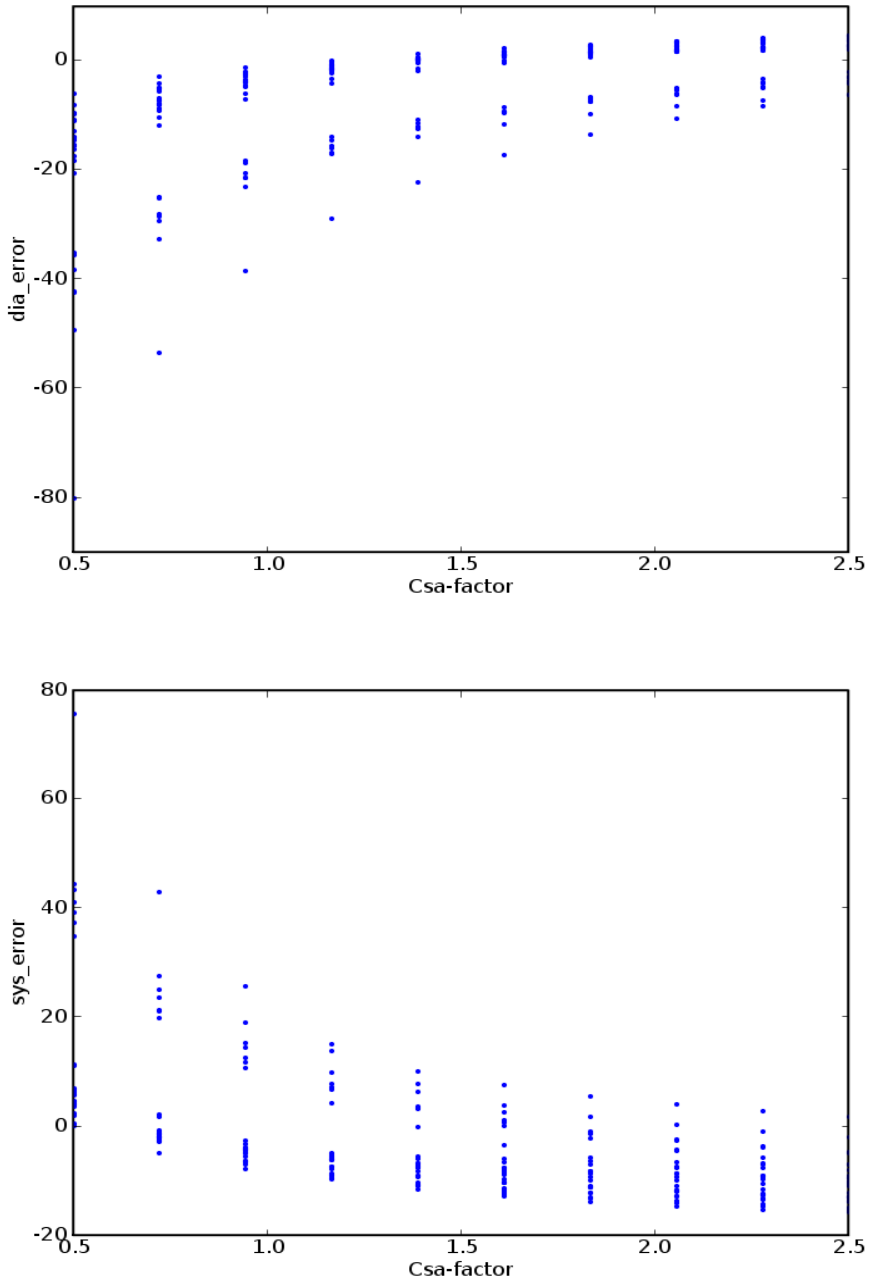

Figure 7.6.: How multiplying compliance with a factor changes the range of diastolic and systolic errors.

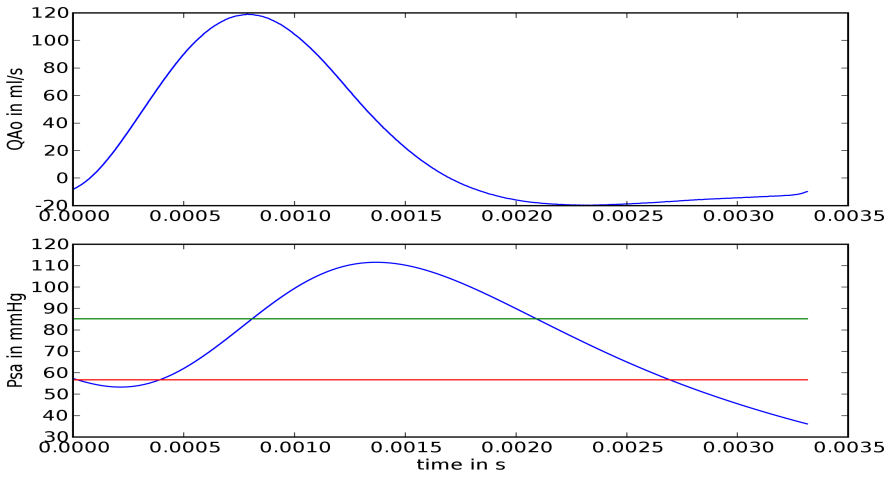

Figure 7.7.: Inverse modeling of the One-Compartment Model.

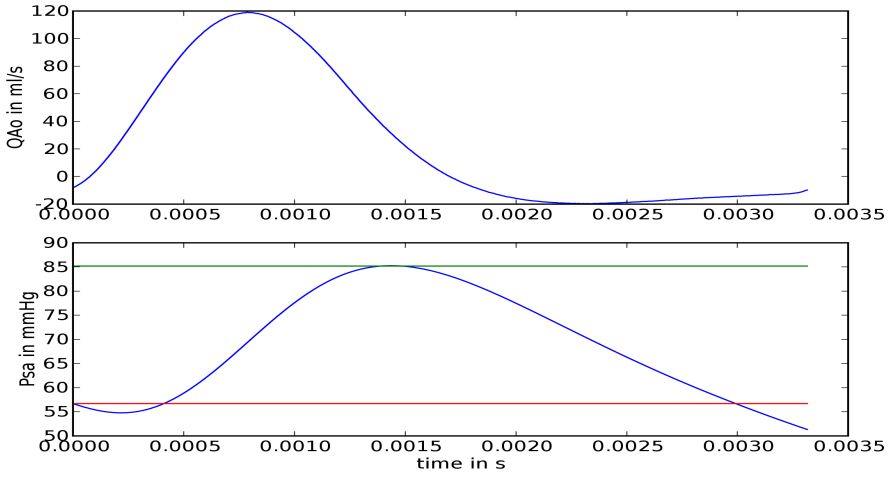

Figure 7.8.: Inverse Modeling of the One-Compartment Model with adapted occurrence of systolic pressure.

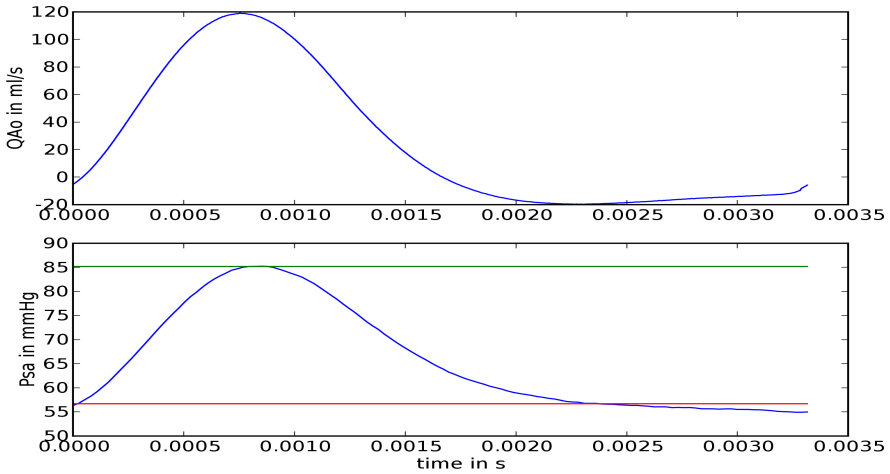

Figure 7.9.: Inverse Modeling of the One-Compartment Model with nonlinear flow - resistance relation.

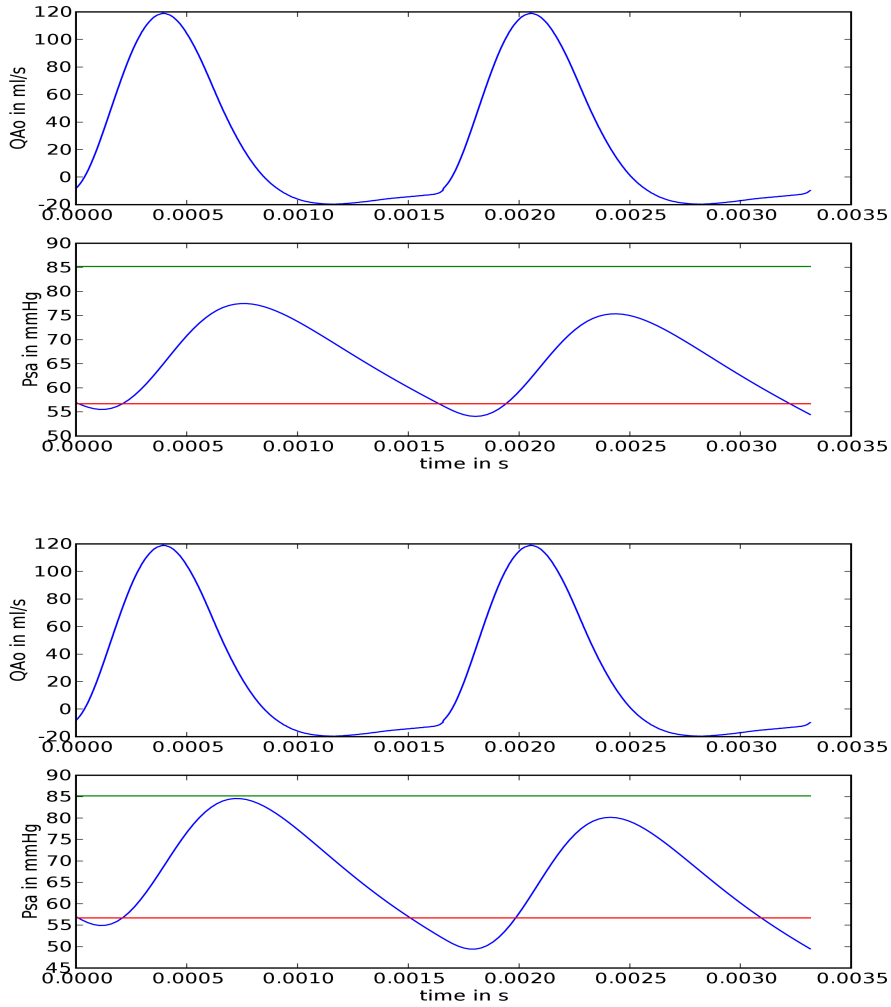

Figure 7.10.: Inverse modeling of the linear One-Compartment Model over two periods; Systole required at flow maximum (a) and at delayed (b).

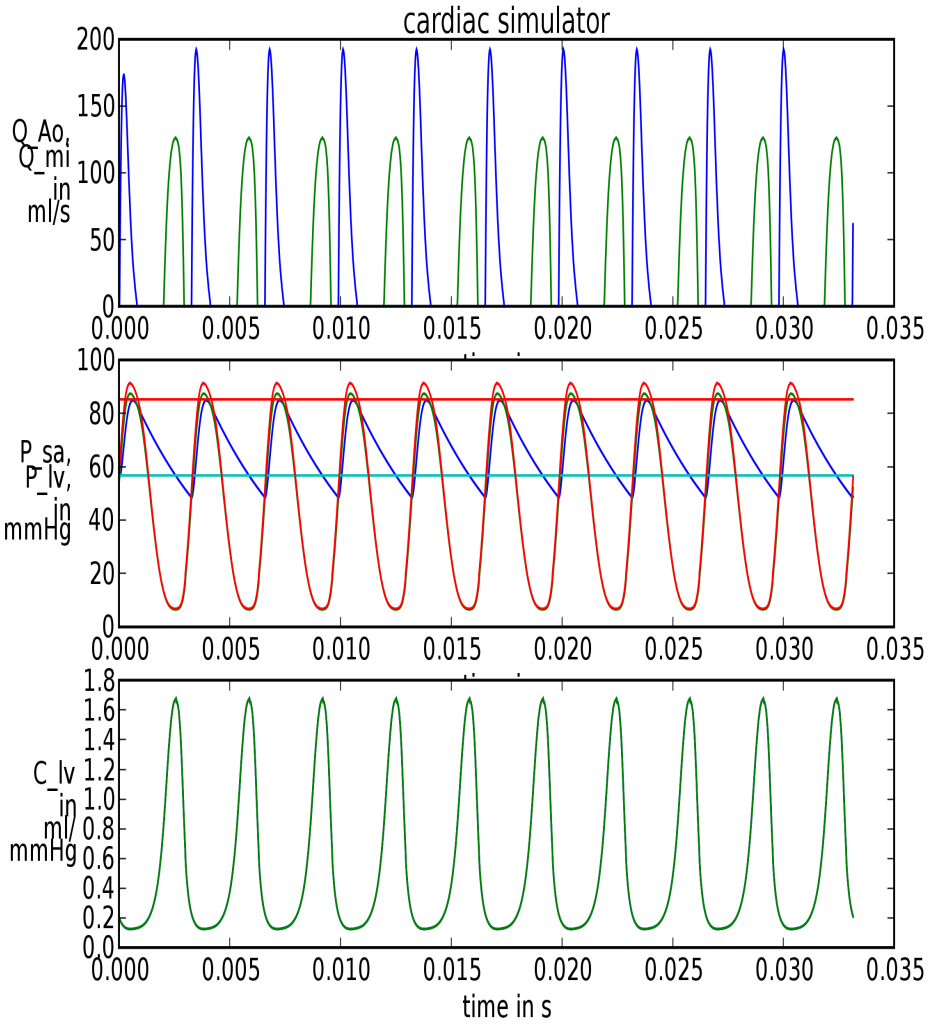

Figure 7.11.: Simulation of the Two-Compartment Model with use of calculated C_{lv}.

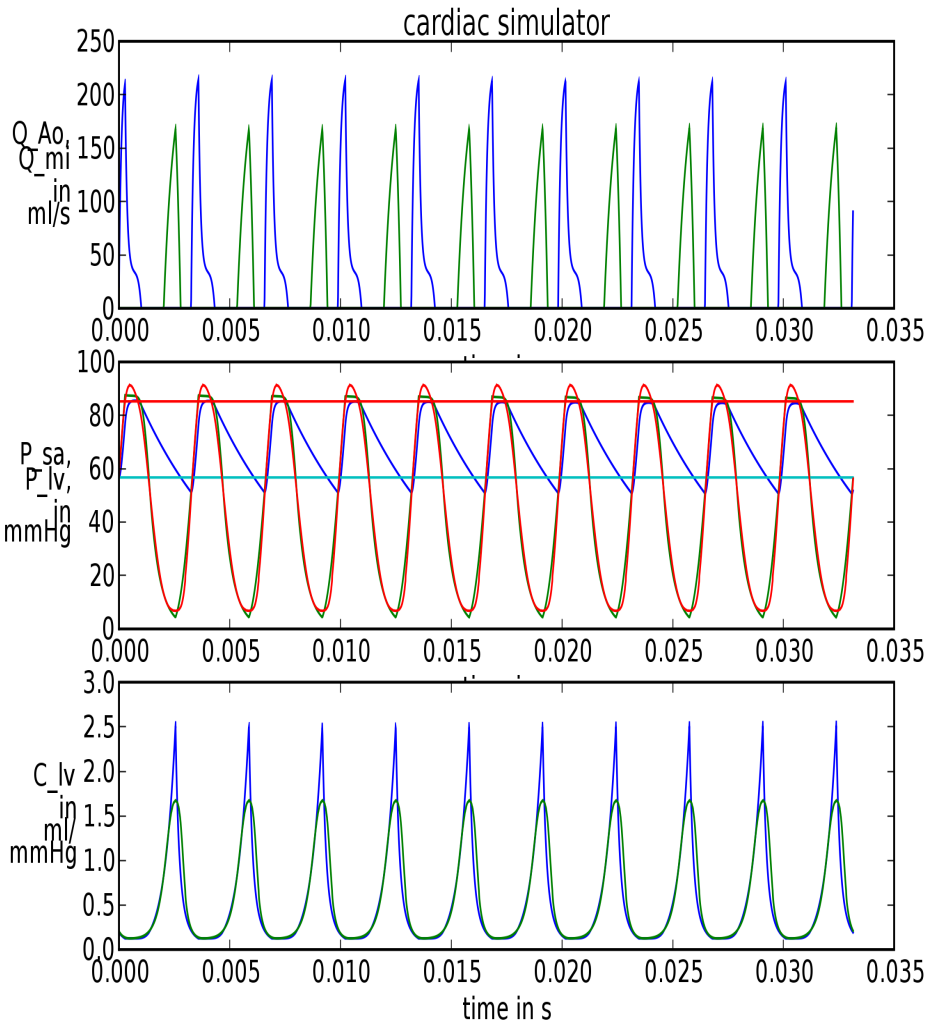

Figure 7.12.: Simulation of the Two-Compartment Model fitted C_{lv}.

Part III.

Extending Basic Models with a Feedback Mechanism responding to Dynamic Changes

8. Experiments and Their Impact on the CVS

8.1. Application of Dynamical Data to the Model

To estimate the model's reaction on dynamical changes, every parameter should be assumed adaptable. However, the present measurements do not contain the necessary information to find out how the parameters change. The only available quantity for approximating systemic resistance is $TPVR$. We have seen before that applying $TPVR$ is not ideal and the problems with applying the approximated $TPVR$ will increase for higher frequencies (Section 2.2). Furthermore, changes in venous pressure and compliance can not be estimated directly from the measurements. Compliance has long been seen as a constant parameter, but [2], [6] and [39] point out that compliance clearly reacts to dynamics in blood pressure. The only measurements that are directly applicable, are those of the heart rate.

8.2. Simulation Results of the Dynamic Model

In a first attempt, the measurements of $TPVR$ and the heart rate were directly applied to the model, trying to reproduce systolic and diastolic pressure over a long run. The Two-Compartment Model was expanded by changing the representation of parameters from concrete values to objects. Every object contains one function that describes the parameter's change in time and one that can return the functions value at a certain time. For every time interval the functions were changed so that they lead linearly from one data point to the next. A collection of all time varying parameters and their approximation for dynamic changes is listed in Table 8.1. The other parameters remain constant.

Figure 8.2 shows the result for a simulation that contains an interval over five minutes. Over most of the time, the resulting arterial pressure is constant while it rises extremely at some local points. Solving these problems would require more investigation. However, if it was possible to get the correct pressure behaviour by applying the measured resistance and heart rate to a static model, the baroreceptor loop could be modeled decoupled from the CVS. In other words, large and small scale modeling could be done separately. This approach is different from e. g. [4], where all the model parameters were fit to approximate the measured dynamic pressure in the arteries. By separating the model into vessel compartments and control mechanism, the parameters can be fitted with physiological details, that might disappear in a lumped model. The compartment model can help to understand the correlations of pressure,

Table 8.1.: The Dynamic Two-Compartment Model

Parameter	Estimation
R_{sys}	$TPVR(t)$
T	$T(t)$
T_s	$T(t)\frac{T(t_0)}{T_s(t_0)}$

heart rate, resistance and compliance, while modeling the baroreceptor loop can give insight into how the different processes in the body act on the chosen parameters.

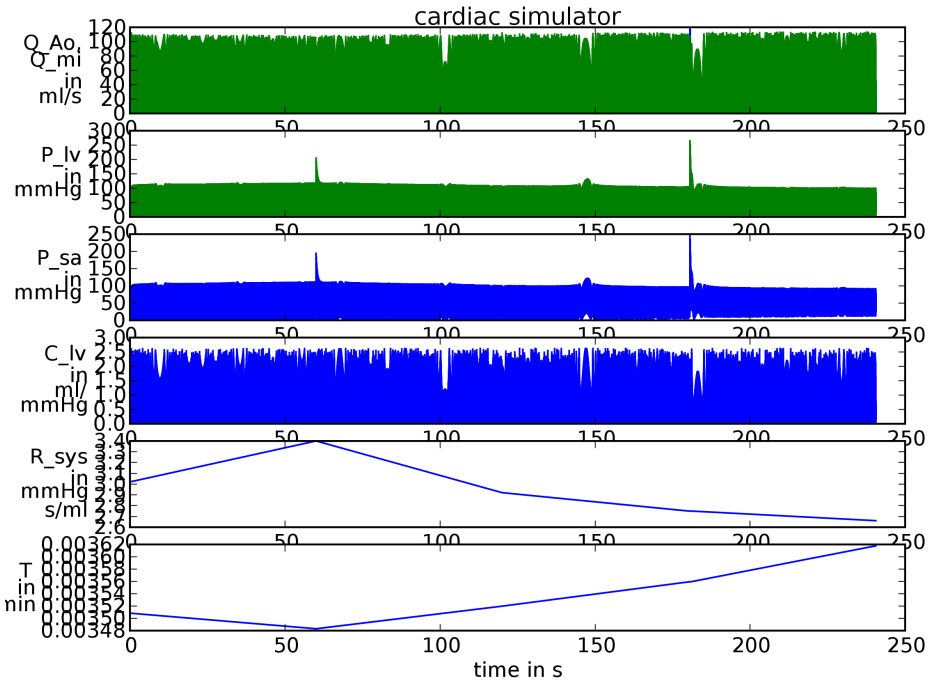

Figure 8.1.: Running the Two-Compartment Model dynamically.

Compared to what was found in *e.g.* [4] the long-term recordings of pressure and heart rate are given in much less detail which makes it difficult to develop physiologically interesting models.

Part IV.

Conclusion

8.3. Summary

8.3.1. Comparing Models

One-Compartment Model. The Simulations in Chapter 7 revealed remarkable differences between the models. The nonlinear flow-resistance relation (Equation 4.3) resulted in more exact pressure values than simulations on a linear flow-resistance relation (Equation 4.2). Also, the time when systolic pressure occurs was simulated more correctly with the nonlinear model.

By forward modeling of the linear models, we could show that the sum of systolic and diastolic simulation errors is approximately equal for compliance values defined by a simple estimation and inverse modeling. However, the inverse simulations were only accomplished for one example and need verification.

A lot of effort has been put into developing a solver for inverse problems. Due to its generality, it can be applied to different kinds of models with different measurements.

Two-Compartment Model. The parameter estimation of the Two-Compartment Model was time–consuming and therefore only performed on one example. Fitting a function to match the shape of the left ventricular compliance function (calculated from measured data of aortic flow and ventricular pressure) was difficult. We could see, that the best fit in a mathematical sense would not necessarily produce the desired simulation results. The characteristics of ventricular compliance had a different level of influence in different regions. Nevertheless, ventricular pressure could be simulated quite exactly.

Another difficulty was to estimate the values of the valves resistances and the venous pressure. However, simulations of systemic arterial pressure were acceptable. The clearest weakness in the model was revealed when comparing the shape of measured and simulated aortic flow. The deviation is probably due to the linear flow-resistance relation.

It remains to simulate a version of the Two-Compartment Model where the flow pressure relation is nonlinear.

Efficiency. Both the forward and the inverse methods were order optimal, i. e. refining the grid increases the computation time by a similar factor.

8.3.2. Can the Models Reveal Additional Information from the Data?

Modeling may introduce parameters that are not measurable. If the chosen model is built upon physiological ideas, new parameters give additional insight into the problem. In all the models, compliance was an important paramter — a parameter that is not part of Berg's research. However, due to the few measurements of systemic arterial pressure per period, compliance could only be estimated roughly. Hence, the role of compliance in hypertension could not be analyzed.

With the developed solver for inverse modeling, we might be able to approximate resistance more exactly than $TPVR$ does.

Earlier research has shown that it is possible to create physiological models of the baroreceptor loop. Among those were models of the parasympathic and sympathic activity of the nervous system that were assumed to be of interest to Prof. Berg.

8.4. Application and Future Prospectives

8.4.1. Possible Application of Computational Experiments

With additional parameters introduced by modeling, it might be easier to understand measurements in more detail. E. g., we expect compliance to be a factor that can help to understand dynamic changes in the CVS. Models of the baroreceptor loop separate certain physiological activities that are not measurable. Thus, such models might give a chance of quantifying changes in these activities. However, replacing real experiments by computational ones is probably not possible today.

8.4.2. Strategies for Improved Models

This thesis is based on data that was produced for other purposes. The aim was to see how these data could be applied to models. When first developing a model, high resolution measurements will be useful in determining its accuracy. Once developed, we only need measurements with a sufficient number of data points to determine its parameters.

We suggest to develop two separate models. First, it is important to understand how compliance and resistance need to be adjusted to simulate pressure correctly over a long period of time. Since heart rate measurements are available, they should be directly applied to the model. When compliance and resistance are known, they can be used to find baroreceptor models, that give more insight into the effects that cause their change. Inverse modeling can be helpful to test different types of models and for finding appropriate parameters. However, forward models are needed to verify the solutions.

In addition to giving good results, it is important that the applied models are based on quantities that have a physiological meaning. The purpose of the models must be to add more insight for medical researchers by allocating non-measurable physiological quantities [9].

Appendices

A. SOLUTIONS

A.1. The One-Compartment Model

A.1.1. A Error - Plots

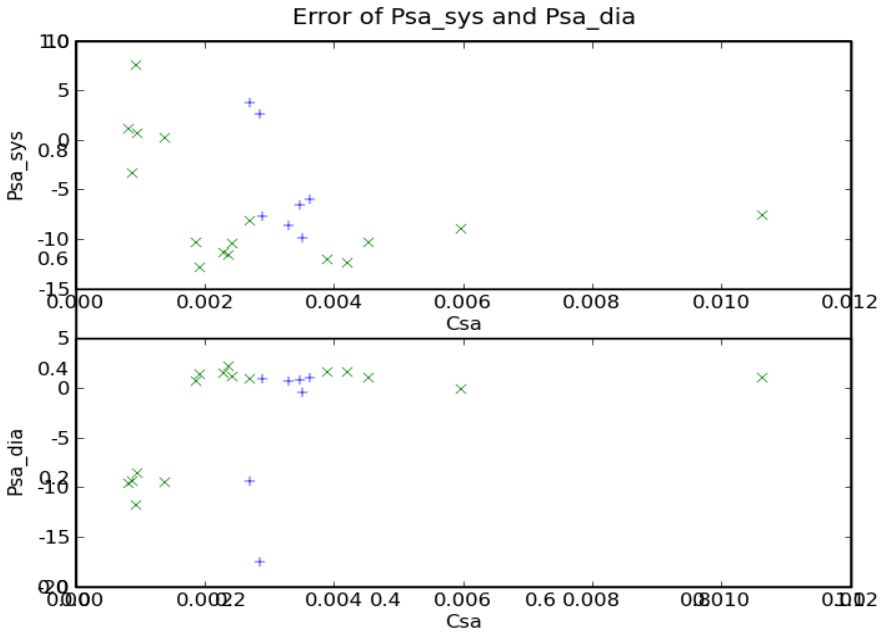

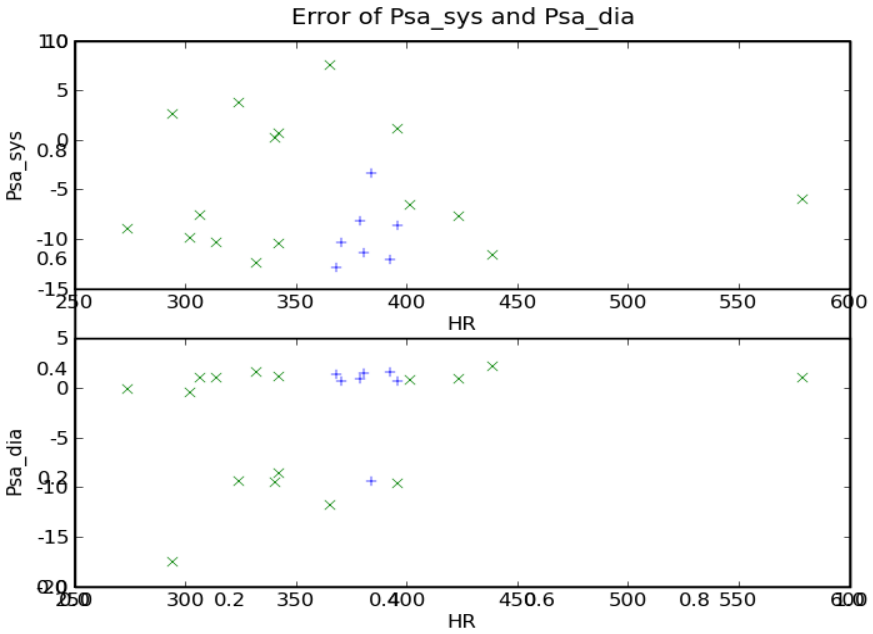
Error of Psa_sys and Psa_dia
Psa_sys
HR
Psa_dia
HR

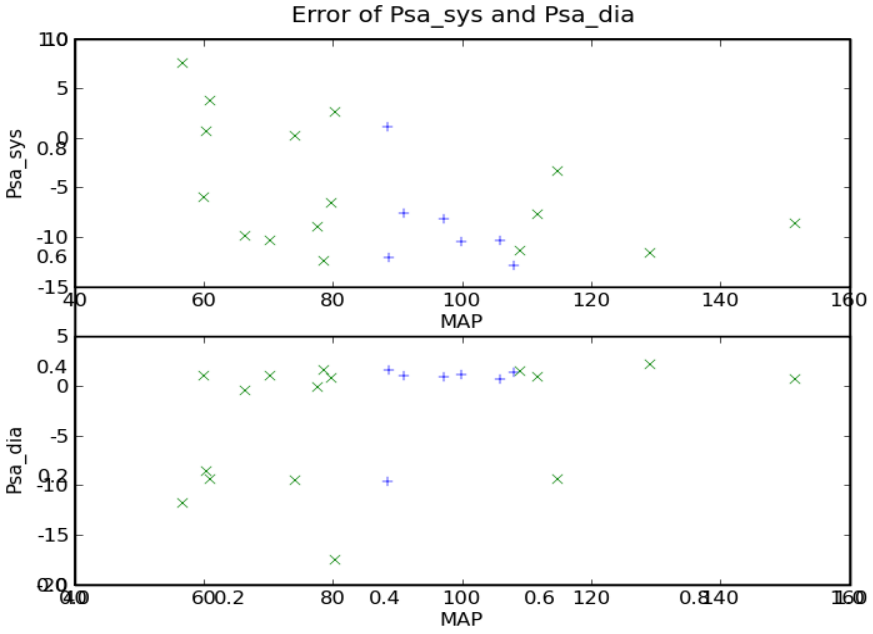
Error of Psa_sys and Psa_dia
Psa_sys
MAP
Psa_dia
MAP

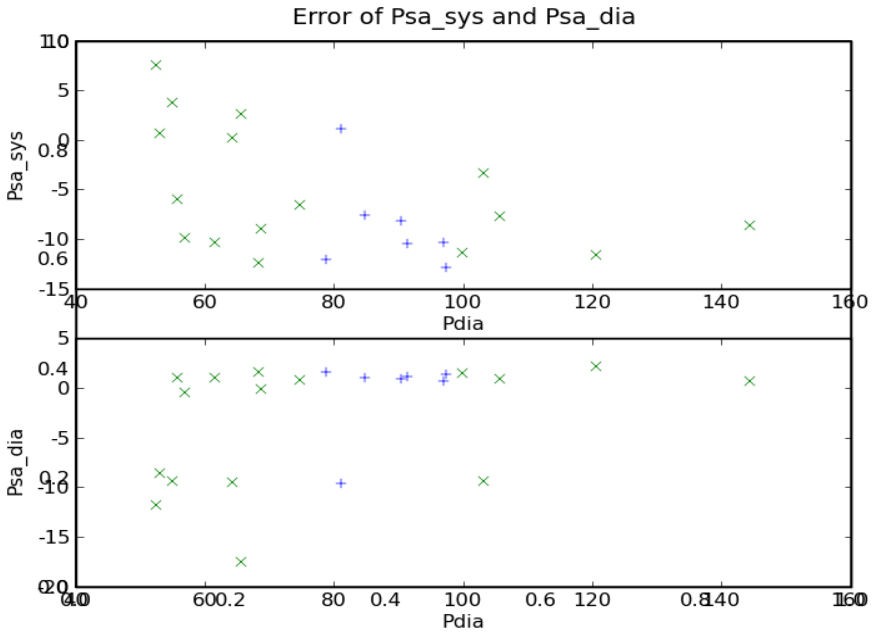
Error of Psa_sys and Psa_dia
Psa_sys
Pdia
Psa_dia
Pdia

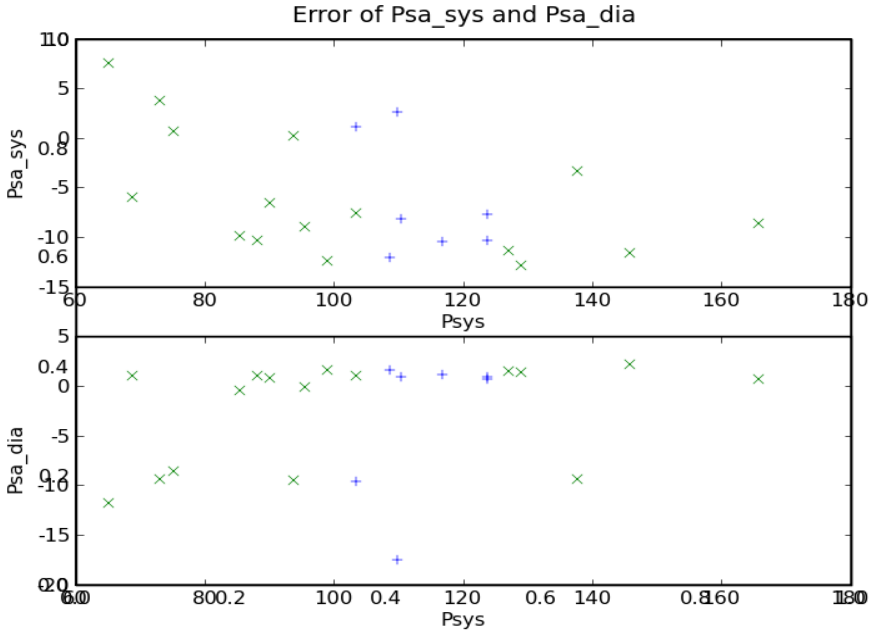
Error of Psa_sys and Psa_dia
Psa_sys
Psys
Psa_dia
Psys

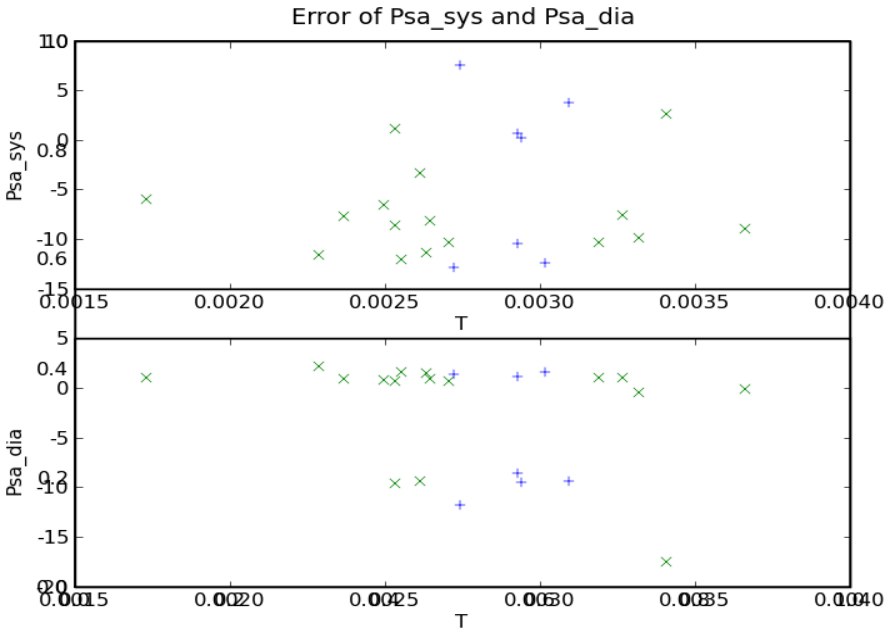
Error of Psa_sys and Psa_dia
Psa_sys
T
Psa_dia
T

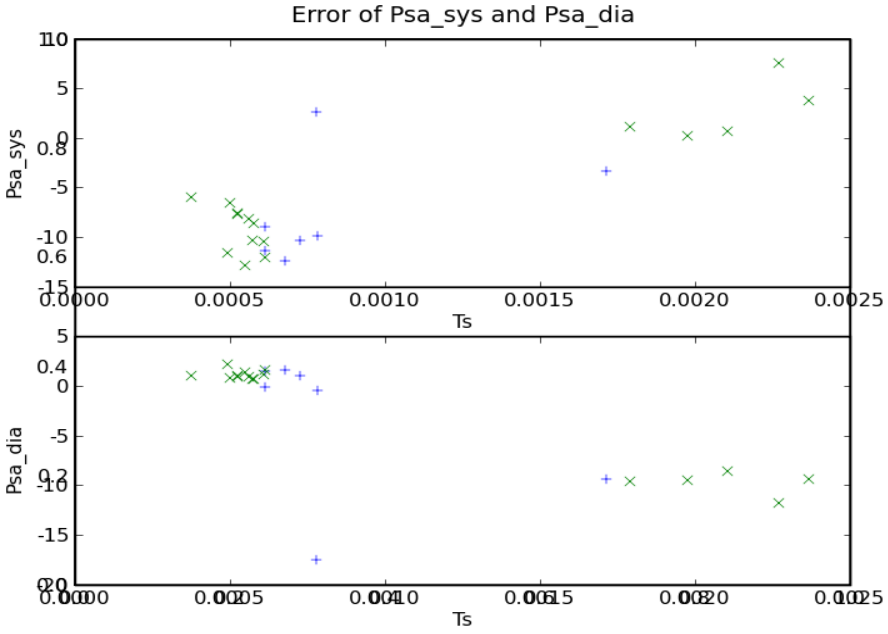
Error of Psa_sys and Psa_dia
Psa_sys
Ts
Psa_dia
Ts

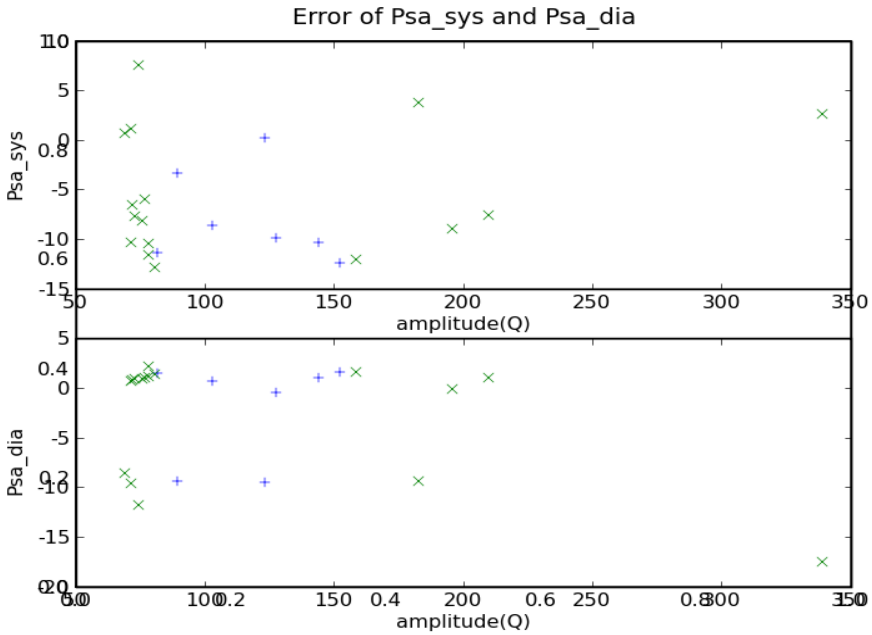
Error of Psa_sys and Psa_dia
Psa_sys
amplitude(Q)
Psa_dia
amplitude(Q)

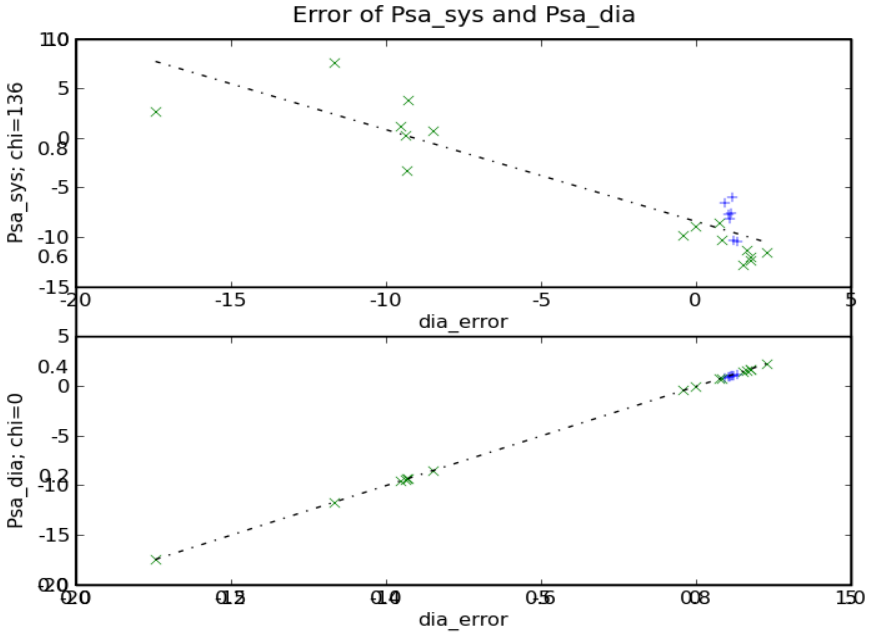
Error of Psa_sys and Psa_dia
Psa_sys; chi=136
dia_error
Psa_dia; chi=0
dia_error

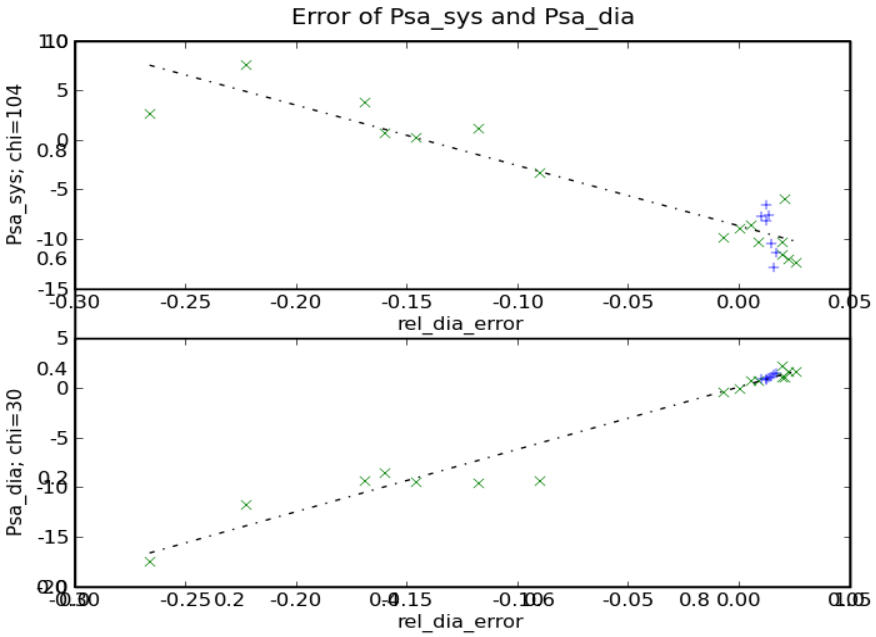
Error of Psa_sys and Psa_dia
Psa_sys; chi=104
rel_dia_error
Psa_dia; chi=30
rel_dia_error

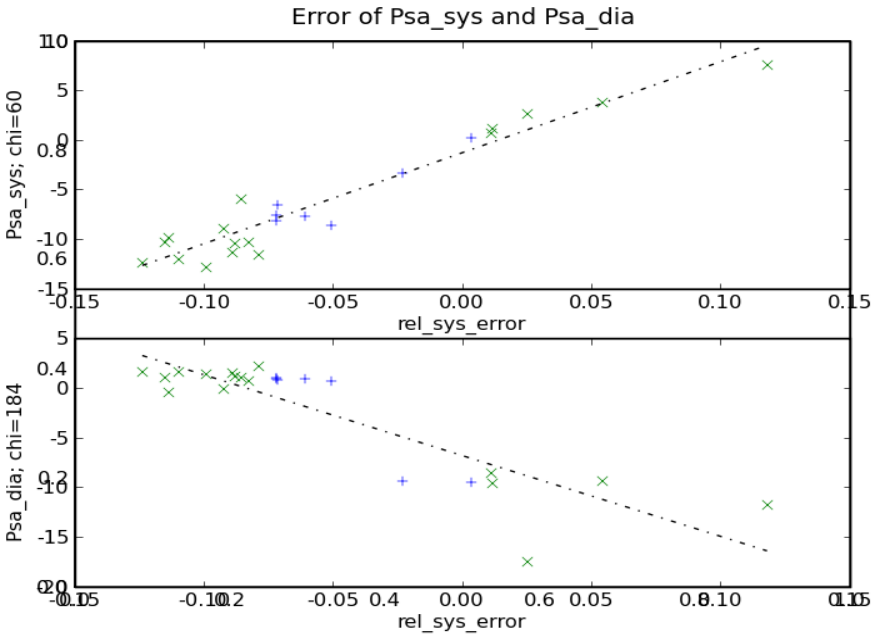
Error of Psa_sys and Psa_dia
Psa_sys; chi=60
rel_sys_error
Psa_dia; chi=184
rel_sys_error

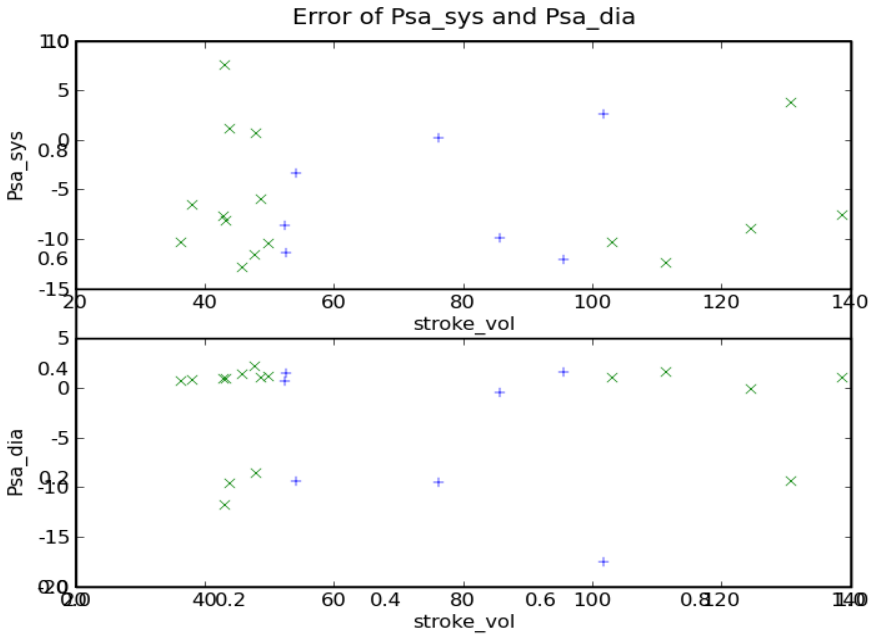
Error of Psa_sys and Psa_dia
Psa_sys
stroke_vol
Psa_dia
stroke_vol

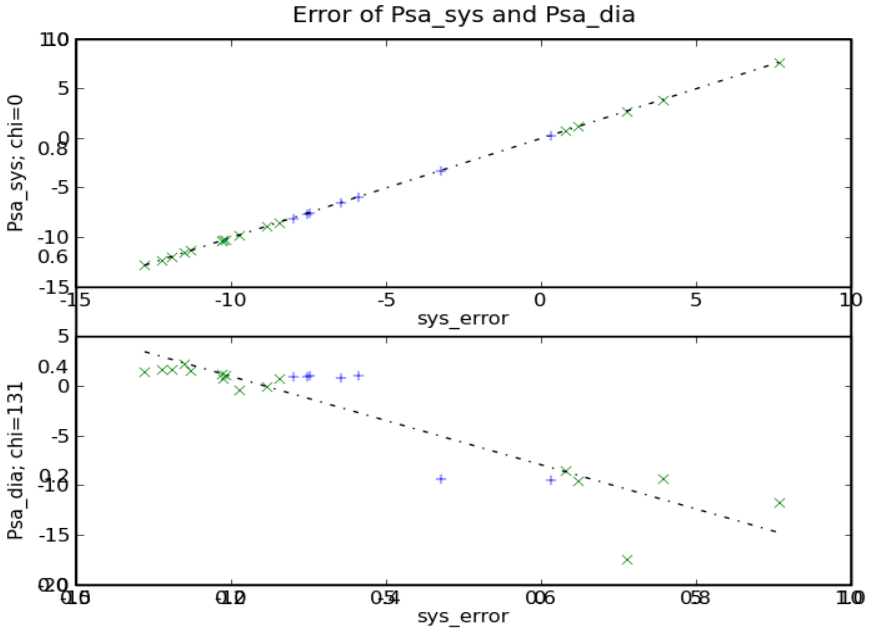
Error of Psa_sys and Psa_dia
Psa_sys; chi=0
sys_error
Psa_dia; chi=131
sys_error

A.1.2. Compliance Correlated to Other Parameters

Compliance Correlated to Heart Rate, Stroke Volume, Ampliute of Flow and Systemic Resistance

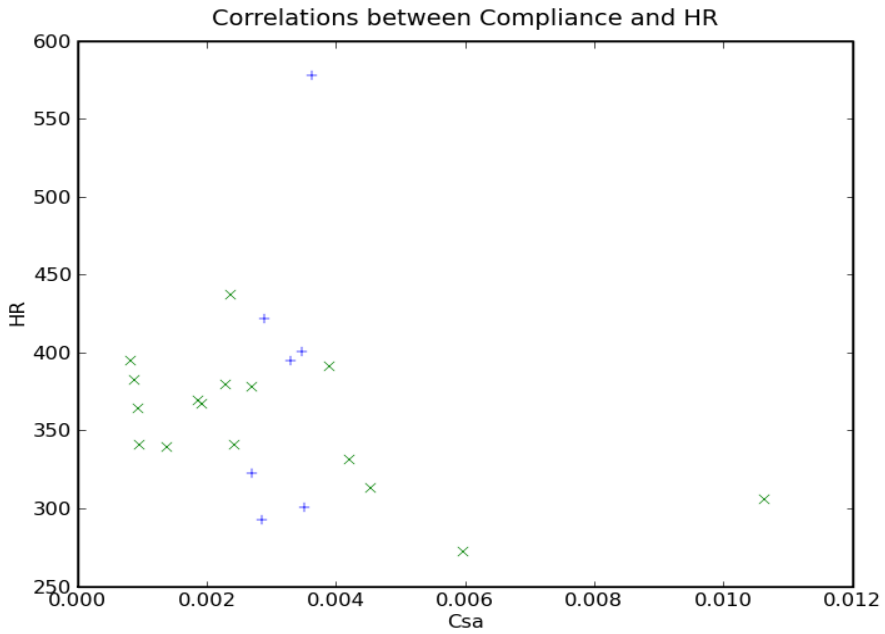

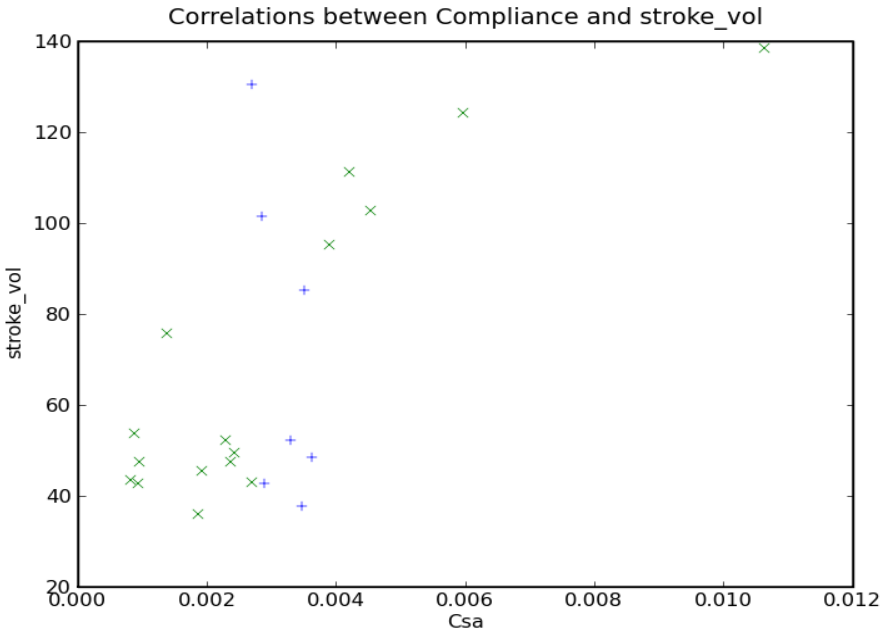

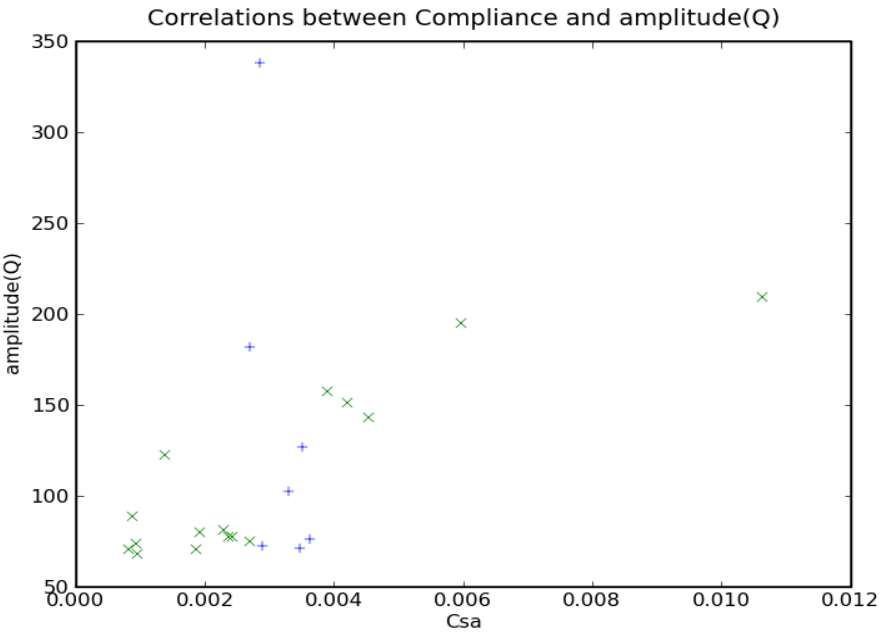

Compliance Correlated to Pressure Values: Mean Pressure, Diastolic Pressure and Systolic Pressure

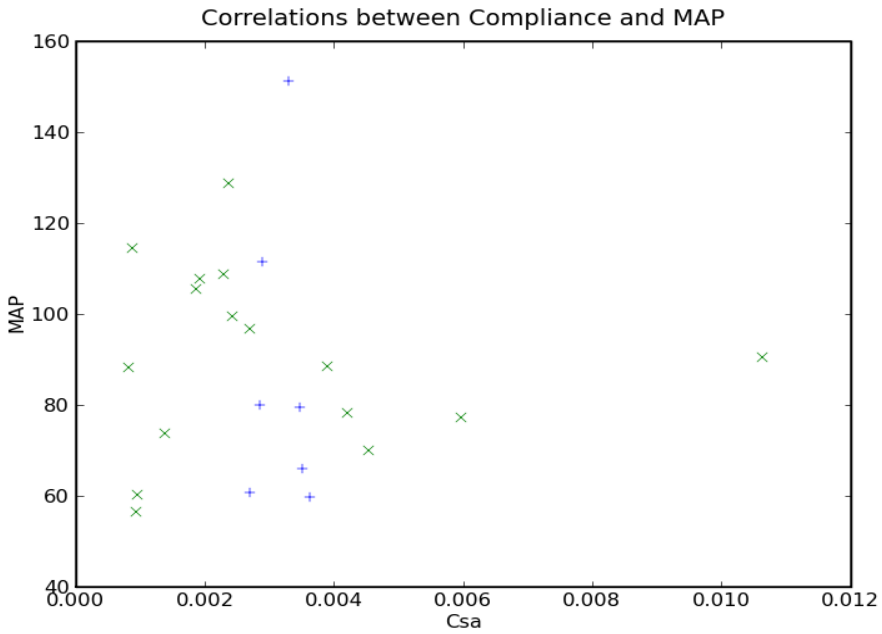

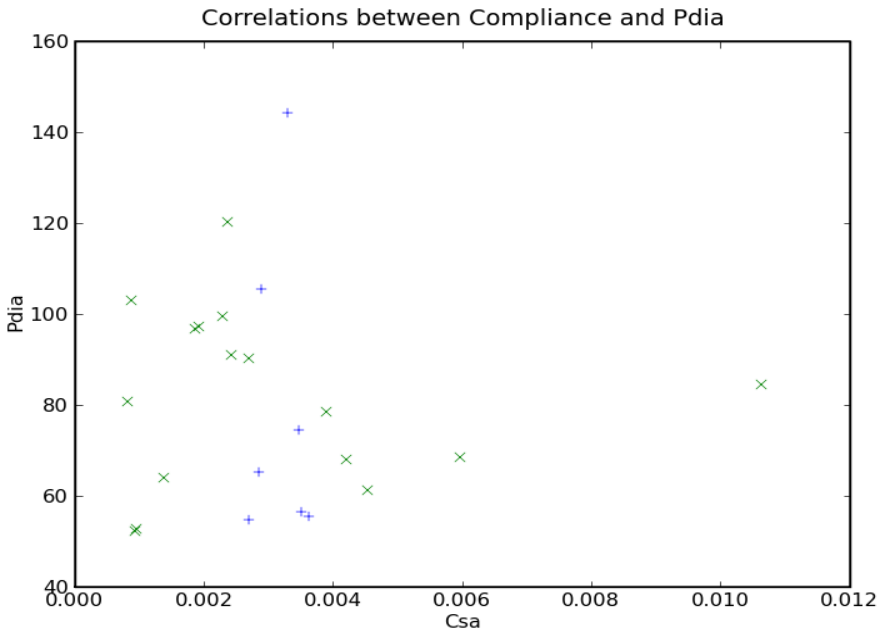
Correlations between Compliance and Pdia
160
140
120
100
80
60
40
Pdia
0.000
0.002
0.004
0.006
0.008
0.010
0.012
Csa

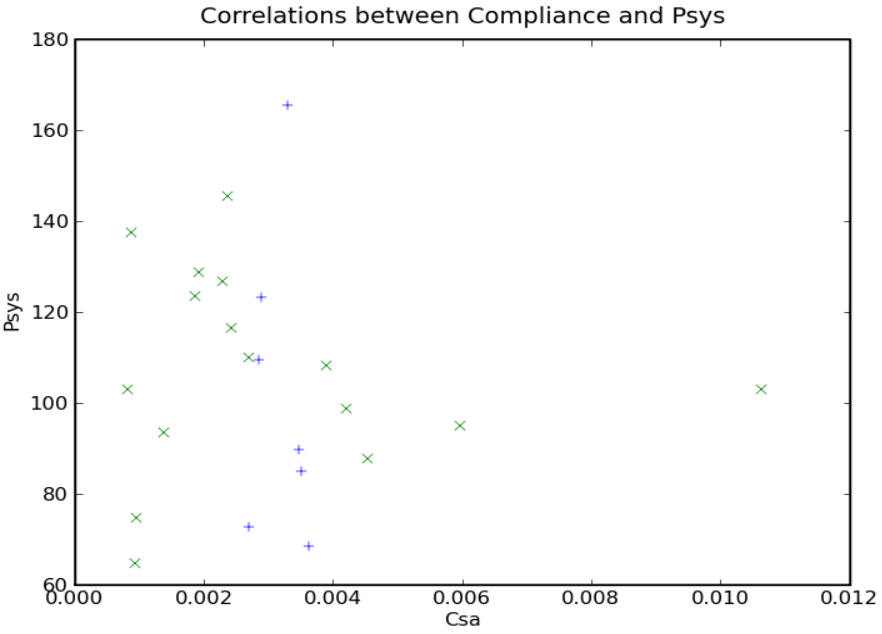
Correlations between Compliance and Psys
180
160
140
120
100
80
60
Psys
0.000
0.002
0.004
0.006
0.008
0.010
0.012
Csa

Compliance Correlated to Duration of Periods and Systoles

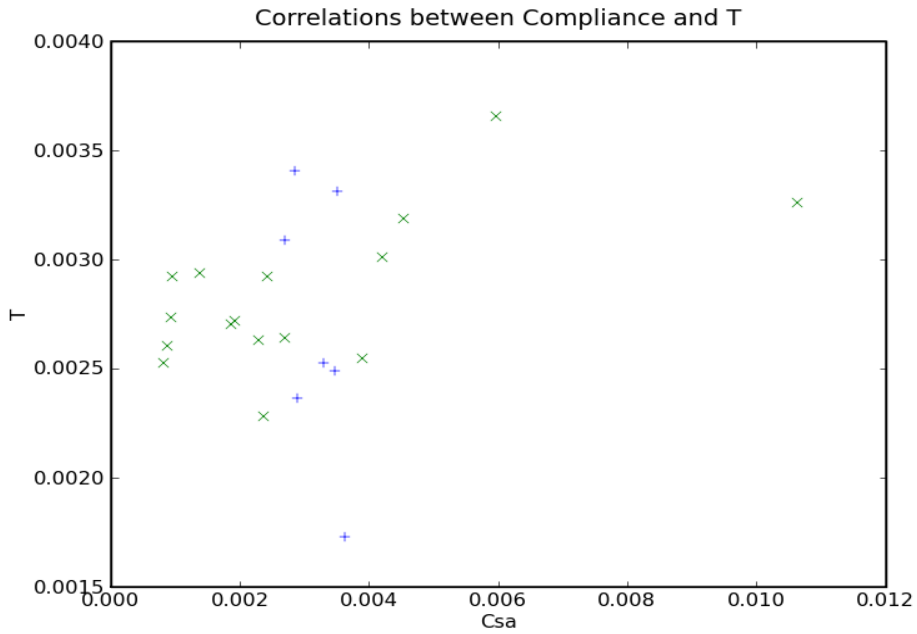

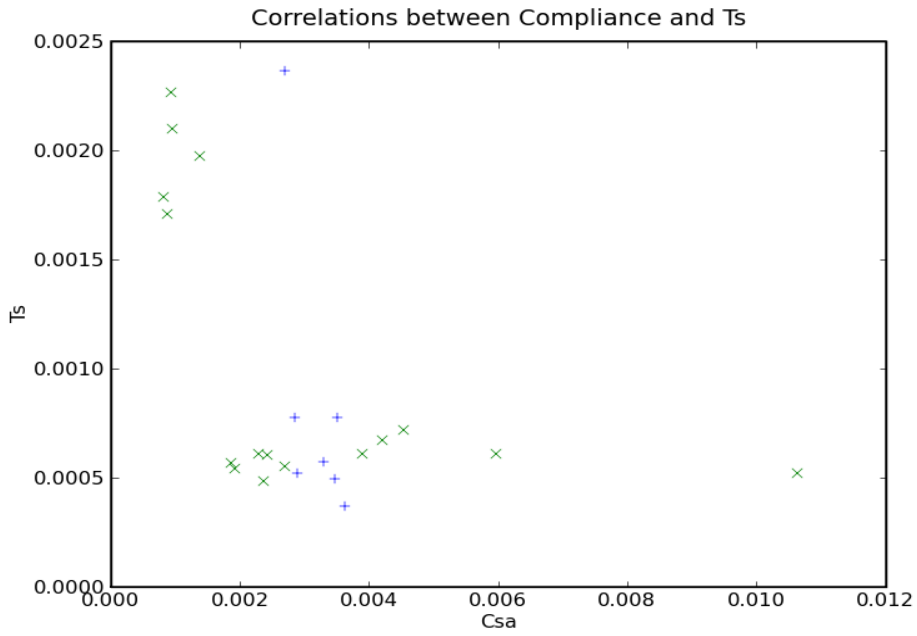

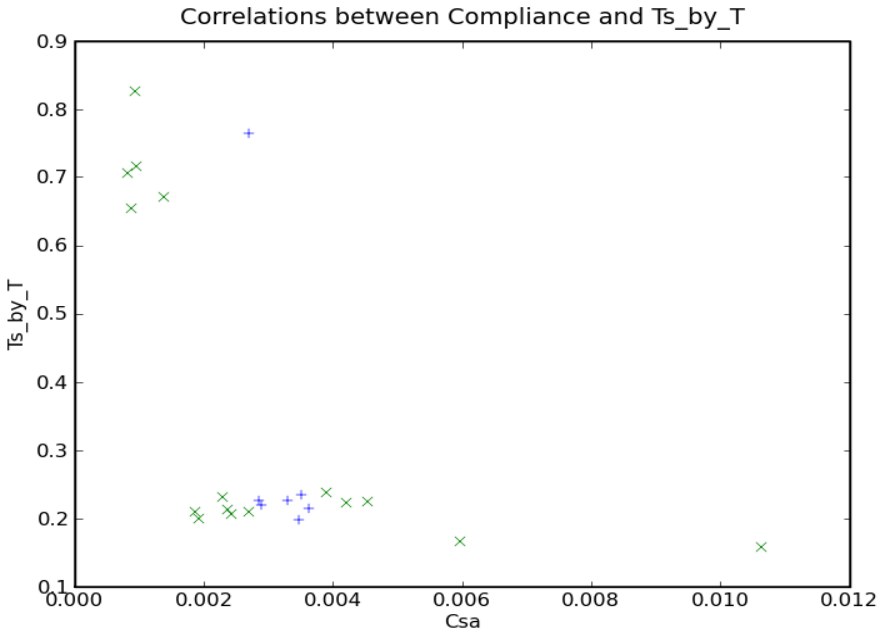

Compliance Correlated to Modeling Errors (Diastolic and Systolic) and Relative Errors (Diastolic and Systolic)

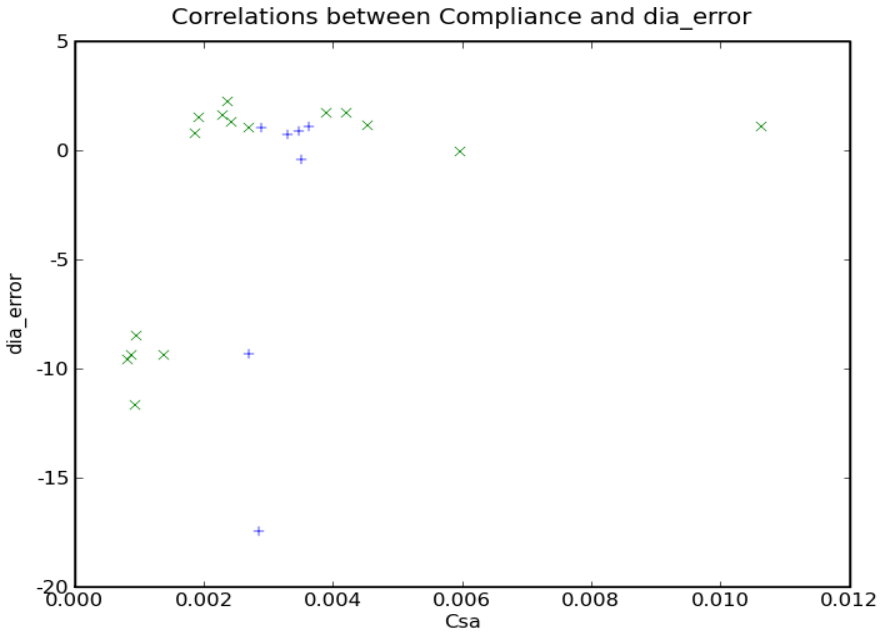

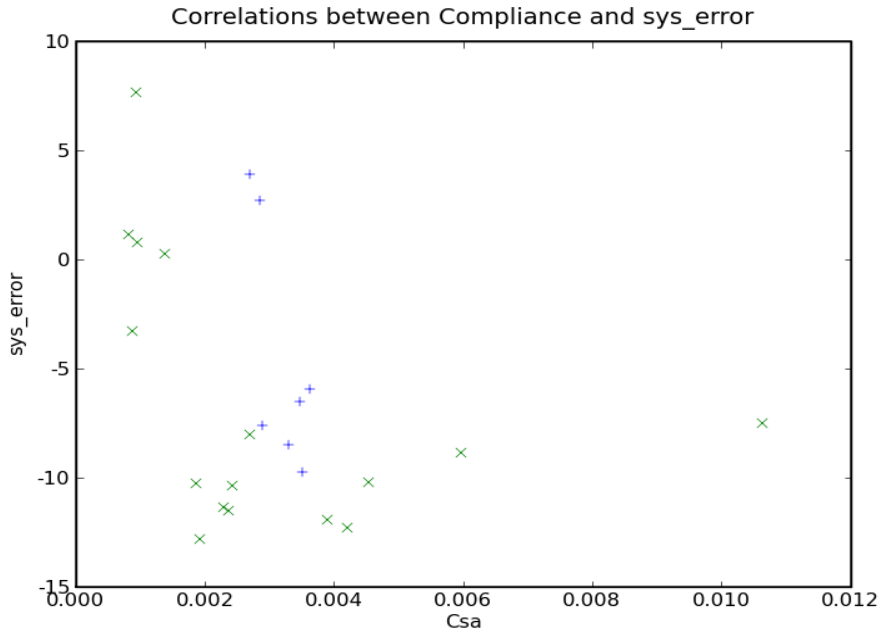
Correlations between Compliance and sys_error
sys_error
Csa
10
5
0
-5
-10
-15
0.000
0.002
0.004
0.006
0.008
0.010
0.012

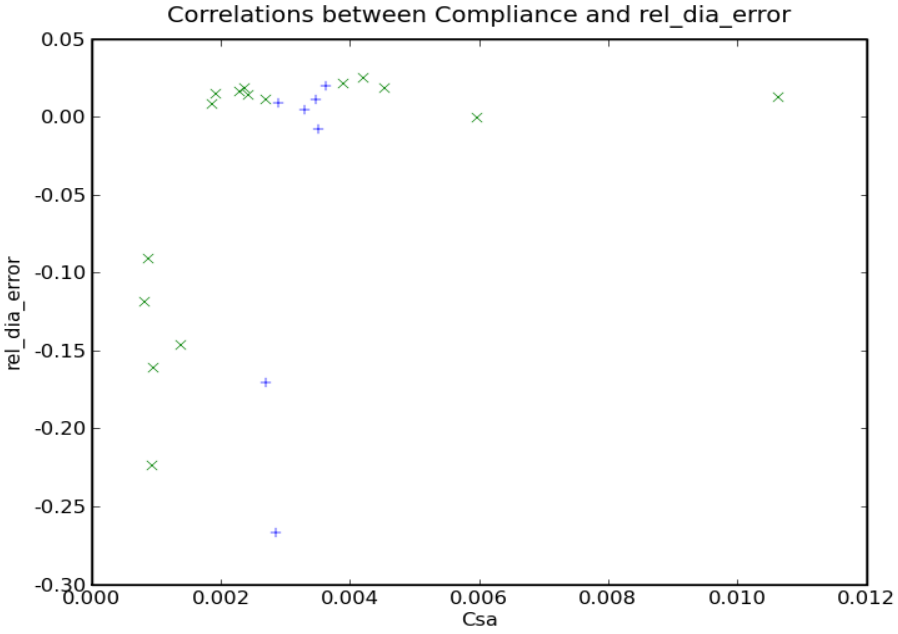
Correlations between Compliance and rel_dia_error
rel_dia_error
Csa
0.05
0.00
-0.05
-0.10
-0.15
-0.20
-0.25
-0.30
0.000
0.002
0.004
0.006
0.008
0.010
0.012

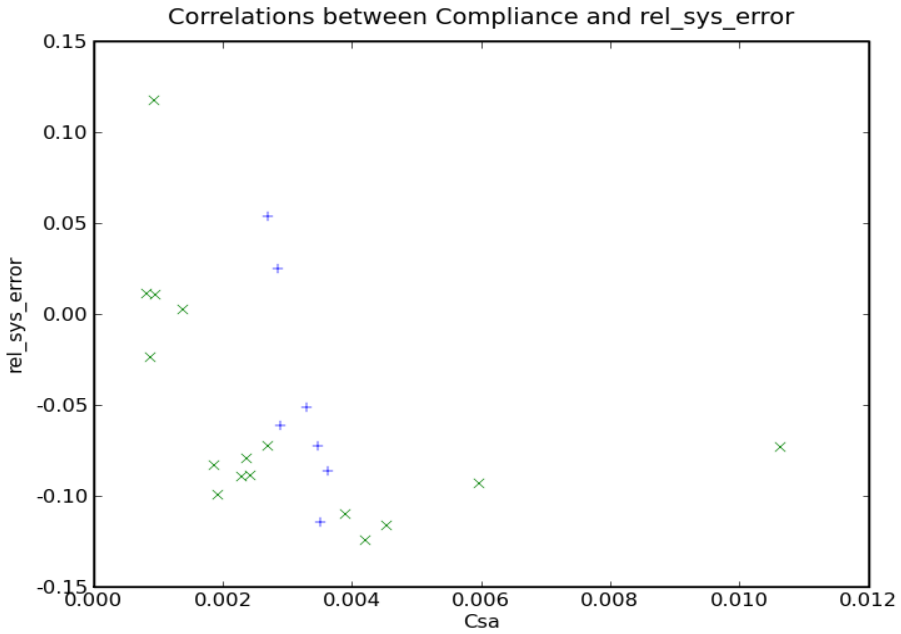
Correlations between Compliance and rel_sys_error
0.15
0.10
0.05
0.00
-0.05
-0.10
-0.15
rel_sys_error
0.000
0.002
0.004
0.006
0.008
0.010
0.012
Csa

A.1.3. Resistance Correlated to Other Parameters

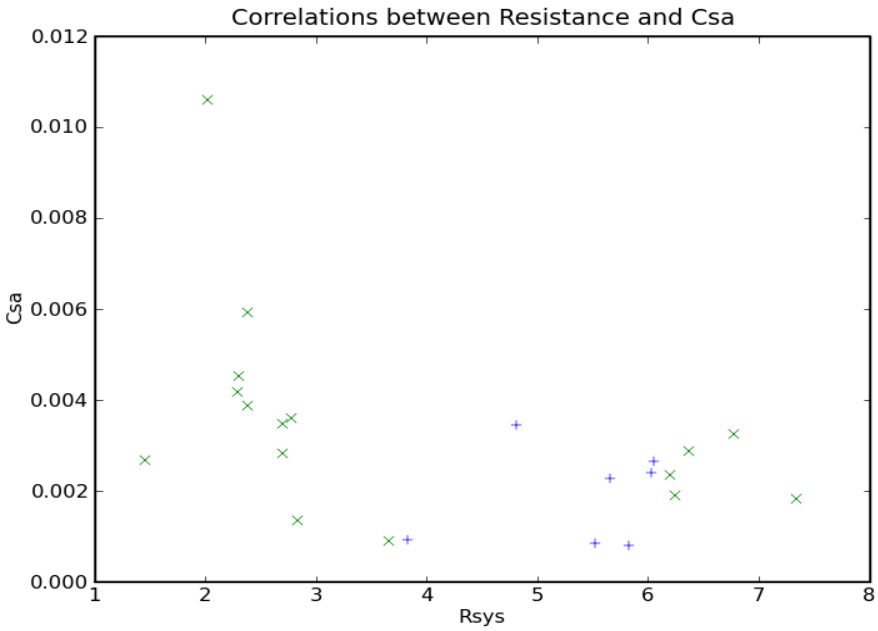

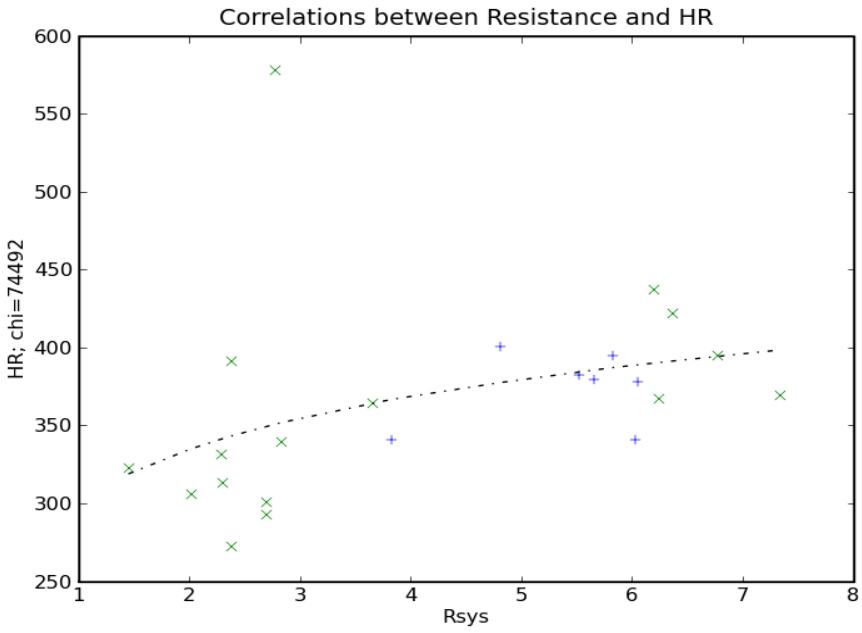

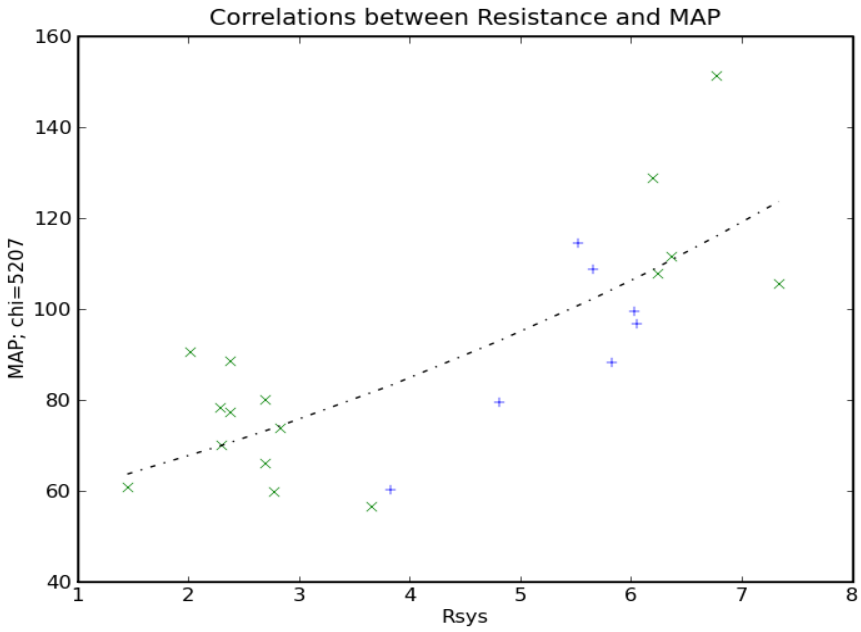
Correlations between Resistance and MAP
MAP; chi=5207
Rsys
160
140
120
100
80
60
40
1
2
3
4
5
6
7
8

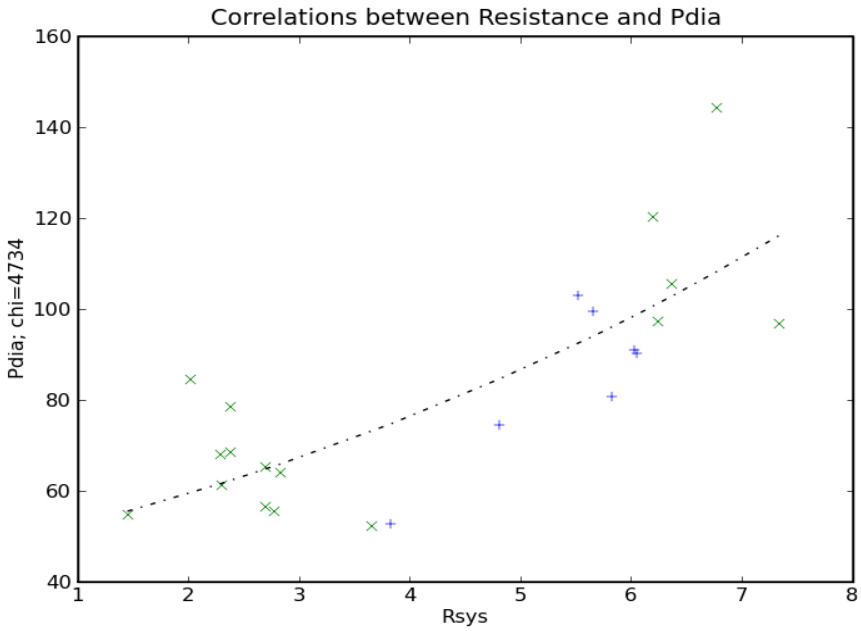
Correlations between Resistance and Pdia
Pdia; chi=4734
Rsys
160
140
120
100
80
60
40
1
2
3
4
5
6
7
8

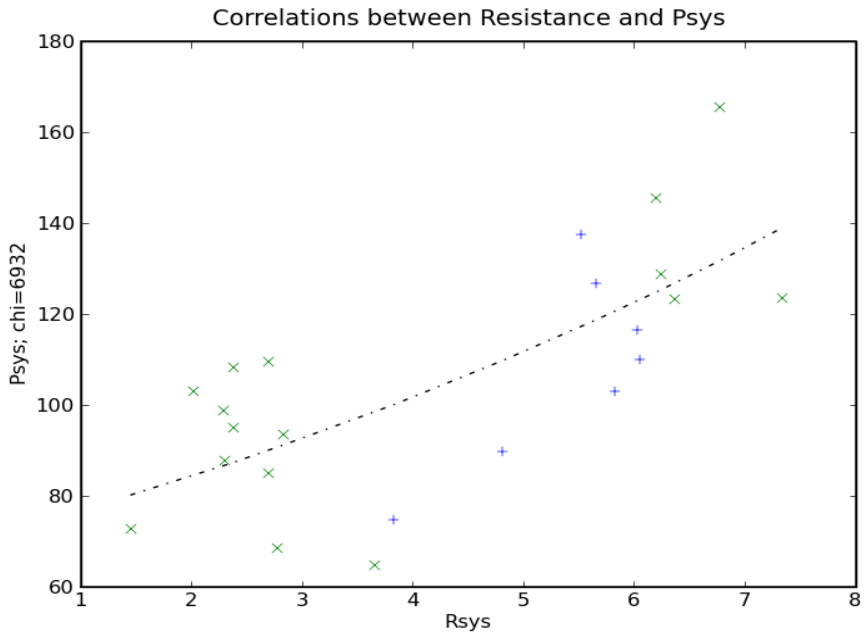
Correlations between Resistance and Psys
Psys; chi=6932
Rsys
180
160
140
120
100
80
60
1
2
3
4
5
6
7
8

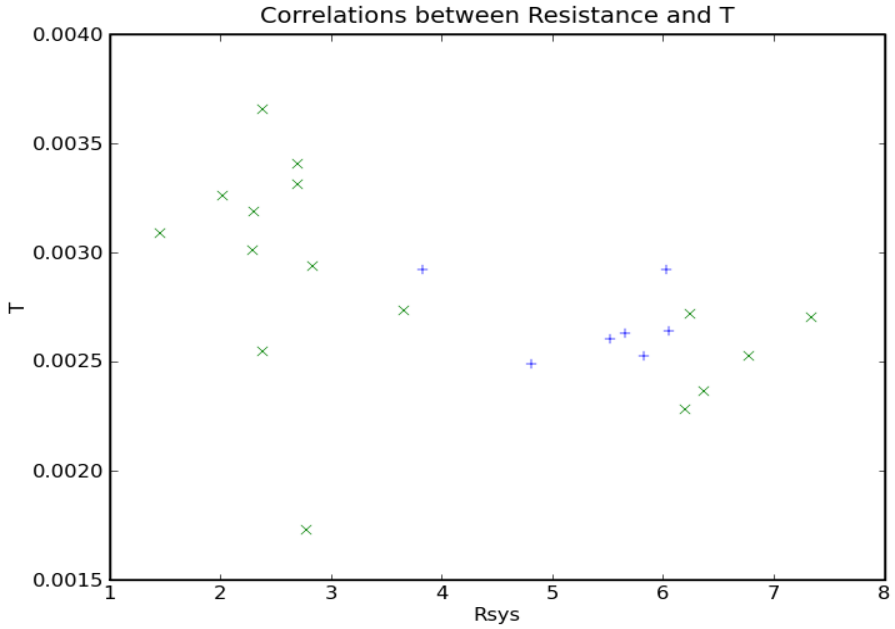
Correlations between Resistance and T
T
Rsys
0.0040
0.0035
0.0030
0.0025
0.0020
0.0015
1
2
3
4
5
6
7
8

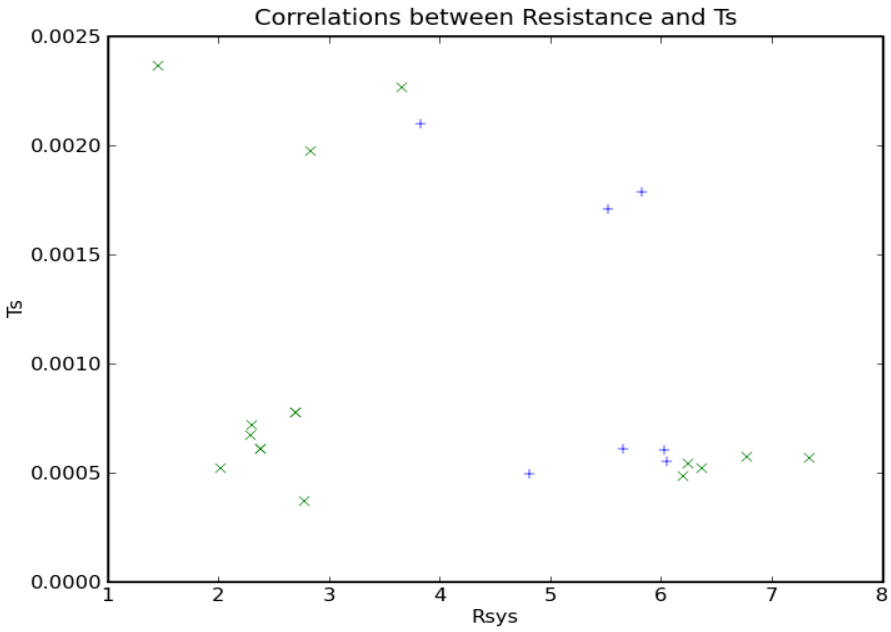
Correlations between Resistance and Ts
0.0025
0.0020
0.0015
0.0010
0.0005
0.0000
Ts
1
2
3
4
5
6
7
8
Rsys

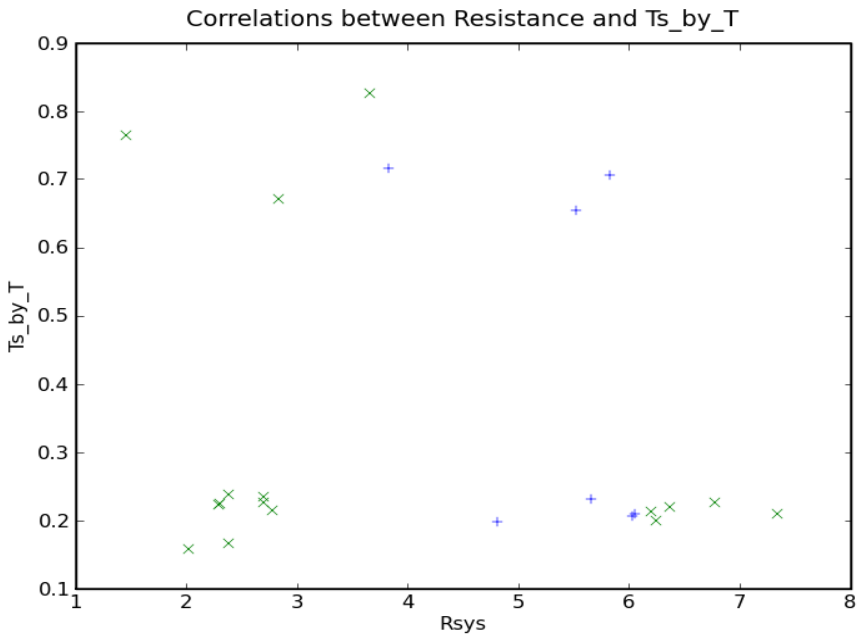
Correlations between Resistance and Ts_by_T
0.9
0.8
0.7
0.6
0.5
0.4
0.3
0.2
0.1
Ts_by_T
1
2
3
4
5
6
7
8
Rsys

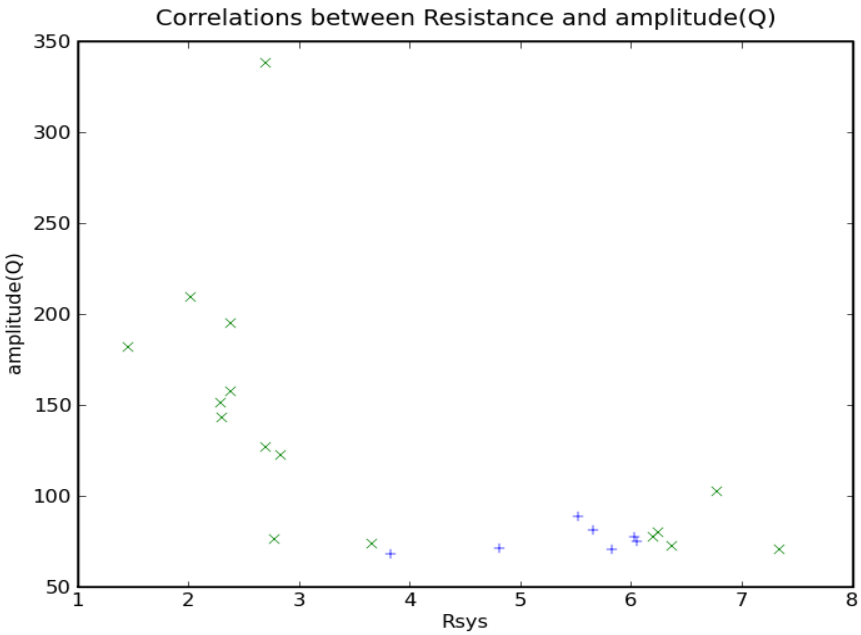
Correlations between Resistance and amplitude(Q)
amplitude(Q)
Rsys
350
300
250
200
150
100
50
1
2
3
4
5
6
7
8

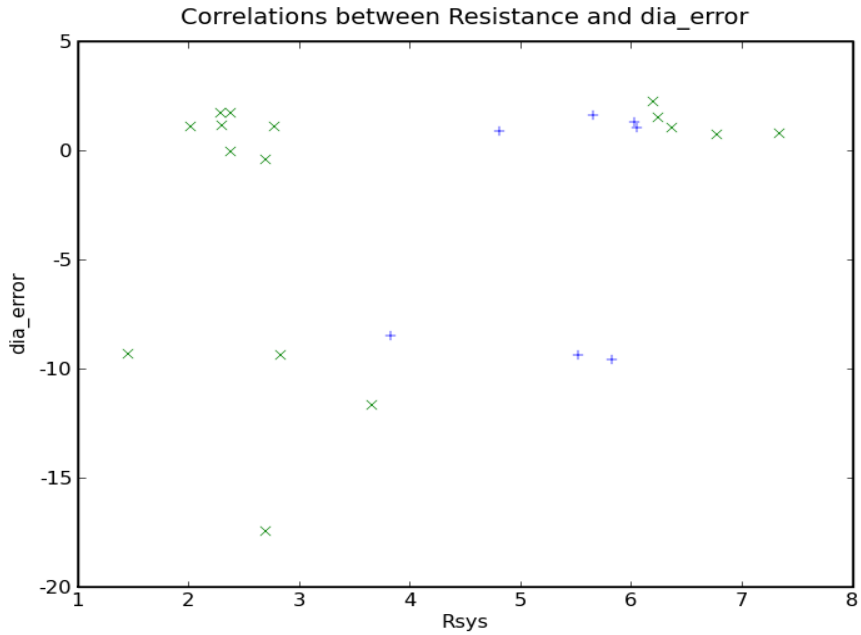
Correlations between Resistance and dia_error
dia_error
Rsys
5
0
-5
-10
-15
-20
1
2
3
4
5
6
7
8

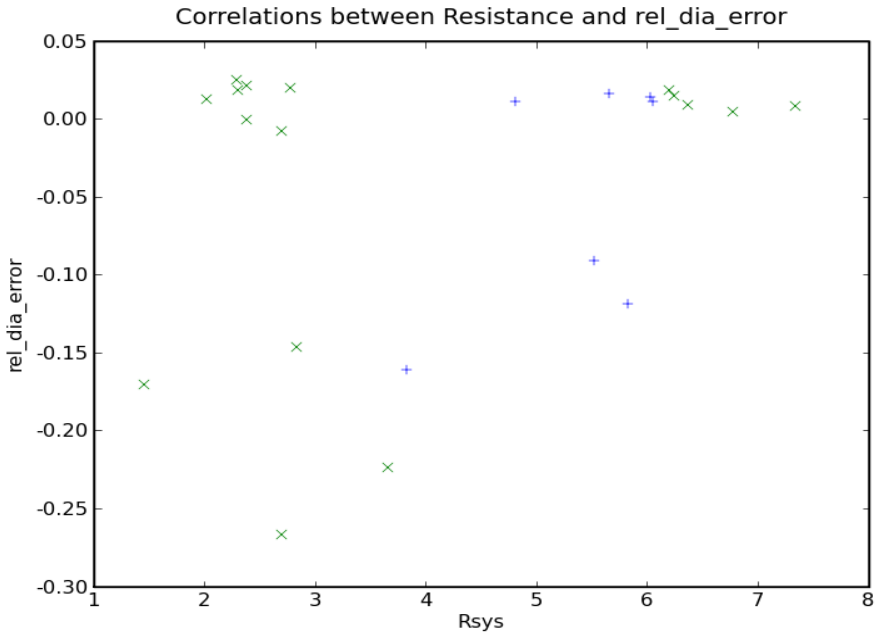
Correlations between Resistance and rel_dia_error
0.05
0.00
-0.05
-0.10
-0.15
-0.20
-0.25
-0.30
rel_dia_error
1
2
3
4
5
6
7
8
Rsys

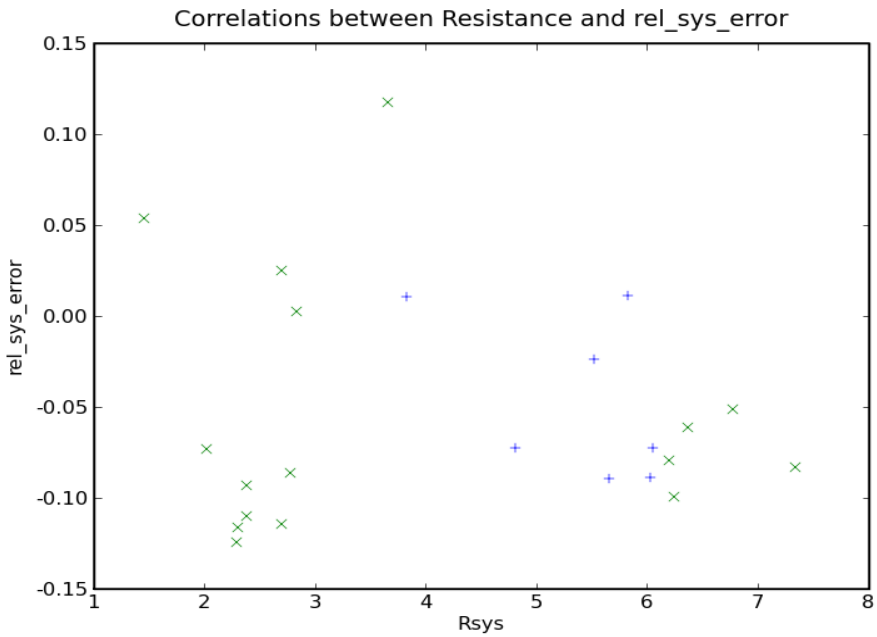
Correlations between Resistance and rel_sys_error
0.15
0.10
0.05
0.00
-0.05
-0.10
-0.15
rel_sys_error
1
2
3
4
5
6
7
8
Rsys

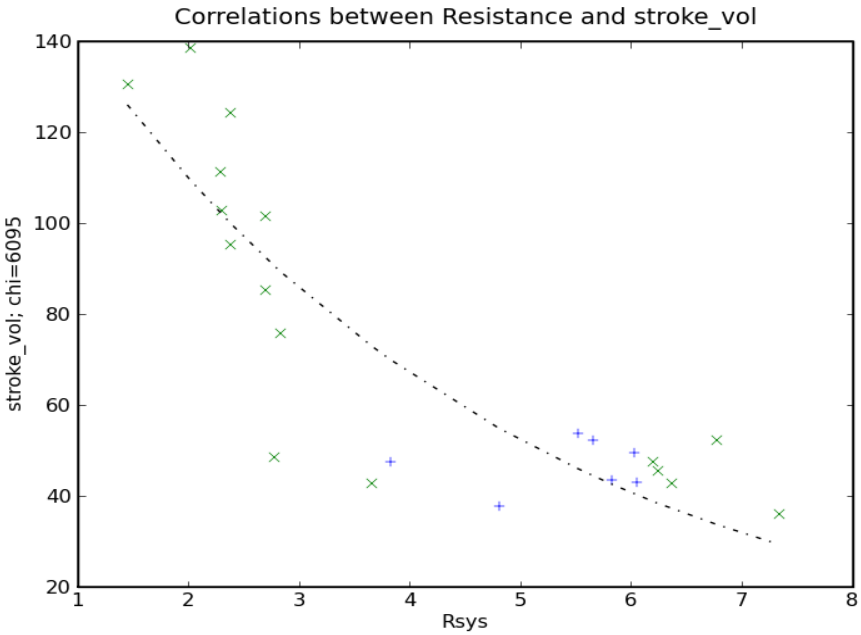
Correlations between Resistance and stroke_vol
stroke_vol; chi=6095
Rsys
140
120
100
80
60
40
20
1
2
3
4
5
6
7
8

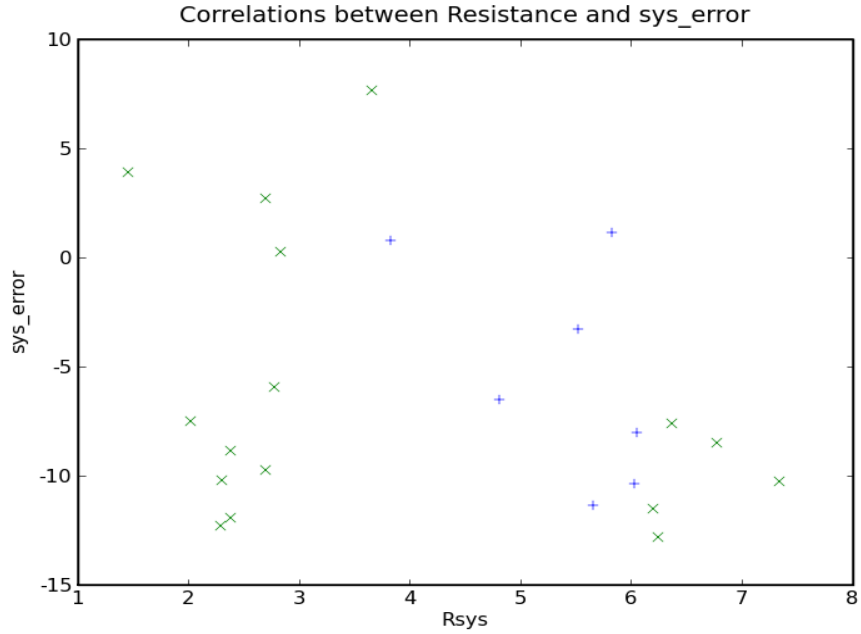
Correlations between Resistance and sys_error
sys_error
Rsys
10
5
0
-5
-10
-15
1
2
3
4
5
6
7
8

A.1.4. Forward Modeling with Different Compliance Values

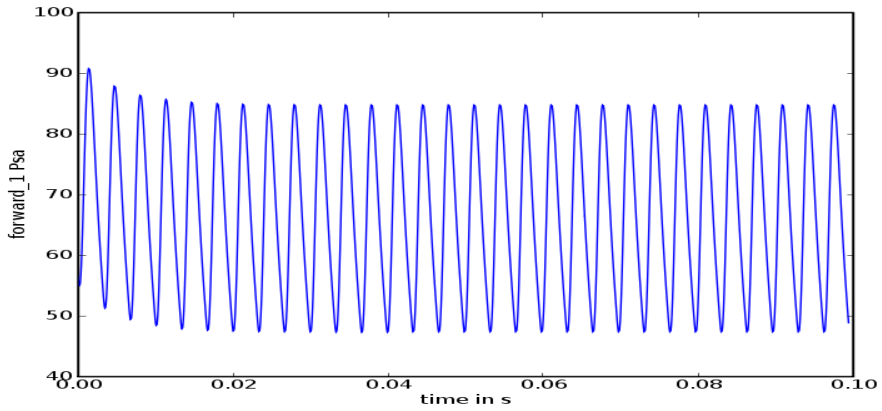

Figure A.1.: Forward model with pre-estimated compliance (Case#1).

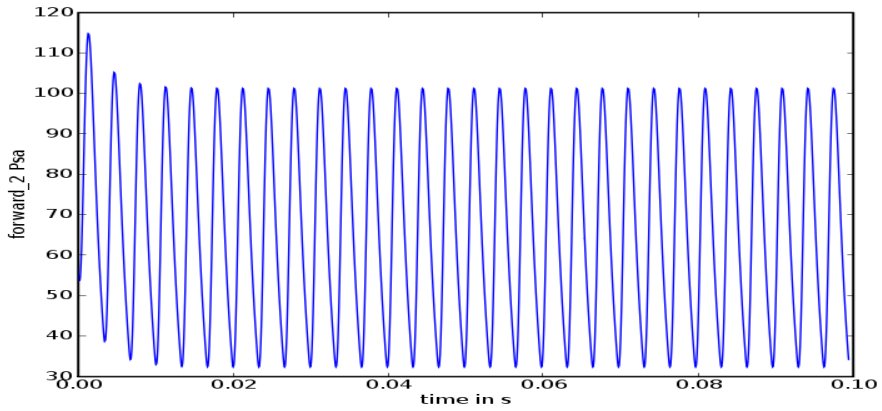

Figure A.2.: Forward model with compliance estimated from inverse modeling over one period with systolic pressure at the flow peak (Case#2).

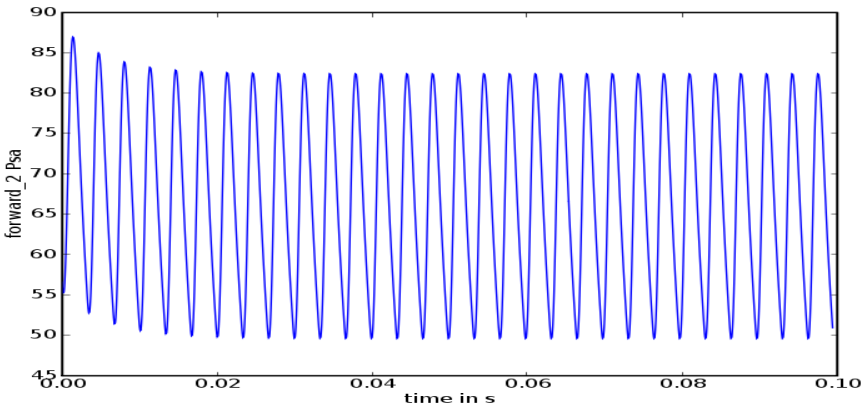

Figure A.3.: Forward model with compliance estimated from inverse modeling over one period with systolic pressure as maximum (Case#3).

A.2. The Two-Comparment Model

A.2.1. Evaluation of Left Ventricular Compliance

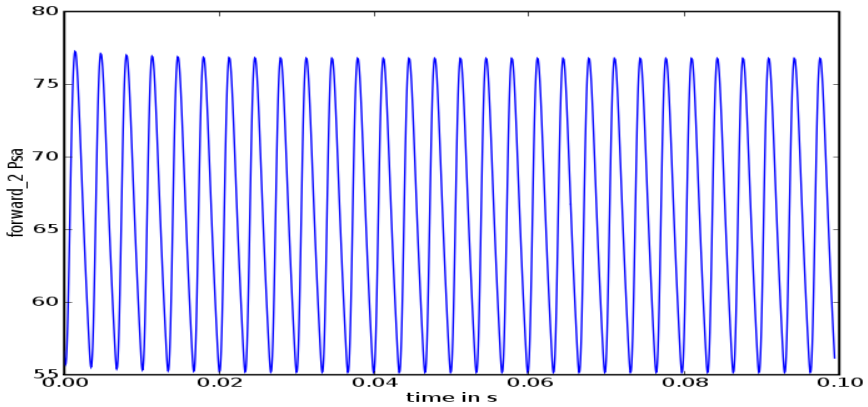

Figure A.4.: Forward model with compliance estimated from inverse modeling over two periods with systolic pressure at the flow peak (Case#5).

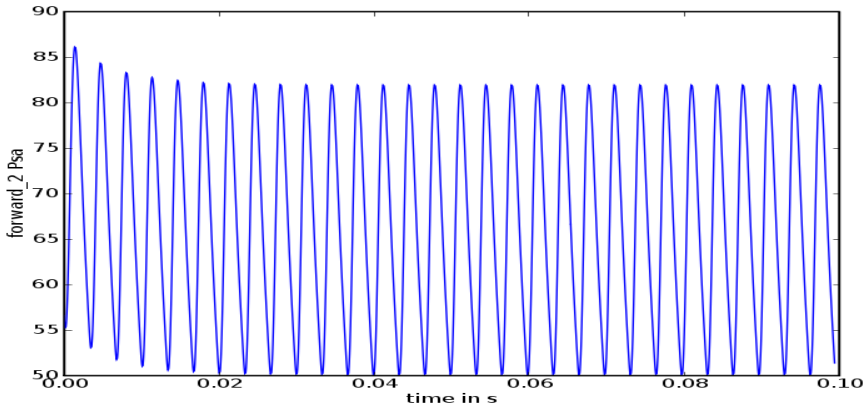

Figure A.5.: Forward model with compliance estimated from inverse modeling over two periods with systolic pressure as maximum (Case#4).

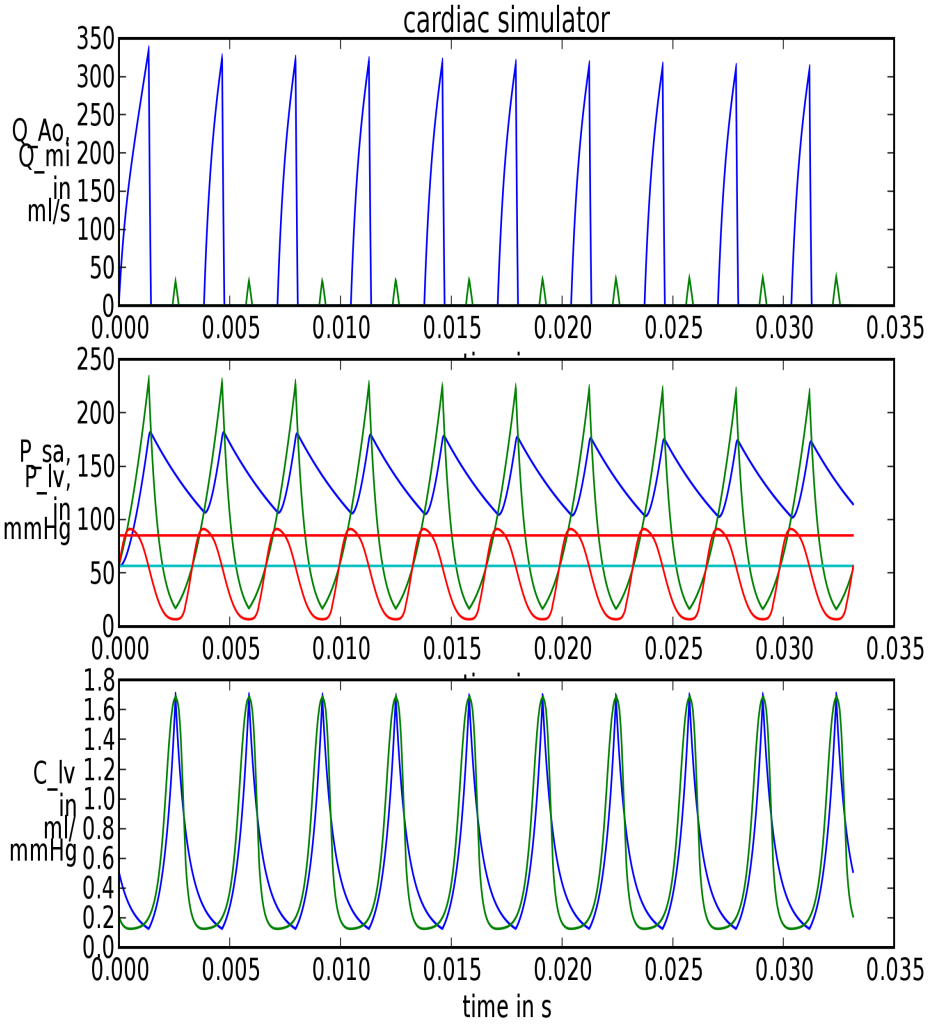

Figure A.6.: Simulation of the Two-Comparment Model with direct use of Sagawa for C_{lv}.

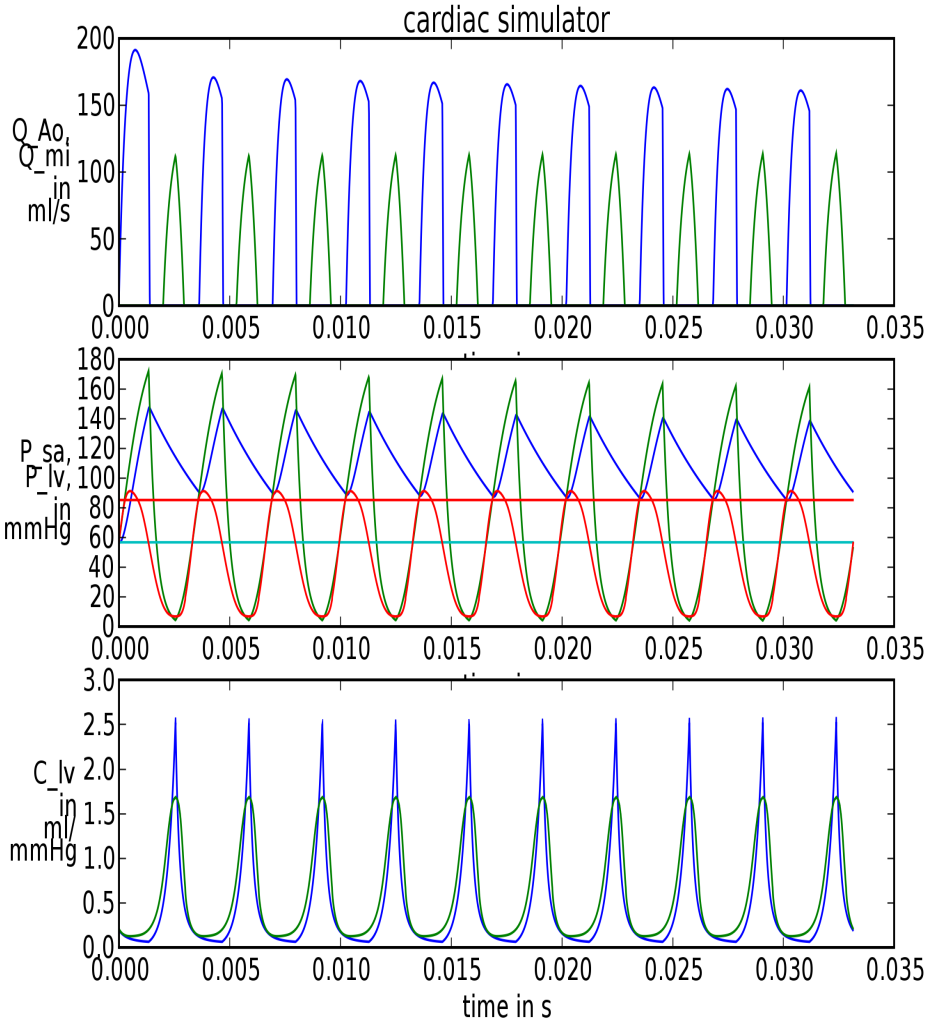

Figure A.7.: Simulation of the Two-Comparment Model with adapted time and changed max and min values of C_{lv}.

B. Programming Issues

All programs are implemented in python [18] with the mathematics package numpy [13] and the plotting tool pylab [29]. The implementation of the linear models were based on [15]. For finding relations between different parameters, the plots of parameters of the one-compartment model were fitted with the tool Scientific Python ([25]). The inverse modeling is based on the use of the packages Swiginac (Symbolic Mathematics, [31]) and SyFi (Symbolic Finite Elements[26]).

All programming code and applied data material can be downloaded from [12]. The following tables give an overview of how the code can be used.

Table B.1.: Forward modeling of the One-Compartment Model

Task	Command	Result
Simulating one model	Simple	Shows the resulting plot
Simulating a series of Models	CollectData	Collects all cases in HTML-files including simulation plots and all known parameters; All parameters are additionally added to the file "Collected_ data.txt"
Correlating the collected data	ProcessData	Generates plots from the collected parameters

An overview of the programs dependencies on exterior packages and other programs is illustrated in Figure B.1. The python script *readData* handles reading of measurement data, averaging high measurement data and algorihms for finding the points in the single experiments, where the registered measurements were reasonalbe. The script *Rat* is based on *readData* and provides the parameters that are used for the different simulations. It also enables plotting of data. *Simple* and *Extended* contain the scripts for simulating the One and Two-Compartment Models respectively. A long sequence of the Two-Compartment Model can be executed by running the script *longRun*. For running and comparing a bunch of One-Compartment simulations, the scripts *CollectData* and *ProcessData* were used.

Solving the inverse problem is based on the script *LagrangeSolver*. This solver is built in a general style that allows to formulate a variety of ordinary differential equations as inverse problems. For using the solver, the unknown variables have to be defined as (swiginac-)symbols and the trial function for every variable has to be given. Additionally, a mesh over the given time, a (SyFi-) reference element and the anverage step length are required. During

Table B.2.: Inverse modeling of the One-Compartment Model

Task	Command	Result
Simulating a linear flow–resistance relation over one period	BasicRatSimulator	generates a HTML–file with results
Simulating a linear flow– resistance relation with adapted maximum over one period	BasicRatSimulator_max	generates a HTML–file with results
Simulating a linear flow– resistance relation over twp periods	RatSimulator_2P	generates a HTML–file with results
Simulating a linear flow– resistance relation with adapted maximum over two periods	RatSimulator_2P_max	generates a HTML–file with results
Simulating a nonlinear flow-resistance relation over two periods	nonlinear _inverse	shows a plot of the solution

Table B.3.: Forward modeling of the Two-Compartment Model

Task	Command	Result
Simulating one model with an adapted C_{lv}-function	Extended	Shows the resulting plot
Simulating one model over five minutes	longRun	Shows the resulting plot

the initialisation of a *LagrangeSolver* object, local-to-global mappings for the variables are generated automatically. The mappings are given as two different types. One mapping for all the variables and a list of mappings, with one mapping for the every parameter.

After building an object of the class *LagrangeSolver*, the variables' variational formulation on the referance element is available. These definitions of the variables are necessary to formulate the Lagrange function and the function for the preconditioner on the reference element. Since the Lagrange equation may include time-dependent functions that are given by discrete values, the *LagrangeSolver* enables to add a list of the functions' symbols and the function definition that returns a value for every node in the mesh. Further, known points in the solution can be inserted into the final matrix. For this purpose, list of indexes, and corresponding values needs to be transferred to the solver. The defined functions, and the mentioned list are necessary input for setting up the system of equations. The final Lagrange equation is then achieved by analytical derivation of the Lagrange function. Then, the Lagrange equation is mapped to the global time mesh, where the list of variable-specific mappings

enables the variables to be defined by symbols with the index of the appropriate time interval. The inverse of the preconditioner is created in the same way and afterwards inversed symbolically.

So far, the system of equations that is given still includes symbols for the parameters in every point of the time interval. Befor solving the system, the current values of the parameters are inserted on every iteration step. The initial values have to be given as input to the *LagrangeSolver*'s solving function, however, the solver disposes of a function that adapts the number of necessary points to the given element type.

The scripts that use *LagrangeSolver* contain combinations of different Lagrange functions and handeling of the input data. *Test* is an additional script that was used for the eigenvalue analysis. In contrast to the others, the initial condition and the requirements on the solutions are set directly into the system of equations.

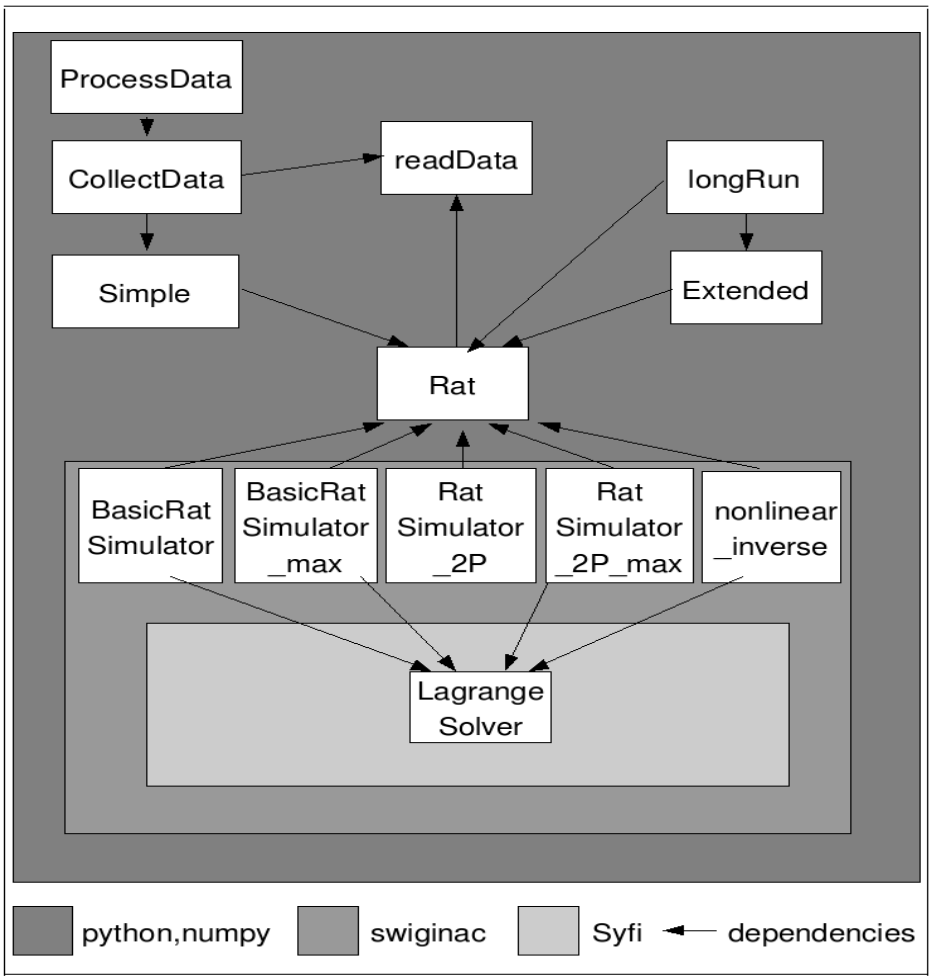

Figure B.1.: Diagram of all components and their dependencies on other components and packages.

Bibliography

[1] 25th Annual Meeting of the American Society of Biomechanics. *Hydraulic Model of the Systemic Resistance*, 2001.

[2] Almoraci S. Algarve, Jorge M. Barreto, and Walter C. Lima. Computer model of overall systemic circulatory system with baroreflex blood pressure control. *12th IEEE Symposium on Computer-Based Medical Systems. 18-20 June 1999, Stamford, CT, USA*, pages 104–109., 1999. IEEE Computer Society.

[3] Jose Luis Rojo Alvarez, Manel Martinez-Ramon, Mario de Prado-Cumplido, Antonio Artes-Rodriguez, and Anibal R. Figueiras-Vidal. Support vector method for robust arma system identification. *IEEE Transactions on Signal Processing*, 52(1):155–164, January. 2004.

[4] Jerry J. Batzel, Franz Kappel, Daniel Schneditz, and Hien T. Tran. *Cardiovascular and Respiratory Systems (Modeling, Analysis and Control).* Siam, Philadelphia, 2007.

[5] Dietrich Braess. *Finite Elements; Theory, Fast Solvers, and Applications in Elasticity Theory.* Camebridge University Press, Edinburgh, third edition, 2007.

[6] R. Burattini, G. Gnudi, N. Westerhof, and S. Fioretti. Total systemic arterial compliance and aortic characteristic impedance in the dog as a function pressure: A model based study. *Computers and Biomedical Research*, 20:154–165., 1987.

[7] Alfredo L. Clavell, Michael T. Mattingly, Tracy L. Stevens, Amiram Nir, R. Scott Wright, Lawrence L. Aarhus, Dennise M. Heublein, and John C. Burnett Jr. Angiotensin converting enzyme inhibition modulates endogenous endothelin in chronic canine thoracic inferior vena caval constriction. *The Journal of Clinical Investigation*, 97(5):1286–1292., 1996.

[8] Linda S. Constanzo. *Physiology.* Elsevier Science, third edition, 2006.

[9] Michael Danielsen. *Modeling of Feedback Mechanisms which Control the Heart Function in a View to an Implementation in Cardiovascular Models.* PhD thesis, Department of Mathematics, Roskilde University, 1998.

[10] Timothy L Davis and Roger G. Mark. Teaching physiology through simulation of hemodynamics. *Computers in Cardiology 1990*, 17:649–652., 1999.

[11] Karima Djabella, Claire Madigue, and Michel Sorine. A differential model of the baroreflex control of the cardiovascular system during a tilt test. *Proceedings of the 44th IEEE Conference on Decision and Control and the European Control Conference 2005, Seville, Spain*, pages 903–908., 2005.

[12] Programing Code for Master Thesis. *http://folk.uio.no/susanhen/*.

[13] Python Package for Scientific Computing. *http://numpy.scipy.org*.

[14] Cardiovascular System II: The Vascular Highway. *http://www.phschool.com/science/biology_place/biocoach/cardio2/intro.html*.

[15] Frank C. Hoppensteadt and Charles S. Peskin. *Modeling and Simulation in Medicine and the Life Sciences*. Springer, New York, second edition, 2002.

[16] H. Suga K. Sagawa and K. Nakayama. Instantaneous pressure-volume ratio of the left ventricle versus instantaneous force-length relation of papillry muscle. *Cardiovarscular System Dynamics, M.I.T. Press, Cambridge*, MA:99–105., 1978.

[17] James Keener and James Sneyd. *Mathematical Physiology*. Springer, New York, 1998.

[18] Python Programmin Language. *http://www.python.org*.

[19] Xinsheng Li, Jing Bai, Shuai Cui, and Shuzhong Wang. Simulation study of the cardiovascular functional status in hypertensive situation. *Computers in Biology and Medicine*, 32:345–362., 2002.

[20] Laila Mathews. Paradigm shift in hemodynamic monitoring. *The Internet Journal of Anesthesiology*, 11(2), 2007.

[21] Alessandro Monti, Claire Medigue, and Laurence Mangin. Instantaneous parameter estimation in cardiovascular time series by harmonic and time-frequency analysis. *IEEE Transactions on Biomedical Engineering*, 49(12):1547–1556, December. 2002.

[22] Ramakrishna Mukkamala and Richard J. Cohen. A forward model-based validation of cardiovascular system identification. *Am J Physiol Heart Circ Physiol*, 281:H2714–H2730., 2001.

[23] Mark Mutsaer, Mostafa Bachar, Jerry Batzel, Franz Kappel, and Stefan Volkwein. Receding horizon controller for the baroreceptor loop in a model for the cardiovascular system. *Cardiovascular Engineering*, 8(1):14–22, March. 2007.

[24] Robert A. O'Rourke and Eugene Braunwald. *Principles of Internal Medicine: Physical Examination of the Cardiovascular System*. McGraw-Hill, seventeenth edition, 2008.

[25] Scientific Python Package. *http://dirac.cnrs-orleans.fr/plone/software/scientificpython/.*

[26] Symbolic Finite Elements Package. *http://www.fenics.org/wiki/SyFi.*

[27] Joseph L. Palladino, Jan P. Mulier, and Abraham Noordergraaf. Defining ventricular elastance. *Proceedings of the 20th Annual International Conference of the IEEE Engineering in Medicine and Biology Society*, 20(1):383–386., 1998.

[28] K. H. Parker. Notes for cardiovascular fluid mechanics. http://www.bg.ic.ac.uk/Staff/khparker/homepage/BSc_lectures/2002/Cardiovascular_Mechanics.pdf.

[29] Python plotting package. *http://www.scipy.org/PyLab.*

[30] William K. Purves. *Life: The Science of Biology.* W.H. Freeman & Company, Gordonsville, fourth edition, 1998.

[31] a C++ library for symbolic maths Python interface to Ginac. *http://swiginac.berlios.de/.*

[32] Christopher M. Quick, David S. Berger, Douglas A. Hettrick, and Abraham Noordergraaf. True arterial system compliance estimated from apparent arterial compliance. *Annals of Biomedical Engineering*, 28:291–301., 2000.

[33] Mansour Rayminia, Atul Trivedi, Janos Molnar, Monther Elbzour, Mayra Guerrero, Yasser Salem, Aziz Ahmed, Sandeep Koshla, and David L. Lubell. Validation of a new formula for mean arterial pressure calculation: The new formula is superior to the standard formula. *Catheterization and cardiovascular interventions*, 63(4):419–425., 2004.

[34] Sat Sharma and Claude Kortas. Hypertension. http://www.emedicine.com/med/topic1106.htm.

[35] Liron Sheffer, William P. Santamore, and Ofer Barnea. Cardiovascular simulation tool. *Cardiovascular Engineering*, 7:81–88., 2007.

[36] Bram W. Smith, J. Geoffrey Chase, Roger I. Nokes, Geoffrey M. Shaw, and Graeme Waked. Minimal haemodynamic system model including ventricular interaction and valve dynamics. *Medical Engineering and Physics*, 26:131–139., 2004.

[37] D. J. Snow, S. J. Gray, S. Ghosh, L. Foubert, A. Oduro, T. W. Higenbottam, F. C. Wells, and R. D. Lattimer. Inhaled nitric oxide in patients with normal and increased pulmonary vascular resistance after cardiac surgery. *British Journal of Anaesthesia*, 72:185–189., 1994.

[38] Joakim Sundnes, Glenn Terje Lines, Xing Cai, Bjorn Frederik Nielsen, Kent-Andre Mardal, and Aslak Tveito. *Computing the Electrical Activity in the Heart.* Springer, Heidelberg, 2006.

[39] G. Paul Toorop, Nico Westerhof, and Gijs Elzinga. Beat-to-beat estimation of peripheral resistance and arterial compliance during pressure transients. *The American Physiological Societey*, 0363-6135/87:H1275–H1283., 1987.